Replies to Reviewer 1

We thank both reviewers for their knowledgeable and valuable comments. Our efforts in addressing them, together with the reviewers' suggestions, led to a revised manuscript that represents a great improvement with respect to the original version. In what follows, reviewer's comments are in black and authors' replies in red.

There is a second order polynomial which is "added to the retrieval", but there is no discussion of the details of this process. If it is fit individually during each retrieval, and is properly included in the error analysis, then it will have a large effect on the lower stratospheric sensitivity. I am therefore somewhat skeptical of the accuracy of the sensitivities shown in Figure 8 at _30km and below. The other choice is to treat this as a systematic term, in which case it affects the systematic error but not the sensitivity. In either case, this can introduce an important uncertainty, and the authors need to discuss exactly what they have done.

We added to the manuscript a discussion on how the retrieval process includes a second order polynomial. This is done by fitting it in each retrieval, individually. It is not a systematic term. It does have a large effect on the sensitivity below 30 km but this is already taken into account in the sensitivity profile of figure 8 (original manuscript, now figure 9). In the figure below, we show the difference in sensitivity between employing the second order polynomial or only a first order one.

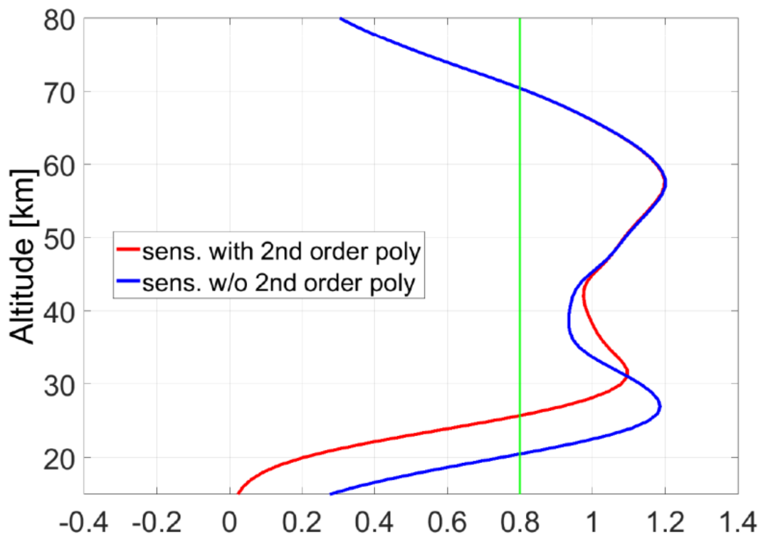

In order to address this issue raised by the reviewer, we estimated the uncertainty in the retrieved profile due to the use of the second order polynomial. The most rigorous way of doing it, in our opinion, is to take the uncertainty associated to the second order coefficient (Δa_2) in the retrieval process (say for example 20%, e.g., $a_2 = (-5 \pm 1) \times 10^{-3}$) and then perform two retrievals for the same spectrum with fixed values of the second order coefficient equal to $a_2 \pm \Delta a_2$ (in our example they would be $a_2 = -4 \times 10^{-3}$ and $a_2 = -6 \times 10^{-3}$). The resulting two vertical profiles would then provide an estimate for the uncertainty of the regular retrieved profile associated with the uncertainty in the second order coefficient. We found that the average uncertainty of the second order coefficient calculated by the optimal estimation routine over the entire dataset is 6%, with few retrievals showing more than 20%. We therefore decided to employ a fixed maximum uncertainty on the coefficient of 20% for the whole data set, rejecting from the data set those few retrievals (less than 5% of the total) that had an uncertainty larger than 20% in the determination of a_2. Displayed below is the updated figure related to the error analysis of the spectrum observed on 23 Dec, 2016, where we added the polynomial uncertainty to the other 2 sources. As expected the polynomial uncertainty has an impact mostly in the lower part of the retrieval.

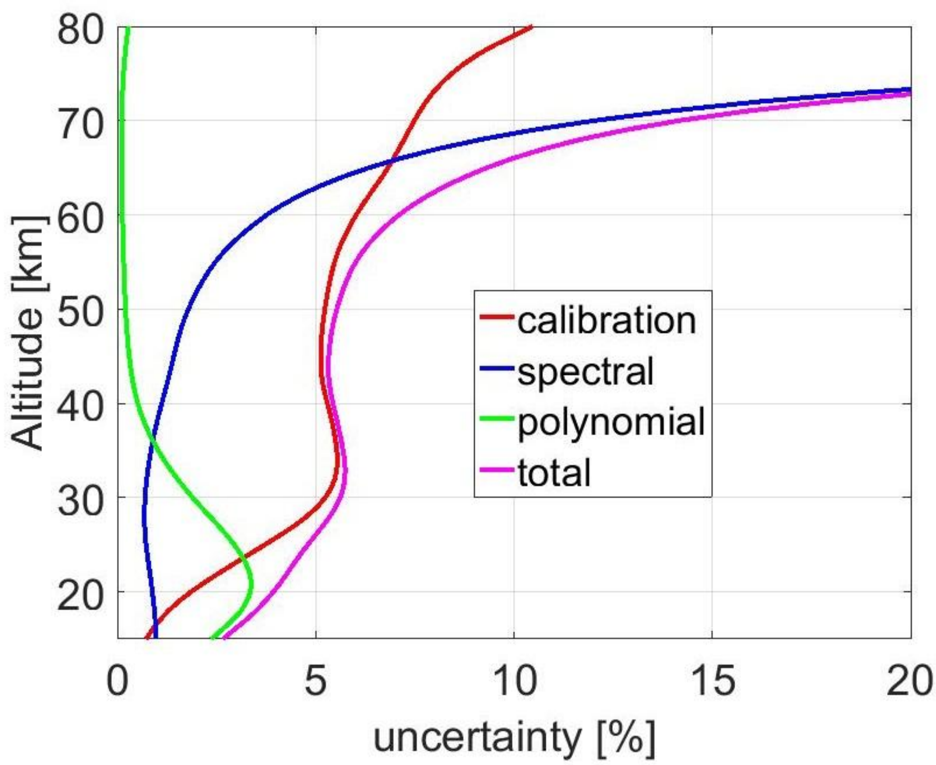

On top of it, in order to demonstrate the good quality of VESPA retrievals down to 25 km altitude, we changed the apriori used for the retrievals, which is now a fixed climatological profile up to about 48 km and a seasonal profile in the mesosphere (see also our reply to this specific issue raised by the reviewer in the following), and we introduced in the manuscript the correlation between VESPA profiles and MLS smoothed profiles. These are the original high resolution MLS profiles smoothed in the vertical with a running average of 10 km. This was done in order to decouple MLS profiles from the apriori and the averaging kernels used in VESPA retrievals (which was a short-coming of the correlation between VESPA and MLS convolved profiles shown in the originally submitted manuscript) and yet make the MLS vertical resolution somewhat similar to that characterizing VESPA profiles.

Figures down below show the relative and absolute average differences between VESPA and MLS smoothed (blue), and between VESPA and MLS convolved (red),

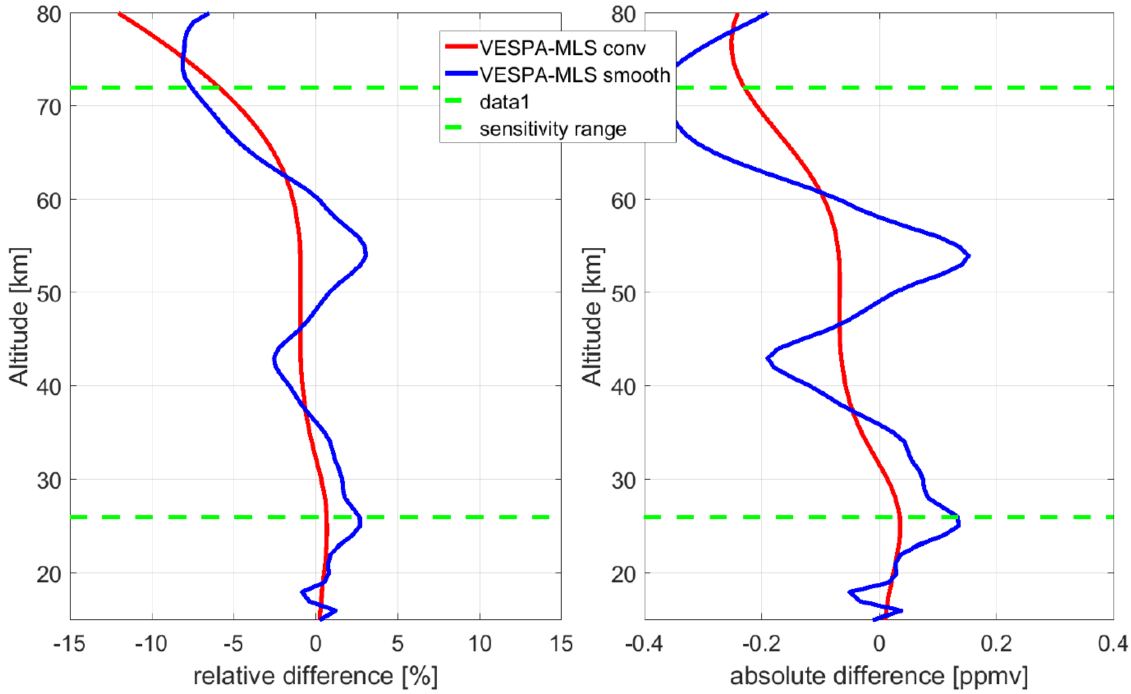

the correlation coefficient between VESPA and MLS smoothed profiles (blue),

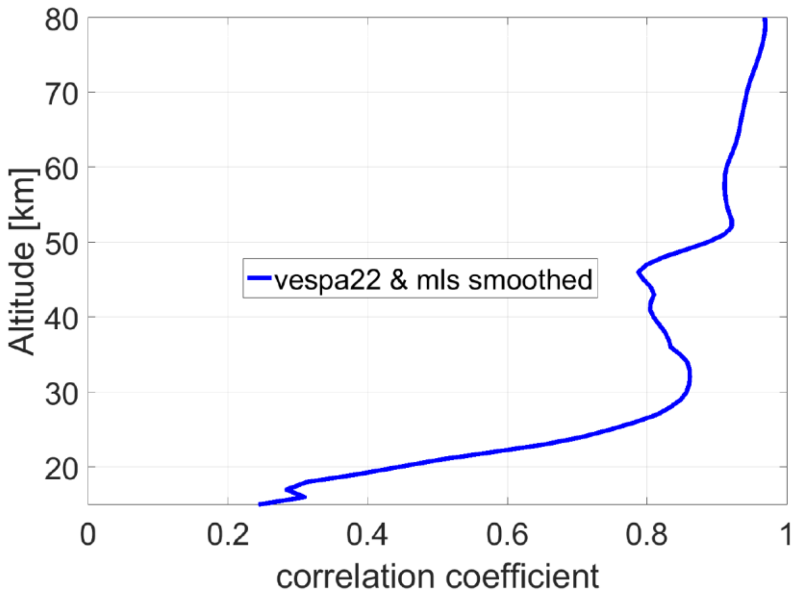

and the time series at 25 km of VESPA22, MLS convolved and MLS smoothed.

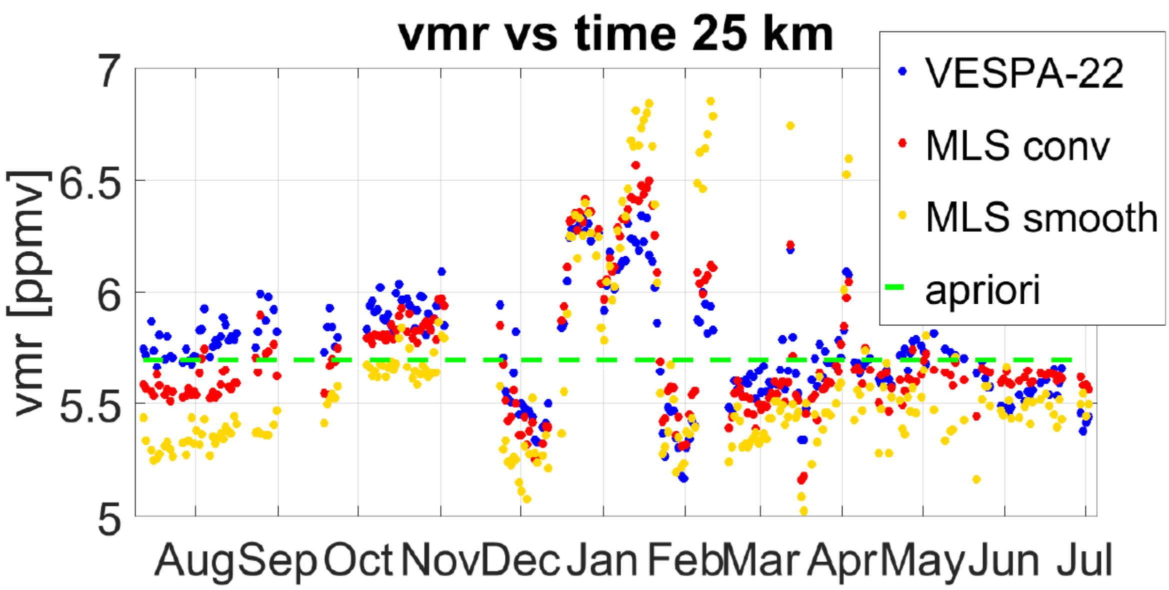

All the figures above demonstrate in our opinion that VESPA22 retrievals are scientifically valuable in the sensitivity range indicated in the manuscript. Please note, however, that we also specified in the revised manuscript that the sensitivity range changes with seasons (see fig. 18 in the revised manuscript) and in summer it is approximately between 30 and 65 km. See figure below.

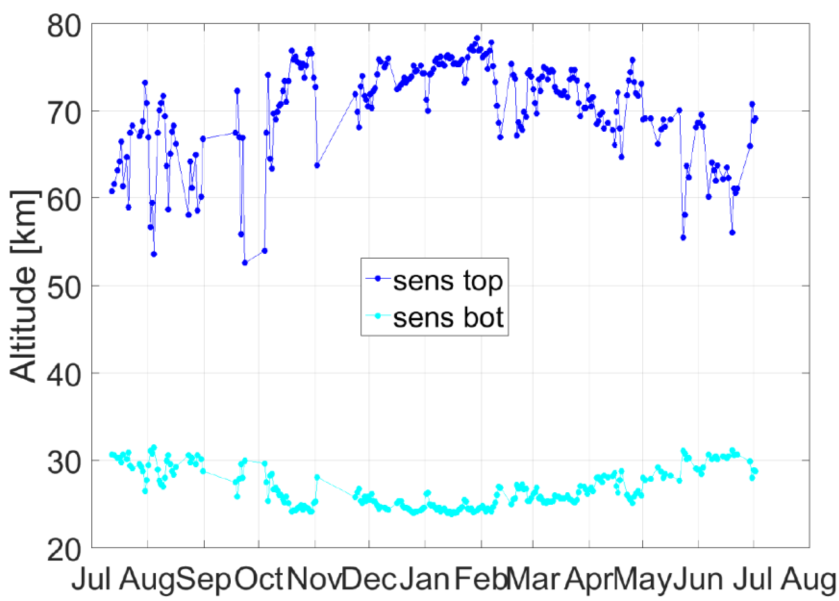

What was changed in the revised manuscript:

- Added discussion in Section 4 on how the second order polynomial is treated in the retrieval process;
- Modified figure 12 with the updated error analysis which includes the polynomial uncertainty;
- Modified figure 9 according to the new error analysis;
- Inserted the MLS smoothed data set, with its correlation with Vespa-22 profiles;

- Introduced the time series of the sensitivity interval, i.e., how the interval of accepted sensitivity changes through time. Added this time series in figure 18;
- Added two altitude levels in former figure 15 (figure 17 in the revised manuscript) to prove the good quality of VESPA-22 retrievals at the lower (25 km) and upper (75 km) limits of the sensitivity interval.

In the error analysis, many of the terms have been classified as systematic, when in truth, with the exception of the spectroscopy, almost all of them have a significant random component. As a result, the "retrieval uncertainty" shown in Figure 11, which by implication is the only random component, is, in my estimation, absurdly small. I think it would be acceptable to not specifically label the bulk of the errors as either completely systematic or random, but the present suggestion that the precision is <1% over much of the atmosphere would require a great deal of additional evidence.

We agree with the reviewer and changed the terminology accordingly. The uncertainty due to spectroscopic and calibration parameters is now indicated with "calibration uncertainty" in the revised manuscript.

The VESPA retrievals are performed using a seasonally varying a priori based upon 3 years of seasonally varying MLS data, hence the statement on page 29 that these are "independent datasets" is not true. Claims of high correlation between the measurements are therefore unsubstantiated. If the authors wish to publish claims related to correlations they should either perform their retrievals with a constant a priori (which would probably still leave them with good correlations), or compare deviations from the a priori for the two datasets (which is a tough test). Alternatively they could drop the whole discussion of correlation, along with Table 6 and Figure 14. Also, as long as the retrievals are done with a varying a priori Figure 15 should include a point indicating the a priori for each month.

We followed the reviewer's suggestion and changed the whole analysis by using only two apriori profiles during 10 out of the 12 months of the year, identical below 48 km and diverging above, due to the large difference in Polar regions between summer and winter water vapor mesospheric profiles. We added figure 7 in the revised manuscript (and below) showing the two apriori profiles. The summer apriori (red line) is used during the period from June 1 to August 31, while the winter apriori (blue line) is used during the period from October 1 to April 31. During the month of May and September, there is a transition period in which we used a linear daily interpolation from one apriori to the other to provide continuity in the retrieved profiles timeseries.

We also added the time series of the apriori mixing ratio values in figure 17 (former figure 15) as suggested by the reviewer.

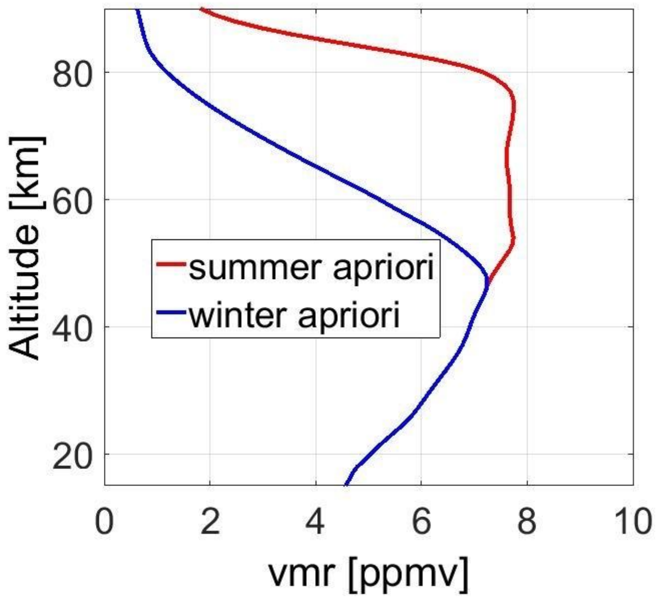

Page 10 line 7 – Where does this "constant in frequency within 1.5%" number come from? The diode data sheets? Or perhaps a calibration measurement?

The indicated 1.5% is half of the maximum difference between brightness temperature values over the spectral passband (see figure below). The noise diodes emission spectra are measured only during the LN_2 calibration. In the revised manuscript we rephrased the "constant in frequency" sentence with "The noise diode produces a signal that is measured to be quite stable in frequency. In fact, single-channel T_{nd} values are always within 1.5% of the spectral mean of the diode temperature brightness T_{nd}."

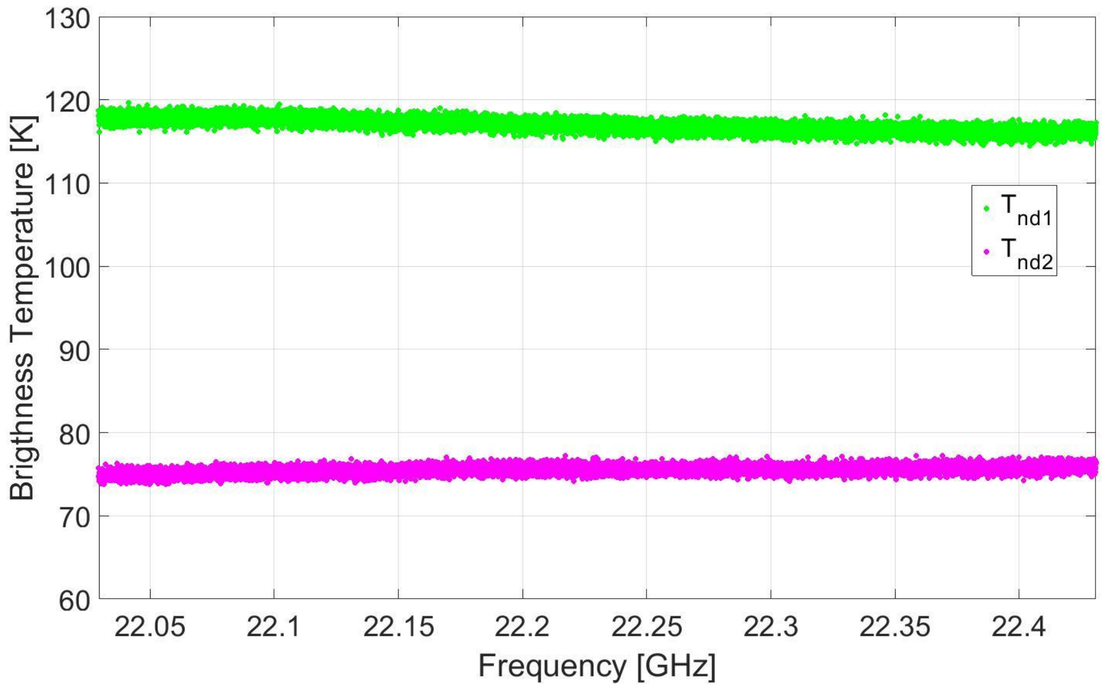

Equation (4) – presumably ‘x’ is known for this transition. What is it?

We added a sentence to direct readers to Table 2 where all the spectroscopic parameters used are listed

Concerning all the comments below, we agree with the reviewer and changed the manuscript accordingly.

Page 6 line 20 “negligible”. Perhaps “small” would be better here. The numbers are given later in the paragraph, so everything here is okay, but for some applications a 1.5% difference might not be considered “negligible”.

The use of Tatm is a bit confusing, as this appears to be the atmospheric temperature for the troposphere, but not for other parts of the atmosphere. Would it be better to label this as Ttrop?

“Tsup” is a rather odd abbreviation for surface temperature.

Page 11 line 7: “explicit” should be “explicitly give”

Page 15 line 13 – “Selee” should be “Seele”

Page 17 line 8 – missing ‘(‘   ?????????

Figure 9 –“specttrocscopy” should be “spectroscopy”

Replies to Reviewer 2

We thank both reviewers for their knowledgeable and valuable comments. Our efforts in addressing them, together with the reviewers' suggestions, led to a revised manuscript that represents a great improvement with respect to the original version. In what follows, reviewer's comments are in black and authors' replies in red.

In general, the introduction in section 3 to 5 repeats the basics of radiative transfer, balancing instruments and optimal estimation, which are already described in detail in the cited literature. In my opinion, these sections could be easily shortened without loss of information.

We shortened the sections as suggested by the reviewer, also eliminating 13 basic equations.

The abstract (p.1 line 13) and section 3 describe the VESPA-22 back-end as an FFTS with 500 MHz bandwidth and 31kHz resolution. However, the schematic in Fig. 1(b) shows a system with 1GHz bandwidth. Is this the actual schematic of the instrument?

No, there was a mistake in the schematics. It has been corrected.

Also P4 line 1 states a 2GS/s sampling rate, which results in a 1 GHz Nyquist bandwidth.

The effective sampling rate is 1 GS/s. It was corrected in the revised manuscript.

P. 3 line 13: The sentence "the waveguide used by VESPA-22 polarizes the incoming radiation with a gain difference between the two polarization modes of 45 dB" is both incorrect and irrelevant. The rectangular waveguide supports only a single polarization by definition. The stated 45dB may refer to the feed horn, but the actual cross-polar with the offset reflector will be much worse. Bertagnolio 2012 states for the same instrument 35dB and 24dB, respectively. This should not affect the observations, so the sentence could be easily removed.

We agree with the reviewer and removed the sentence.

P. 6 line 28 states that the opacity in Fig 3 was calculated for water vapor profiles measured by AURA/MLS. However, the dominant effect in this figure is due to tropospheric water vapor which is not measured by MLS.

We clarified this statement in the revised manuscript. The profiles used were obtained merging tropospheric and stratospheric measurements collected by radiosondes from Eureka (80.0°N -85.9°W), Canada, and Aura/MLS, respectively.

P. 9 line 24 states that a 6 MHz wide interval around the line center is kept at 31kHz resolution, while all other channels are binned with 50 channels. In Fig 6(b) the interval without binning looks much smaller than 6MHz.

The interval without binning is indeed 6 MHz and was correctly showed in Figure 6b of the original manuscript. However, the x-axis unit in figure 6b was MHz and there was a 10^4 multiplicative factor on the bottom right of the figure. We realized that this indication was misleading and we changed the frequency unit for all the figures of the revised manuscript from MHz to GHz.

According to p. 14 line 1 the matrix with the measurement error Se was assumed with constant diagonal elements which are calculated from the residuals after an initial run of the retrieval. However, the central channels without binning will have a higher measurement error as the ones without binning. Please provide also the range of measurement errors which were used in Se for the daily retrievals. The retrieval errors in Fig 11 seem to be very small. Could this be an artifact of an underestimation of the measurement errors in Se due to the binning at the line wings?

The reviewer is correct and in the original manuscript Se was underestimated. In the new analysis inserted in the revised manuscript Se is now calculated before the smoothing process of the spectrum and this brought an increase of the retrieval uncertainty (now indicated as “spectral uncertainty”) of approximately 70% over the entire vertical profile. The figure below (also inserted in the revised manuscript) shows the new error analysis where we also added the uncertainty due to the use of the second order polynomial (see later comment of this reviewer and a similar comment of reviewer 1).

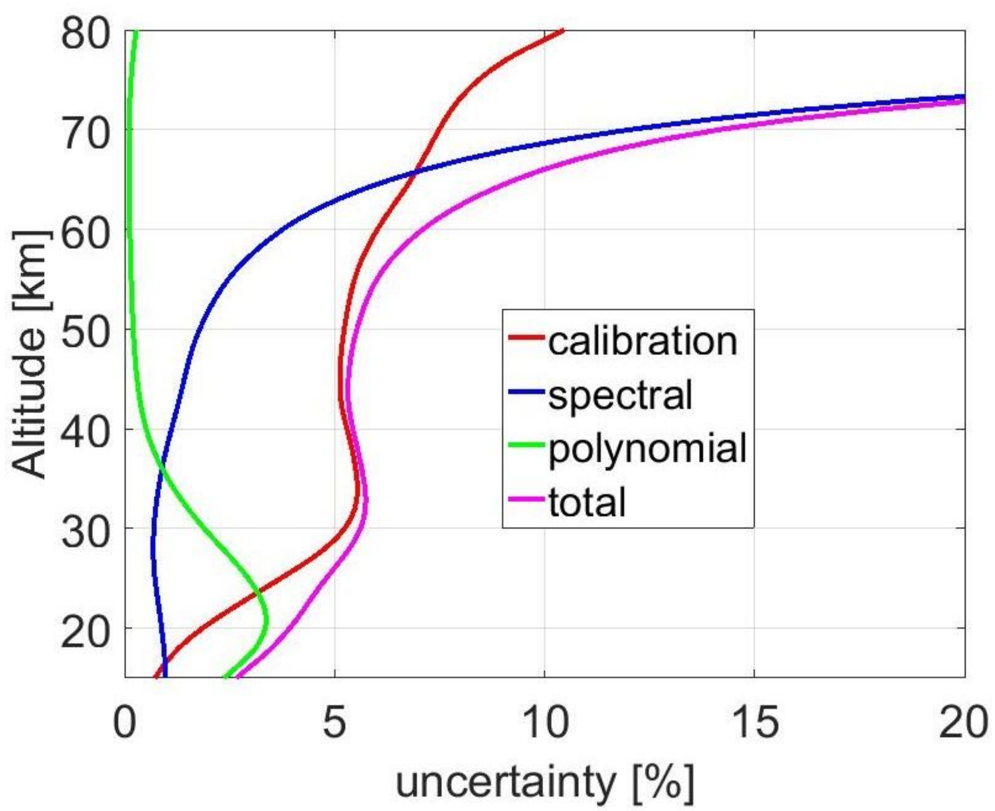

The retrieval uncertainty (now “spectral uncertainty”) is still small, especially in the lower stratosphere, but we underline that it represents only the uncertainty due to spectral noise and potential spectral artifacts.

The figure below shows the time series of the Se values. The range of Se values has been indicated in the revised manuscript.

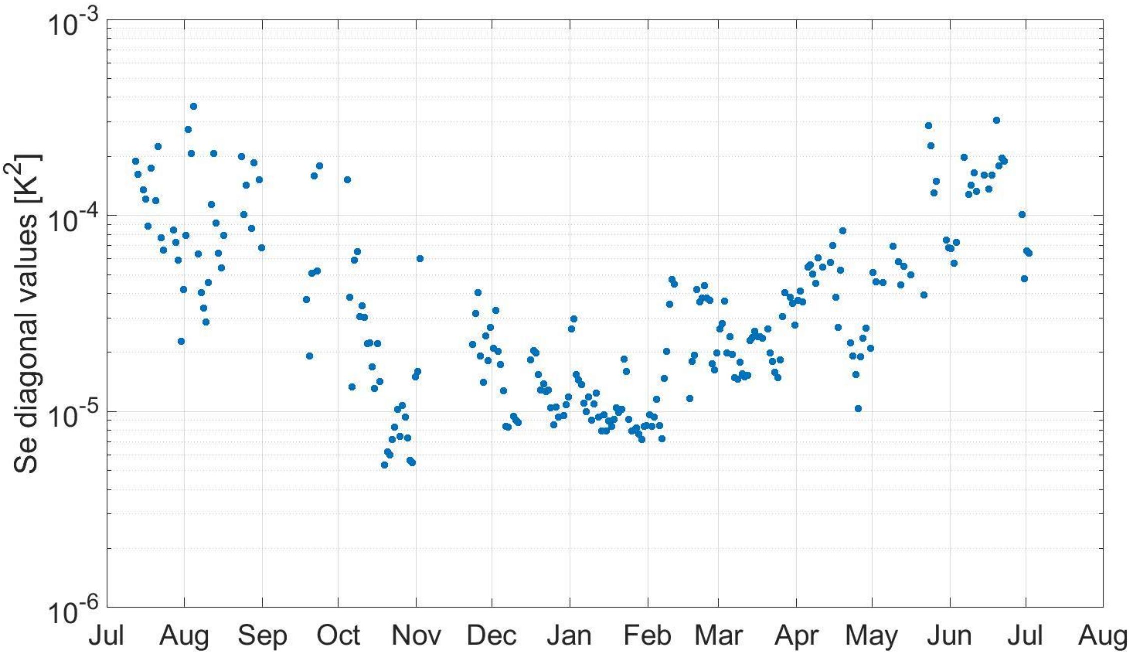

Where do the values for the apriori covariance in Fig. 5 come from?

The Sa matrix values were chosen empirically in order to optimize the characteristics of the retrieval (i.e., maximize sensitivity range and vertical resolution without introducing unphysical oscillations in the retrieved vertical profile). We added this information in the revised manuscript. In the new analysis, we also adopted a slightly rescaled σ profile with respect to the one used in in the original manuscript (and of course updated former figure 5, now figure 6).

P. 14 line 7: "A second-order polynomial is also added to the retrieval . . .". At which stage is it taken into account in the retrieval, and how does it affect the measurement response at the lower altitudes? Is it really a second order polynomial, or just a straight line?

This issue was raised by both reviewer so we report here the same detailed answer we provided to reviewer 1.

We added to the manuscript a discussion on how the retrieval process includes a second order polynomial. This is done by fitting it in each retrieval, individually. It is not a systematic term. It does have a large effect on the sensitivity below 30 km but this is already taken into account in the sensitivity profile of figure 8 (original manuscript, now figure 9). In the figure below, we show the difference in sensitivity between employing the second order polynomial or only a first order one.

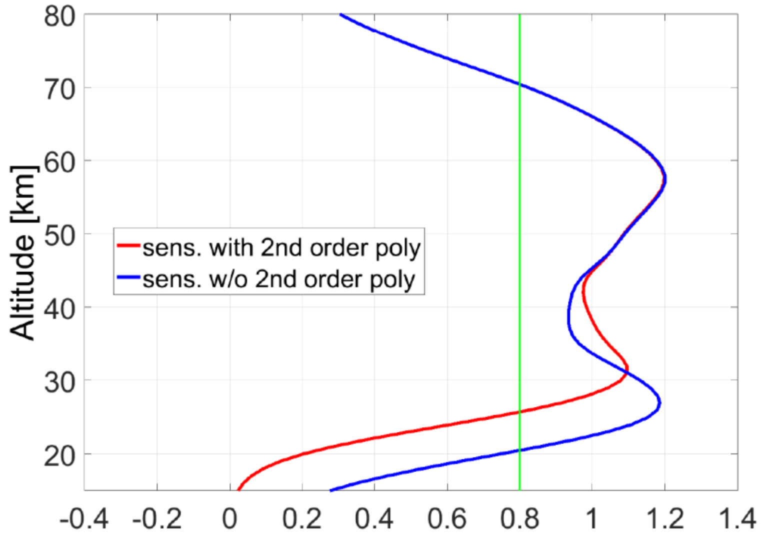

In order to address this issue raised by the reviewer, we estimated the uncertainty in the retrieved profile due to the use of the second order polynomial. The most rigorous way of doing it, in our opinion, is to take the uncertainty associated to the second order coefficient (Δa_2) in the retrieval process (say for example 20%, e.g., $a_2 = (-5 \pm 1) \times 10^{-3}$) and then perform two retrievals for the same spectrum with fixed values of the second order coefficient equal to $a_2 \pm \Delta a_2$ (in our example they would be $a_2 = -4 \times 10^{-3}$ and $a_2 = -6 \times 10^{-3}$). The resulting two vertical profiles would then provide an estimate for the uncertainty of the regular retrieved profile associated with the uncertainty in the second order coefficient. We found that the average uncertainty of the second order coefficient calculated by the optimal estimation routine over the entire dataset is 6%, with few retrievals showing more than 20%. We therefore decided to employ a fixed maximum uncertainty on the coefficient of 20% for the whole data set, rejecting from the data set those few retrievals (less than 5% of the total) that had an uncertainty larger than 20% in the determination of a_2. Displayed below is the updated figure related to the error analysis of the spectrum observed on 23 Dec, 2016, where we added the polynomial uncertainty to the other 2 sources. As expected the polynomial uncertainty has an impact mostly in the lower part of the retrieval.

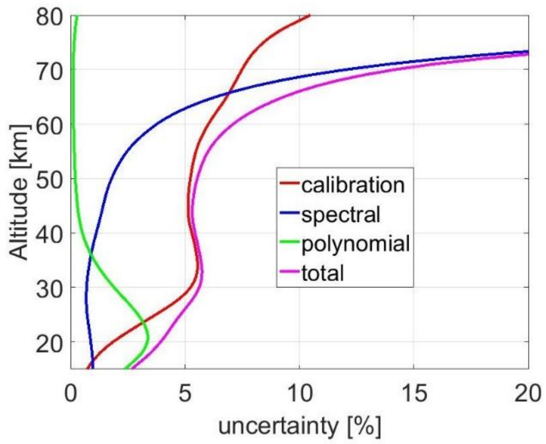

On top of it, in order to demonstrate the good quality of VESPA retrievals down to 25 km altitude, we changed the apriori used for the retrievals, which is now a fixed climatological profile up to about 48 km and a seasonal profile in the mesosphere (see also our reply to this specific issue raised by the reviewer in the following), and we introduced in the manuscript the correlation between VESPA profiles and MLS smoothed profiles. These are the original high resolution MLS profiles smoothed in the vertical with a running average of 10 km. This was done in order to decouple MLS profiles from the apriori and the averaging kernels used in VESPA retrievals (which was a short-coming of the correlation between VESPA and MLS convolved profiles shown in the originally submitted manuscript) and yet make the MLS vertical resolution somewhat similar to that characterizing VESPA profiles. Figures down below show the relative and absolute average differences between VESPA and MLS smoothed (blue), and between VESPA and MLS convolved (red),

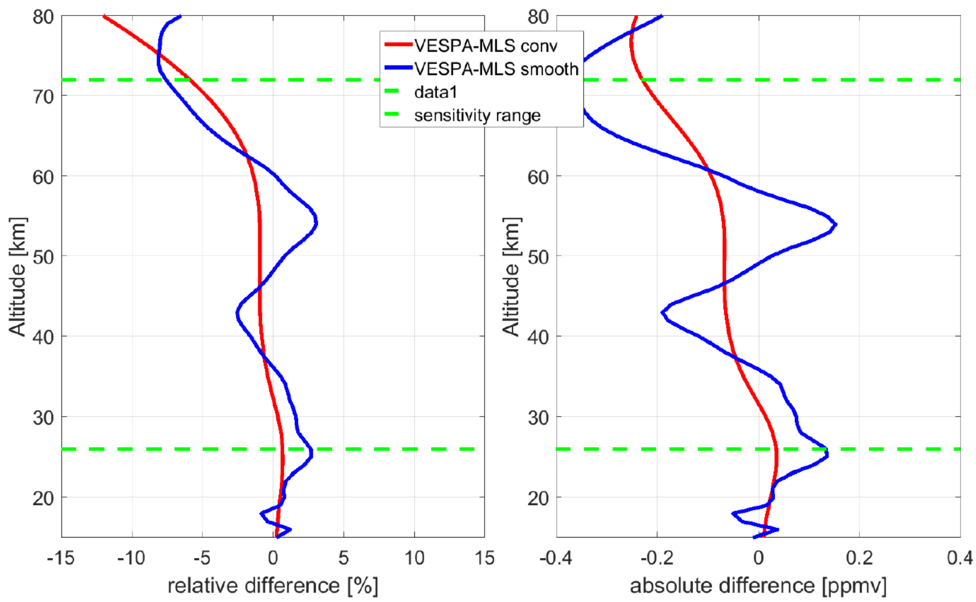

the correlation coefficient between VESPA and MLS smoothed profiles (blue),

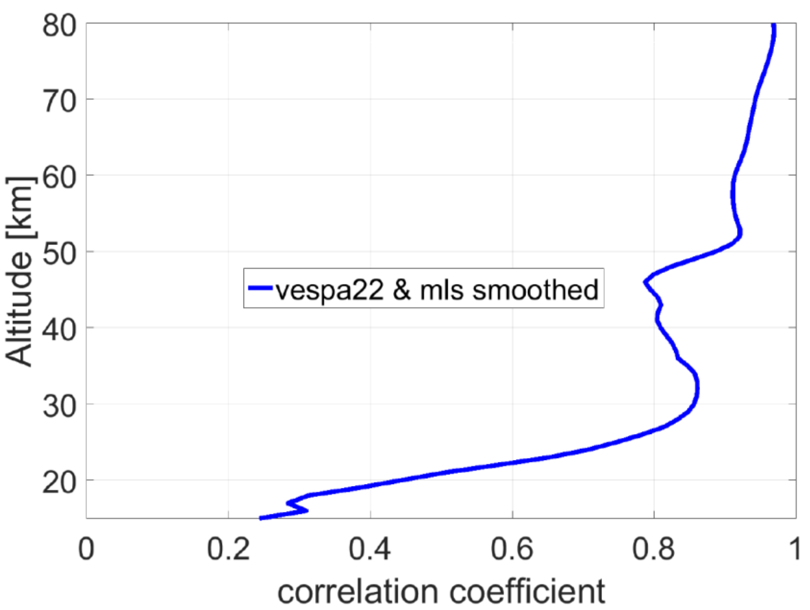

and the time series at 25 km of VESPA22, MLS convolved and MLS smoothed.

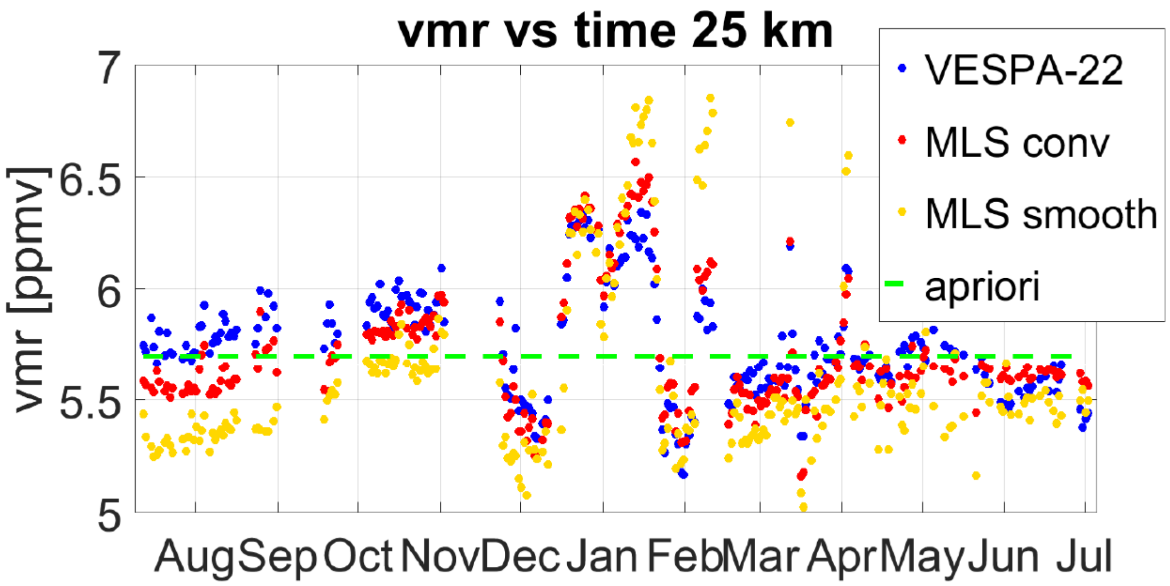

All the figures above demonstrate in our opinion that VESPA22 retrievals are scientifically valuable in the sensitivity range indicated in the manuscript. Please note, however, that we also specified in the revised manuscript that the sensitivity range changes with seasons (see fig. 18 in the revised manuscript) and in summer it is approximately between 30 and 65 km. See figure below.

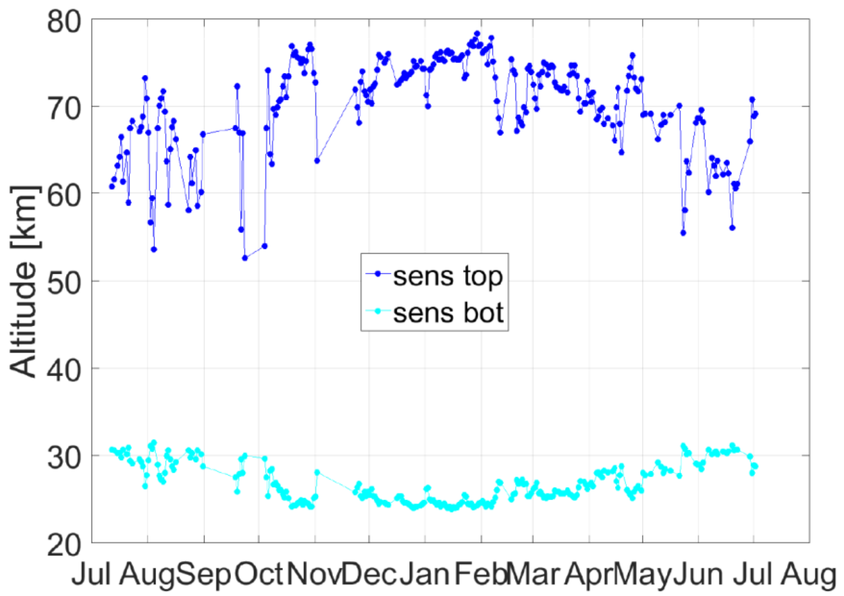

What was changed in the revised manuscript:

- Added discussion in Section 4 on how the second order polynomial is treated in the retrieval process;

- Modified figure 12 with the updated error analysis which includes the polynomial uncertainty;
- Modified figure 9 according to the new error analysis;
- Inserted the MLS smoothed data set, with its correlation with Vespa-22 profiles;
- Introduced the time series of the sensitivity interval, i.e., how the interval of accepted sensitivity changes through time. Added this time series in figure 18;
- Added two altitude levels in former figure 15 (figure 17 in the revised manuscript) to prove the good quality of VESPA-22 retrievals at the lower (25 km) and upper (75 km) limits of the sensitivity interval.

P. 10 line 7 "The noise diode produces a signal that can be considered constant in frequency within 1.5%". Where does this number come from, and can it be demonstrated in the VESPA22 measurements? Over which bandwidth is it valid? Presumably only 40MHz are used for the retrieval, but according to Eq. 20 the mean T_ND is calculated for a much wider frequency range.

The indicated 1.5% is half of the maximum difference between brightness temperature values over the spectral passband (see figure below). The noise diodes emission spectra are measured only during the LN_2 calibration. In the revised manuscript we rephrased the "constant in frequency" sentence with "The noise diode produces a signal that is measured to be quite stable in frequency. In fact, single-channel T_{nd} values are always within 1.5% of the spectral mean of the diode temperature brightness T_{nd}." This is valid over the full 400 MHz bandwidth used in the spectral inversion process.

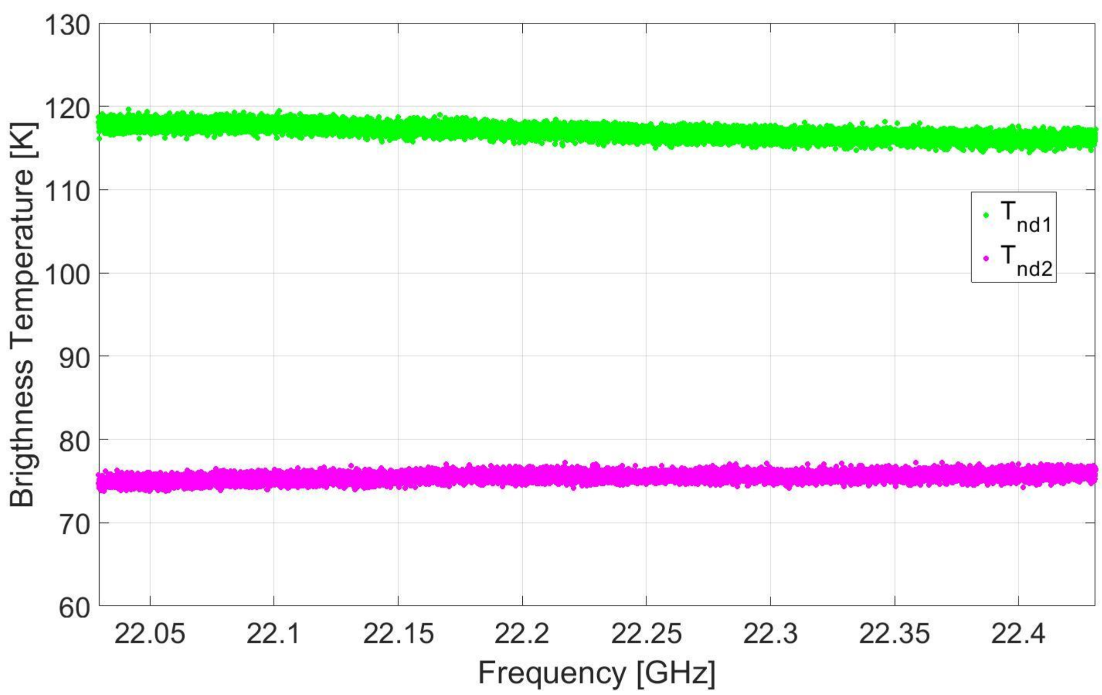

Also the opacity of the Delrin sheet is assumed to be frequency independent. Is this really the case, or does e.g. the polynomial baseline fit change after changing the thickness of the Delrin sheet?

The reviewer is probably correct in suggesting that the delrin sheets have an opacity that varies over the 400 MHz of spectral measurement. We can infer it from the change of the polynomial baseline that we find when we change delrin sheet (in the figure below we indicate the average polynomial baselines when using a 5 mm or 9 mm sheet), as suggested by the reviewer.

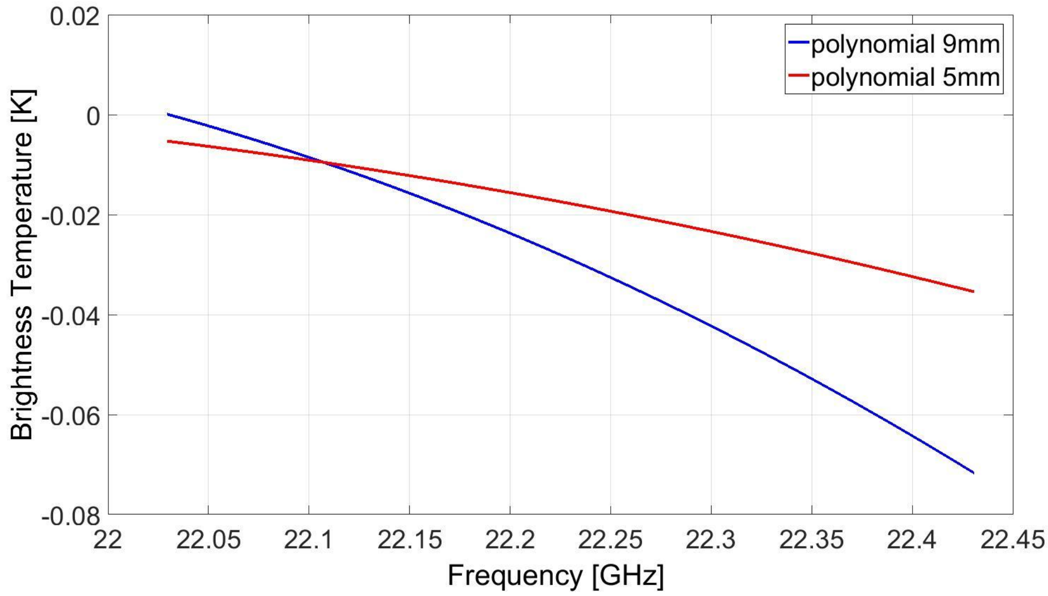

However, we take into account the potential dependency of delrin opacity on frequency in the uncertainty associated to the measurement of the delrin opacity. Delrin opacity measurements have a maximum error (max-min/2) of approximately 2% but we conservatively estimated such an uncertainty to be ±10%.

We added a phrase clarifying that the indicated τ_d is the delrin "mean opacity value over the spectral passband".

P. 12 line 6 claims that the noise diode temperatures measured with LN2 and tipping curve agree within 0.4%. However, the fluctuations of the tipping curve results in Fig. 4 seem to be in the order of several Kelvin, which should result in a higher discrepancy.

Are these fluctuations measurement errors caused e.g. by an inhomogeneous atmosphere, or do they represent a real fluctuation of the noise diode ENR caused e.g. by changes of the laboratory temperature? Which value was used in the actual retrievals?

The 0.4% agreement stated in the manuscript is calculated as the mean difference between the noise diodes temperature measured during the LN_2 calibration and the diodes temperature measured by means of the tipping curve immediately before or after the LN_2 calibration. We confirm that the number is correct and it is approximately 0.4%. We clarified this in the revised manuscript with the sentence "The mean relative difference between T_{nd} values calculated with LN_2 and with tipping curves carried out immediately before or after LN_2 calibrations is (0.4±0.4)% and (0.2±0.3)% for the calibration and the backup diodes, respectively."

Most of the fluctuations in the Fig. 4 of the original manuscript are caused by an inhomogeneous atmosphere. However, some are caused by changes in the ambient temperature inside the observatory (such as that visible on the end of February). We checked this against measurements of the temperature inside the observatory. As a result of this reviewer's comment, we decided to set a stricter rule for accepting tipping curve measurements and now use a threshold of 0.4 instead of 0.8 (see P12 L2 of original manuscript). The figure below shows the time series of T_{nd} values obtained by tipping curves that comply to this new criterion. In the revised manuscript this figure substitutes former Figure 4. In order to better discuss the tipping curve procedure we also added a new figure in the revised manuscript, also attached below.

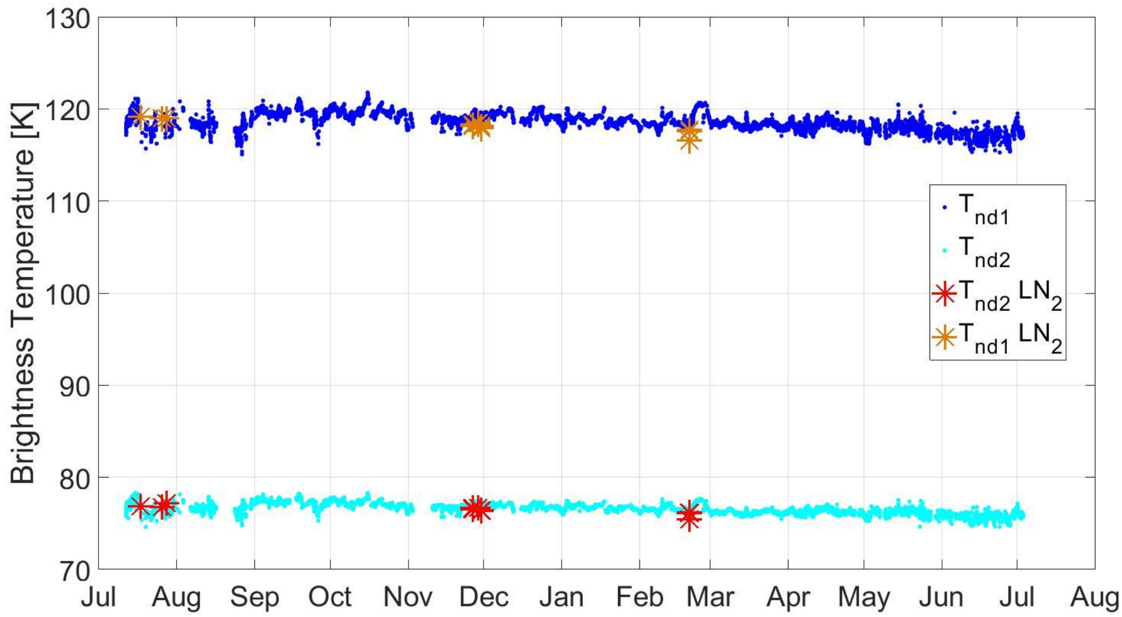

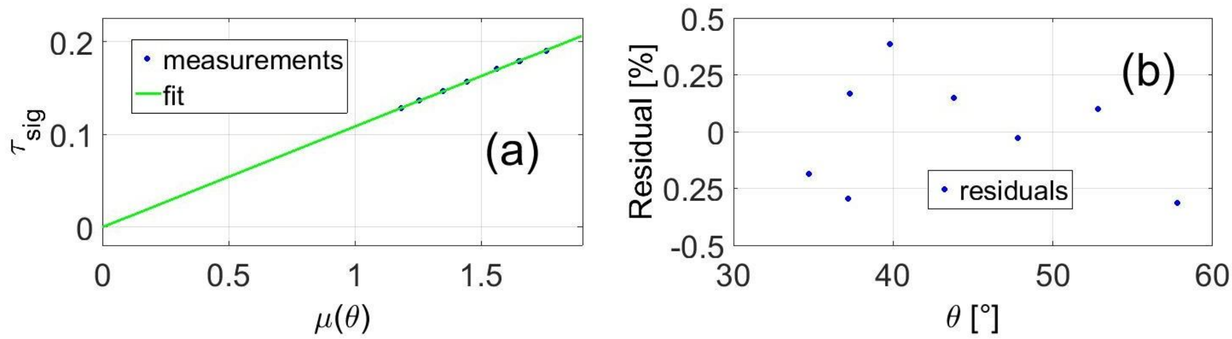

P 11 line 3: "T_atm is the average temperature obtained from radiosonde data by weighting the tropospheric temperature vertical profile with the water vapor concentration profile." Is this weighting done with the water vapor vmr or with vmr*p ?

Yes, the weighting is done with the water vapor vmr*p.

Several occasions: replace "depending from" with "depending on"

We modified the manuscript as suggested.

The abstract (p.1 line 3) mentions an integration time in the order of hours, but the paper discusses only the results of daily mean values.

We calrified this in the abstract, mentioning first the potential capabilities of the instrument (“The integration time for a measurement ranges from 6 to 24 hours, depending on season and weather conditions”), and then specifying twice that for this work we use only 24-hour averaged spectra (“The VESPA-22 water vapor mixing ratio vertical profiles discussed in this work are obtained from 24-hour averaged spectra and are compared with version 4.2 of concurrent Aura/Microwave Limb Sounder (MLS) water vapor vertical profiles”).

P. 2 line 17: The statement "Positive trends were observed during the last two decades" is followed by citations from 1999-2001. This sentence should be reworded or backed by more recent citations.

We modified the manuscript as suggested.

P. 3 line 10: instead of "full beam at half power" the term "full width at half maximum" (FWHM) would be more common and is also used in the cited Bertagnoli 2012 paper

We modified the manuscript as suggested.

P. 3 line 19: "Two noise diodes are inserted in the IF chain" should read "RF chain". Preferably "IF" and "RF" should be explained at first instance.

We modified the manuscript as suggested.

P. 4 line 19 mentions the brand name "eccofoam", but earlier the window was identified as LD-15 which is a different material.

We modified the manuscript as suggested.

P. 9 line 3: The statement "The ’zero’ signal is measured and subtracted to every acquired spectrum..." is misleading and could be understood that V0 is measured with every spectrum. Please clarify when and how often V0 is measured and whether it has a significant effect. Presumably it does not contribute at all to the result since the calibration with Eq. 13 and 16 uses always differences between two raw spectra.

The V_0 signal is measured every 15 minutes, at the beginning of each spectral integration which is the time resolution of the VESPA-22 spectral dataset. Although the measurement of V_0 is not required before the regular spectral measurement (as correctly argued by the reviewer), we do need to provide the FFTS with a “zero” signal at the input for its calibration, which VESPA performs every 15 minutes. We therefore measure and save such “zero” signal as a check on the performed FFTS calibration.

V_0 is also measured at the beginning of each tipping curve procedure (which is run every 30 minutes). Here we do not use S-R but S only and if we did not subtract the zero signal from S we could potentially introduce a small error in tipping curve measurements. However, V_0 is only about 0.5% of S and this error is possibly negligible.

We tried to clarify this aspect with the sentence “The “zero” signal, which amounts to approximately 0.5% of the incoming signal to the FFTS, is measured approximately every 15 minutes and it is subtracted to each S and R 15-minute integration spectra which are eventually saved on the control & acquisition PC (see figure 1b).” and by adding V_0 in the equation of Mu*Tau.

P. 9 line 5: "..and subtracts the counts number from these two sources" should probably read "...numbers...".

We modified the manuscript as suggested.

P. 13 line 16 states that the central 400MHz are used in the retrieval. Since the Fig 6a) shows only 40 MHz this is most likely a typo.

As mentioned above the frequency range showed in the figure is indeed 400MHz. This misunderstanding is caused by the factor 10^4 that was not clearly visible in the bottom right of the panel. We fixed this by using GHz instead of MHz.

P. 17 line 6+8: There seems to be a copy and paste error in the sentences "... integrated for second-degree polynomial 24 hours . . ." and "The cyan line is the retrieved by the inversion..."

We modified the manuscript as suggested.

P. 22 line 20 and following: These paragraphs repeat the principles of the Delrin balancing, Eq 42 is very similar to Eq.8. Also the details of the sheets and how their opacity is determined are presented. In my opinion this would fit better to section 4.1 where the instrument and calibration are discussed, than into this section 6 "retrieval uncertainty".

We modified the manuscript as suggested, removing equation 42 and moving the discussion on the measurement of the delrin sheets opacity to former Section 4.1, now Section 3.2.

P23 line 30: "...of the datasets obtained with the different models [. . .] respect to the reference model dataset..." Apparently a missing "with" in [. . .], otherwise the sentence does not make sense to me.

We modified this sentence in the revised manuscript and this comment no longer applies.

Fig. 10: The labels (c) and (d) are missing in the lower two subplots. Fig. 17: The labels (a) and (b) are missing in the two subplots.

These figures have been removed and this comment no longer applies.

LIST OF CHANGES

The manuscript has been modified in the text to follow all the suggestions from the two reviewers. This implied addition of text throughout the manuscript and, in some cases, minor changes to the figures. Rev 2 suggested we cut some of the discussion on the general principles of microwave remote sensing, radiative transfer, and retrieval algorithm, and this also contributed to a significant change in the text.

Specifically,

- a discussion on the use of the second order polynomial was added in Section 4, as suggested by both reviewers;
- the discussion on the Delrin opacity was moved from section 6 to section 3.2, as suggested by Rev 2;
- the number of sections was reduced and topics consolidated in fewer sections;
- 13 basic equations, and their relative discussions, were eliminated as requested by rev 2;
- former figures 3, 14 and 17, and their corresponding discussions, were removed;
- in all equations and related text we clarified where there are frequency dependent terms as opposed to constant terms or mean values.

Additionally,

- the uncertainty due to second order polynomial was added, and figure 11 was changed accordingly;
- the data analysis was changed with a new apriori profile which is held constant in time up to 48 km, following a suggestion of Rev 1 (see new Figure 6);
- the matrix Se calculation was improved as suggested by Rev 2 which led to the new spectral contribute to the uncertainty as shown in the new figure 11;
- the correlation with MLS smoothed instead of MLS convolved was inserted in Section 5, Figure 13c, following a comment from Rev 1;
- the time series of the sensitivity range (which changes with seasons) was presented instead of showing only the average of the sensitivity altitude interval over the entire period (see updated figure 15);
- the time series of two additional altitude levels (25 and 75 km) were added in former figure 15, now figure 14;
- more data were added to the analysis, extending the discussed period of VESPA-22 data from May to July 2017.

VESPA-22: a ground-based microwave spectrometer for long-term measurements of Polar stratospheric water vapor

Gabriele Mevi[1,2], Giovanni Muscari[1], Pietro Paolo Bertagnolio[1,~~4~~a], Irene Fiorucci[1,b], and Giandomenico Pace[3]

[1]Istituto Nazionale di Geofisica e Vulcanologia, Rome, 00143, Italy
~~[2]Roma Tre University, Mathematics~~[2]Mathematics and Physics Department, Roma Tre University, Rome, 00146, Italy
[3]ENEA, Laboratory for Observations and Analyses of Earth and Climate, ~~Santa Maria di Galeria~~Rome, 00123, Italy
~~[4]Now~~[a]Now at: AECOM, Croydon, CRO 2AP, United Kingdom
[b]Now at Istituto Paritario Vincenzo Pallotti, Rome, 00122, Italy

Correspondence to: Gabriele Mevi (gabriele.mevi@ingv.it)

Abstract. The new ground-based 22 GHz spectrometer, VESPA-22 (water Vapor Emission Spectrometer for Polar Atmosphere at 22 GHz) measures the 22.23 GHz water vapor emission line with a bandwith of 500 MHz and a frequency resolution of 31 kHz. The integration time for a measurement ~~is of the order of~~ranges from 6 to 24 hours, depending on season and weather conditions. Water vapor spectra are collected using the beam switching technique. VESPA-22 is designed to operate automatically with ~~minimum need of~~little maintenance; it employs an uncooled front-end characterized by a receiver temperature of about 180 K and its quasi-optical system presents a full width at half ~~power full beam angle~~maximum of 3.5°. Every 30 minutes VESPA-22 measures also the sky opacity~~ with a temporal resolution of two measurements an hour~~ using the tipping curve technique. The instrument calibration is performed automatically by a noise diode; the emission temperature of this element is ~~measured two times~~estimated twice an hour ~~through the observation of~~by observing alternatively a black body at ambient temperature and ~~of ~~the sky at ~~60° of~~an elevation~~.~~ of 60°. The retrieved profiles obtained inverting ~~a ~~24-hour integration spectra present a sensitivity ~~higher~~larger than 0.8 from about 25 to ~~72~~75 km of altitude during winter and from about 30 to 65 km during summer, a vertical resolution from about 12 to 23 km (depending on altitude~~)~~), and an overall 1σ uncertainty ~~between 5 and 12 %.~~lower than 7% up to 60 km altitude and rapidly increasing to 20% at 75 km.

In July 2016, VESPA-22 was installed at the ~~THAAO (~~Thule High Arctic Atmospheric Observatory~~)~~ located at Thule Air Base (76.5° N, 68.8° W), Greenland, and it has been operating almost continuously since then~~, with very few interruption periods characterized by poor weather.~~. The VESPA-22 water vapor mixing ratio vertical profiles discussed in this work ~~cover~~

~~the period~~are obtained from ~~July 2016 to May 2017~~24-hour averaged spectra and are compared with ~~Version~~version 4.2 of concurrent Aura/Microwave Limb Sounder (MLS ~~(Waters et al., 2006~~) water vapor vertical profiles. In the sensitivity range of VESPA-22 retrievals, the intercomparison from July 2016 to July 2017 between ~~the~~ VESPA-22 dataset and Aura/MLS dataset convolved with VESPA-22 averaging kernels ~~reveals a correlation coefficient of about 0.9 or higher and~~ shows an average difference ~~reaching its maximum of~~ within 1.4% up to 60 km altitude and increasing to about 6% ~~or~~ (0.2 ppmv) at ~~the top of the sensitivity range.~~72 km.

1 Introduction

The Polar atmosphere is a very complex system in which water vapor plays an important role. Water vapor has a major impact on the radiative balance affecting both infrared radiation by greenhouse effect and visible radiation by clouds coverage. The importance of water vapor in the Arctic region is enhanced by the so called Arctic ~~Amplification~~amplification effect (Serreze and Francis, 2006), a positive feedback that links the quantity of water vapor in the atmosphere, the presence of clouds, the ice coverage, and the surface temperature. Additionally, about 10% of the surface warming measured during the last two decades can be ascribed to stratospheric water vapor, as shown by Solomon et al. (2010).

The characterization of the water vapor profile, particularly in the ~~mesosphere and~~ stratosphere and mesosphere, is important to understand many chemical processes. Polar water vapor is directly involved in the ozone chemistry as the main source of the OH radical in reactions that cause the ozone destruction (Solomon, 1999). It is also related to the formation of polar stratospheric clouds (PSCs~~),~~) that grant the catalytic surfaces on which heterogeneous reactions take place.

The main sources of middle atmosphere water vapor are transport through the tropical tropopause and methane oxidation, whereas the main sink is photolysis in the Lyman-band. In the middle atmosphere, the lifetime of ~~this gas~~water vapor varies from several days to weeks~~. This long lifetime makes its~~, making it a valuable tracer for the investigation of dynamical processes that characterize the Polar regions~~,~~ especially during winter and ~~the Polar vortex in particular~~spring.

The processes that lead to long-term variations in stratospheric and mesospheric water vapor are not completely understood. Positive trends were observed during the ~~last two decades~~1980-2000 period (Nedoluha et al., 1999; Rosenlof et al., 2001) and Oltmans et al. (2000) suggested that only one half of these changes are related to anthropogenic activities.

The comprehension of the change in climate that affects the Arctic and the peculiar characteristics of this region’s atmosphere calls for long-term measurements. For this task, ground-based microwave remote sensing is a powerful tool to measure water vapor profiles and total amount of precipitable water vapor (PWV).

In this manuscript, VESPA-22 (water Vapor Emission Spectrometer for Polar Atmosphere at 22 GHz), a microwave spectrometer developed at the INGV (Istituto Nazionale di Geofisica e Vulcanologia) is presented. In July 2016, during the Study of the water VApor in the polar AtmosPhere (SVAAP) measurements campaign, a key part of a research effort devoted to the study of the impact of water vapor and clouds on the radiation budget at the ground, VESPA-22 was installed at the Thule High Arctic Atmospheric Observatory (THAAO) located at Thule Air Base (76.5° N, 68.8° W), Greenland. ~~Here the~~The instrument general features, the measurement physics and technique, ~~and~~ a comparison between VESPA-22 and the Aura/Microwave Limb Sounder (MLS) (Waters et al., 2006) version 4.2 datasets are ~~presented, with data ranging from July 2016 to May 2017. MLS is an instrument on board of NASA's Aura satellite. Due to its Sun-synchronous polar orbit the satellite overpasses Thule two times a day at fixed local times. For the comparison shown~~discussed in this ~~manuscript we used version 4.2 (v4.2) MLS data.~~work

2 Instrumental setup

VESPA-22 collects the microwave radiation emitted by the water vapor transition at 22.235 GHz with a spectral resolution of 31 kHz and a bandwidth of 500 MHz. From the spectral measurements water vapor profiles can be retrieved with a temporal resolution of ~~2~~1-4 profiles a day, depending ~~from~~ on season and weather conditions~~ and season~~. The instrument also measures the sky opacity ~~with a temporal resolution of~~ in few minutes by performing a scan of the sky at various angles called tipping curve.

~~In Figure 1~~In Figure 1, a photo and the layout of the spectrometer are displayed. VESPA-22 collects the sky signal coming from different elevation angles using a parabolic mirror. The signal is reflected by the mirror to a Gaussian choked horn antenna (Teniente et al., 2002). This antenna has a far field directivity of 23.5 dB with a pattern that can be approximated at 99.85% to a Gaussian beam with a beam waist of 22.4 mm (Bertagnolio et al., 2012). The quasi-optical system, antenna and parabolic mirror, has a full ~~beam~~width at half ~~power~~maximum (FWHM) $\theta_{3dB} = 3.5°$ (Bertagnolio et al., 2012). This high directivity of the system allows the observation at angles as low as 12° above the horizon, therefore maximizing the number of emitting molecules and the Signal-to-Noise ratio of the measurement. ~~The waveguide used by VESPA-22 polarizes the incoming radiation with a gain difference between the two polarization modes of 45 dB.~~

~~(a)~~ 

~~(b)~~

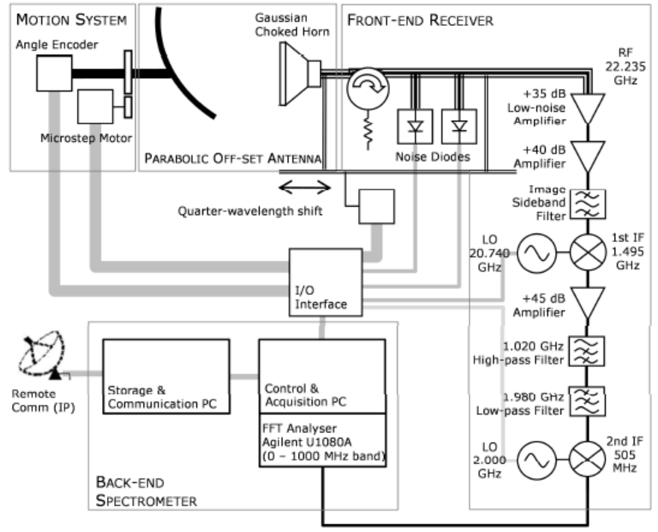
MOTION SYSTEM
Angle Encoder
Microstep Motor
Gaussian Choked Horn
PARABOLIC OFF-SET ANTENNA
FRONT-END RECEIVER
RF 22.235 GHz
+35 dB Low-noise Amplifier
Noise Diodes
+40 dB Amplifier
Image Sideband Filter
Quarter-wavelength shift
LO 20.740 GHz
1st IF 1.495 GHz
I/O Interface
+45 dB Amplifier
1.020 GHz High-pass Filter
1.980 GHz Low-pass Filter
Remote Comm (IP)
Storage & Communication PC
Control & Acquisition PC
FFT Analyser Agilent U1080A (0 – 1000 MHz band)
LO 2.000 GHz
2nd IF 505 MHz
BACK-END SPECTROMETER

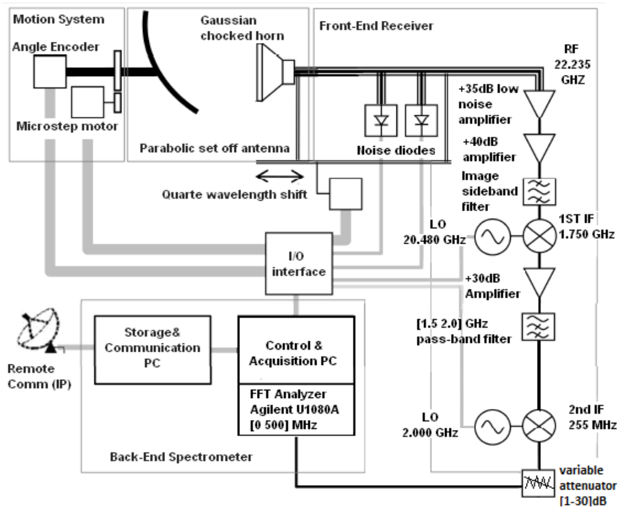

Figure 1: ~~(a), a picture~~**A photo of** ~~the instrument~~**VESPA-22 installed at the THAAO, Thule Air Base, Greenland** ~~where~~**(left), and the** ~~two eccofoam windows can be seen. (b), a scheme~~**layout of the instrument** ~~VESPA-22.~~**(right).**

A first uncooled low noise amplification stage amplifies the incoming signal with a gain of 35 dB. Two noise diodes manufactured by Noisecom are inserted in the ~~IF~~Radio Frequency (RF) chain after the choke antenna by means of two 20 dB broadwall direction couplers. These two diodes produce a signal which is measured to ~~be~~average at about 119 K and 78 K and are used to calibrate the sky signal observed by VESPA-22, as described in ~~the next section~~Section 3.3.

After the 20 dB couplers the signal is amplified and down-converted to lower frequencies and eventually sampled at ~~2Gs~~1 Gs/s by a Fast Fourier Transform Spectrometer (FFTS) Acquiris AC240/Agilent U1080A-001 with 16384 channels, resulting in a spectral resolution of 31 kHz for a total bandwidth of 500 MHz.

~~The receiver temperature T_{rec} of the instrument is measured using a LN$_2$ calibration scheme that is described in the next section and has a mean value of 181 K.~~

~~During the development of the instrument every effort was made~~During measurements, the antenna is moved back and forth to change its distance from the mirror by $\lambda/4 = 3.34$ mm in order to avoid multiple internal reflections of the signal which would cause the formation of standing waves affecting the observed spectrum. ~~For this reason, during measurements, the antenna is moved back and forth to change its distance from the mirror by $\lambda/4 = 3.34\ mm$.~~ One full spectrum is obtained by averaging together two 6-minute spectra collected with the antenna positioned at these two different distances from the mirror. ~~The destructive interference minimizes the standing waves caused by multiple~~

~~reflections internal to the system. Two~~Once a day, two photodiodes are employed to check and reset~~ daily~~ the correct distance between the antenna and the mirror.

VESPA-22 is installed indoor to preserve it from the strong winds and storms which can occur during most of the ~~Polar winter season.~~year. The indoor installation prevents the deposition on the quasi-optical system of snow ~~or~~in winter and dust in summer, as well as the condensation of water droplets~~, on the quasi-optical system~~, therefore improving the durability of the equipment. Additionally, the parabolic mirror and its driving motor are not exposed to strong winds, and VESPA-22 is therefore characterized by a pointing offset very stable with time. The instrument is located in a small wooden annex (Figure 2) to the main observatory in order to minimize the presence of metal surfaces which could also yield standing waves in the observed spectrum.

The spectrometer observes the sky through two 5~~-~~ cm thick Plastazote LD15 windows, one covering the observation at angles from 10° to 60° above the horizon, and a smaller one covering the zenith direction (~~showed in Figure 1 and Figure 2).~~see Figures 1 and 2). This material was tested in the laboratory and proved to have a negligible absorption in the microwave region of interest. ~~The~~ Furthermore, the windows are ~~however~~ not perpendicular ~~with respect~~ to the antenna beam in order to minimize ~~the~~any potential formation of standing waves. The ~~eccofoam~~ opacity of the LD15 window sheets was estimated during VESPA-22 installation and it was measured to be less than 0.0005 Nepers. ~~Two~~Three powerful fans are ~~utilized~~employed to blow off the snow from the observing windows, preventing deposition or ice formation on the external side of the windows. ~~The instrument is located in a small wooden annex (Figure 2)~~VESPA-22 compares the sky emission

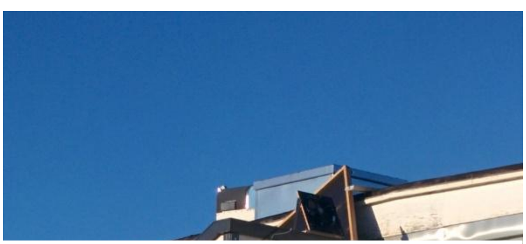

~~**Figure 2: a photo of the exterior of the wooden annex hosting VESPA-22. The observing window of the signal beam is visible on the side of the annex.**~~

from the zenith direction (also called reference direction) to the ~~main observatory~~sky emission from an angle close to the horizon (also called signal direction) in order to perform a stratospheric measurement, as it will be explained in the Section 3.2. The zenith is observed through a white Delrin® acetal homopolymer resin sheet, hereafter simply delrin, (see Figure 1a) which adds a grey body emission to the reference beam; this sheet is set at the Brewster's angle with respect to the incident beam in order to minimize reflections and the ~~presence~~formation of ~~metal surfaces which could produce~~ standing waves.

~~VESPA-22 compares the sky emission from the zenith direction (also called reference beam) to the sky emission from an angle close to the horizon (also called signal beam) in order to perform a stratospheric measurement, as it will be explained in the section 4.1. The zenith is observed through a Delrin® acetal homopolymer resin sheet, hereafter simply delrin, (see Figure 1 a) that adds a grey body emission to the zenith emission; this element forms an angle with the incident beam equal to the Brewster's angle, in order to minimize the reflection and the formation of standing waves.~~

During an hour of standard instrument operations, about 3 minutes are dedicated to tipping curves (~~section~~ see Section 3.4~~.3~~) used to measure tropospheric opacity, about 35 minutes are dedicated to measure the ~~observation of~~emissions from the signal and reference beams, ~~while~~and the rest of the ~~time~~hour is dedicated to instrumental operations, such as the rotation of the parabolic mirror or the instrument calibration by means of the noise diodes.

Figure 2: A photo of the exterior of the wooden annex hosting VESPA-22. The observing window of the signal beam is visible on the side of the annex.

3 Measurement ~~physics~~technique

VESPA-22 collects the 22.235 GHz radiation emitted by water vapor molecules. At this frequency, the Rayleigh Jeans approximation for the Plank's Law can be used and the radiation intensity can be expressed in terms of brightness ~~Temperature T_ν. This quantity is a function of the frequency ν. The radiation intensity collected at the ground can be described using the radiative transfer equation for the elevation angle θ~~temperature. The line shape of the emission from a stratospheric altitude z is mainly a function of atmospheric pressure:

$$\cancel{T_\nu(z_0) = T_0 e^{-\mu(\theta)\tau_\nu(z_{toa})} + \mu(\theta)\int_{z_0}^{z_{toa}} T(z)\alpha_\nu(z) e^{-\tau_\nu(z)\mu(\theta)} dz} \quad , \Delta\nu \propto P(z)\left(\frac{T_0}{T(z)}\right)^n \tag{1}$$

,

where ~~$T_\nu(z_0)$~~$\Delta\nu$ is the ~~radiation measured by the instrument located at an altitude z_0, T_0 is the incoming radiation at the top of the atmosphere z_{toa}, $\alpha_\nu(z)$ is the absorption coefficient, $T(z)$ is the physical temperature at altitude z, $\tau_\nu(z)$ is the opacity defined as~~

$$\tau_\nu(z) = \int_{z_0}^{z} \alpha_\nu(s)\,ds\ , \qquad (2)$$

~~and $\mu(\theta)$ is the air mass factor at the elevation angle θ, computed according to de Zafra (1995).~~

$$\mu(\theta) = \frac{R + z_{trop}}{\sqrt{\left(R + z_{trop}\right)^2 - \left(\left(R + z_{obs}\right)\cos(\theta)\right)^2}}\ . \qquad (3)$$

~~In the latter expression, R is the Earth's radius, $z_{trop} = 3\ km$ is the~~ line width ~~of the tropospheric layer in which most of the atmospheric water vapor is present, and z_{obs} is the altitude of the instrument (0.2 km).~~

~~In the stratosphere, the line shape of the emission from an altitude z is mainly a function of atmospheric pressure~~

$$\Delta\nu \propto P(z)\left(\frac{T_0}{T(z)}\right)^x , \qquad (4)$$

~~where Δν is the line width, x~~, $n < 1$ is a constant coefficient and $T_0 = 300\ K$~~.~~ (see Table 3, Section 4.1, for the spectroscopic values used for VESPA-22 retrievals). Using this dependence and knowing the pressure and temperature atmospheric profiles, the measured spectrum can be inverted using the reverse problem theory to obtain the vertical water vapor mixing ratio profile.

In the mesosphere, the Doppler broadening overcomes the pressure broadening of Eq. (1) determining an upper limit to the altitude range in which the water vapor profile can be retrieved. In the lower stratosphere, the broadening makes the line width comparable to ~~VEPSA~~the VESPA-22 spectral ~~bandwidth~~bandpass, therefore setting a lower altitude limit for the deconvolved profile.

~~4 Measurement technique~~

3.1 Atmospheric opacity

The ~~major part~~majority of the incoming radiation measured by VESPA-22 comes from the troposphere. The tropospheric emission needs to be filtered in order to ~~evidence~~study the stratospheric signal.

In order to simplify ~~Eq. (1),~~the radiative transfer equation, the following approximations can be adopted (e.g., Nedoluha et al., 1995).

- The troposphere is represented as an isothermal layer absorbing the signal to be measured. The first kilometers of the atmosphere produce the greatest part of this layer emission which has a line width larger than VESPA-22 bandwidth. This contribution is treated as an emission constant in frequency.
- The contribution of the stratospheric water vapor absorption to the opacity τ is ~~negligible~~small. This approximation was tested by calculating the atmospheric opacity by means of the radiative transfer simulation software ARTS (Eriksson et al., 2011) and using water vapor vertical profiles with and without their stratospheric component. At the frequency of maximum absorption, the contribution of the stratospheric profile to the overall atmospheric opacity ~~in the 22 GHz region~~ is between 2% and 5% depending ~~from~~on the season. When averaged over the VESPA-22 frequency range, the difference between the opacity calculated using a ~~normal vertical~~ full water vapor vertical profile and a profile with no water vapor above the tropopause is between 0.4% and 1.5~~% depending from the season. In Figure 3, the opacity calculated by ARTS using complete water vapor profiles from the ground to 110 km altitude and the opacity calculated with the same profiles but no water vapor above the tropopause are compared. The profile used were measured by MLS/Aura above Thule on different seasons.~~%.
- The opacity τ_ν can be substituted by its mean value τ. The maximum difference between τ_ν and its mean value τ is between 1.6% and 3.6~~-~~% depending ~~from the~~on season.
- The only signal coming from outside the atmosphere, T_0, is the cosmic background radiation with a constant brightness temperature of 2.73 K.

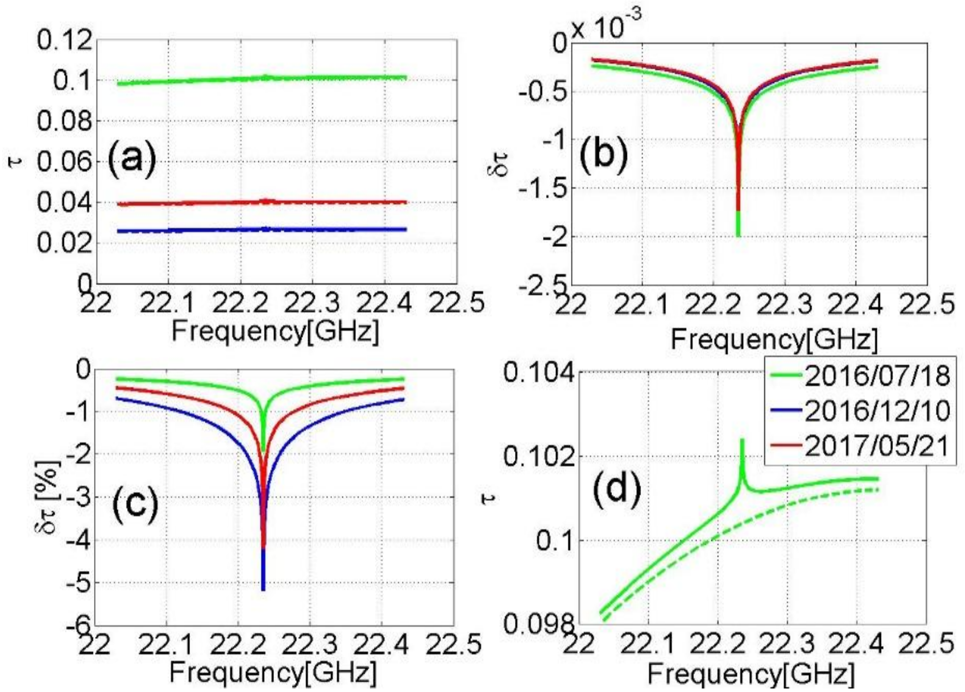

~~**Figure 3: (a) atmospheric opacity calculated by ARTS for complete water vapor profiles measured by AURA/MLS above Thule region on different seasons (solid lines) and for the same profiles with no water vapor above 10 km (dashed lines); (b) and (c) absolute and relative difference between the tropospheric and total opacity; (d) particular of the opacity of the 2016/07/18 profile.**~~

With these approximations ~~Eq. (1)~~the radiative transfer equation describing the radiation received at the ground from an elevation angle θ can be written as:

$$\cancel{T_S = T_0 e^{-\mu\tau} + T_{atm}\left(1-e^{-\mu\tau}\right) + \mu T(\nu) e^{-\mu\tau}\ .} \qquad \cancel{(5)}$$

$$T_S(\nu) = T_0 e^{-\mu\tau} + T_{trop}(1 - e^{-\mu\tau}) + \mu T(\nu) e^{-\mu\tau}. \qquad (2)$$

The left term is the radiation received by the spectrometer ~~from~~ when pointing at the elevation angle θ~~, the~~. The first term ~~in~~on the right side is the extra-atmospheric emission~~. The~~, the second term ~~in right side~~ is the solution of the radiative transfer equation for an isothermal domain ~~and it represents~~where the tropospheric emission is indicated with ~~T_{atm} as~~T_{trop} and represents the mean ~~troposphere~~tropospheric temperature weighted with the water vapor concentration. The third term on the right is the emission coming from the stratosphere and mesosphere, $T(\nu)$, proportional to the air mass factor μ and attenuated ~~by~~in the troposphere~~. In all the previous terms~~ by a factor $e^{-\mu\tau}$ ~~is the tropospheric signal absorption.~~. The ~~third term on the right side approximates the integral term of Eq. (1),~~air mass factor at the elevation angle θ is computed according to ~~Eq. (6) and (7)~~ the formula presented in the work of de Zafra (1995).

$$\mu\int_{z_0}^{z_{toa}} T_\nu(z)\, e^{-\tau_\nu(z)\mu(\theta)}dz \sim \mu e^{-\tau\mu}\int T_\nu(z)\,dz \quad \text{and} \tag{6}$$

$$T(\nu)=\int T_\nu(z)\,dz\ , \tag{7}$$

~~where it was used the relation between physical and brightness temperature in the Rayleigh Jeans approximation $T_\nu=\alpha_\nu T$. $T(\nu)$ is the stratospheric signal that has to be inverted in order to retrieve the water vapor stratospheric profile.~~

~~4.1 The balancing beams~~3.2 Beam switching technique

The technique that VESPA-22 employs to measure the stratospheric signal is called ~~balancing~~ beam switching technique or Dicke switching technique (e.g., Parrish et al., 1988). The instrument compares the emission coming from an observation angle θ (signal beam) with a reference signal with the same mean power over the passband. The observation angle depends ~~from~~on the atmospheric opacity and for VESPA-22~~;~~ it varies from 12° to 25° above the horizon. The reference signal used by VESPA-22 ~~-~~is the sky emission at the zenith (reference beam). In clear sky conditions, the emission at the zenith is smaller than the emission at a much larger zenith angle. Therefore, in order to ensure that the reference beam has the same mean power of the signal beam, a thin sheet of delrin is inserted in the reference beam. The delrin sheet acts as a grey body so that:

$$T_R = T_0 e^{-\tau-\tau_d} + T_{atm}\left(1-e^{-\tau}\right)e^{-\tau_d} + T(\nu)e^{-\tau-\tau_d} + T_d\left(1-e^{-\tau_d}\right)\ , \tag{8}$$

$$T_R(\nu) = T_0 e^{-\tau-\tau_d} + T_{trop}(1-e^{-\tau})e^{-\tau_d} + T(\nu)e^{-\tau-\tau_d} + T_d(1-e^{-\tau_d})\ , \tag{3}$$

where T_R is the radiation observed by VESPA-22 coming from the zenith, partially absorbed ~~and reemitted~~ by the delrin sheet, T_d is the physical temperature of the sheet and τ_d its mean opacity value over the spectral passband. In this equation, the air mass factor μ is equal to 1.

During data taking operations, VESPA-22 alternates ~~zenith~~reference and signal ~~angle~~ observations. The instrument constantly checks if the two beams have the same mean power and continuously changes the signal angle to minimize the difference between them. When the two beams have the same intensity, the frequency independent terms of Eq. ~~(8) and Eq.~~ (3) and Eq. (2) can be equated obtaining:

$$T_0 e^{-\tau-\tau_d} + T_{atm}\left(1-e^{-\tau}\right)e^{-\tau_d} + T_d\left(1-e^{-\tau_d}\right) \approx T_0 e^{-\mu\tau} + T_{atm}\left(1-e^{-\mu\tau}\right)\ , \tag{9}$$

$$T_0 e^{-\tau-\tau_d} + T_{trop}(1-e^{-\tau})e^{-\tau_d} + T_d(1-e^{-\tau_d}) \approx T_0 e^{-\mu\tau} + T_{trop}(1-e^{-\mu\tau})\ , \tag{4}$$

where the stratospheric contribution to the mean beam intensity (about 1%) is neglected (de Zafra, 1995).

The stratospheric signal $T(\nu)$ is obtained by subtracting ~~the signal and the~~ reference ~~beams~~from signal. Using Eq. ~~(5)~~(2), ~~(8)~~(3) and (4) it is possible to write:

$$\cancel{T_S - T_R \approx T(\nu)\left(\mu e^{-\mu\tau} - e^{-\tau-\tau_d}\right)} \text{ ~~and~~} \quad \cancel{(10)}$$

$$\cancel{T(\nu) = \frac{T_S - T_R}{\mu e^{-\mu\tau} - e^{-\tau-\tau_d}}} . \quad \cancel{(11)}$$

$$T_S(\nu) - T_R(\nu) \approx T(\nu)(\mu e^{-\mu\tau} - e^{-\tau-\tau_d}) \text{ and} \quad (5)$$

$$T(\nu) = \frac{T_S(\nu) - T_R(\nu)}{\mu e^{-\mu\tau} - e^{-\tau-\tau_d}} . \quad (6)$$

Three delrin sheets with different ~~thickness~~thicknesses (3, 5, and 9 mm) and ~~opacity~~opacities can be employed, depending ~~from~~on the season, in order to maintain the ~~observation~~signal angle between 12° and 25° above the horizon. Spectra collected are smoothed using a 50-channel moving average. This smoothing process is not performed in a 6 MHz interval centered around the emission line to maintain the maximum frequency resolution near the line peak.

In order to estimate τ_d, the mean opacity value of delrin over the spectral passband, during normal data taking operations the signal angle is locked to its balanced position and the delrin sheet is removed from the reference beam. τ_d can then be calculated using:

$$\tau_d = -ln\left(\frac{T_d - \bar{T}_S}{T_d - \bar{T}_{R\_nod}}\right), \quad (7)$$

where $\bar{T}_{R\_nod}$ is the mean intensity of the reference beam without the sheet and $\bar{T}_S$ is the mean value of the signal beam. The brightness temperatures $\bar{T}_S$ and $\bar{T}_{R\_nod}$ are calculated using parameters obtained by means of a calibration performed using liquid nitrogen (LN_2, see Section 3.3) which is always carried out before estimating τ_d. In order to run these operations, qualified personnel must be at the observatory and therefore τ_d was measured only in July and November, 2016, and February 2017 (Table 1). A total of seven measurements of the compensating sheet opacity were performed, two in July, three in November, and two in February 2017. Half of the difference between the minimum and maximum τ_d values obtained during the same period is used as measurement uncertainty. The mean value of the delrin opacity changes with time, possibly due to a certain level of degassing, i.e., the property of absorbing/releasing water vapor molecules from/to the environment, which depends on atmospheric humidity and it is often noticed in plastic materials. During winter, as the air is drier, the compensating sheets appear to release some water vapor and lower their opacities. VESPA-22 spectral data are calibrated using a linear interpolation between the τ_d values measured over time.

Table 1: Mean values and standard deviations of the measured opacity for the two used delrin sheets during different seasons.

Thickness	July 2016	November 2016	February 2017

9 mm	0.159 ± 0.004	0.128 ± 0.003	0.123 ± 0.003
5 mm	0.088 ± 0.001	0.072 ± 0.001	0.070 ± 0.001

~~4.2~~3.3 Calibration ~~method~~scheme

The broad-band response of VESPA-22 to the signal coming from the sky can be written as:

~~The broad-band response of VESPA-22 to the signal coming from the sky can be written as:~~

$$\cancel{V = \alpha\left(T + T_{rec}\right) + V_0} \qquad \cancel{(12)}$$

$$V(\nu) = \alpha(\nu)\big(T(\nu) + T_{rec}(\nu)\big) + V_0(\nu). \qquad (8)$$

In this equation, V is the incoming signal in counts ~~number~~numbers of the FFT back-end spectrometer, T is the signal brightness temperature, α the gain of the instrument, T_{rec} the receiver noise temperature and V_0 the “zero” signal of the FFTS. All the quantities represented in Eq. ~~(12)~~(8) are frequency dependent. The “zero” signal, which amounts to approximately 0.5% of the incoming signal to the FFTS, is measured approximately every 15 minutes and it is subtracted to ~~every acquired spectrum so it is not explicitly written in what follows in order to simplify the notation.~~

~~VESPA-22 collects the sky radiation from signal~~ each Signal and ~~reference beams and subtracts~~Reference 15-minute integration spectra which are eventually saved on the ~~counts number from these two sources.~~control & acquisition PC (see Figure 1b). Using Eq. ~~(12), Eq.~~(8), Eq. (6) can be written as:

$$\cancel{T(\nu) = \frac{1}{\alpha}\frac{V_S - V_R}{\mu e^{-\mu\tau} - e^{-\tau-\tau_d}}} \qquad \cancel{(13)}$$

$$T(\nu) = \frac{1}{\alpha(\nu)}\frac{V_S(\nu) - V_R(\nu)}{\mu e^{-\mu\tau} - e^{-\tau-\tau_d}}. \qquad (9)$$

VESPA-22 measures the gain parameter α ~~using a noise diode manufactured by Noisecom, an element producing a stable signal and inserted between the choked horn antenna and the first stage low noise amplifier~~ by means of ~~a 20 dB broadwall coupler (see Figure 1 b).~~the noise diode. As mentioned before, VESPA-22 has two different noise diodes, one used to perform regular calibrations and the second inserted to ensure the stability over time of the first one, as described by Gomez et al. (2012).

During regular measurements, the calibration noise diode is switched on and its emission is added to the reference signal. The noise diode is then switched off and VESPA-22 measures only the radiation coming from the zenith. ~~Therefore, the received radiation is~~The gain parameter can be obtained by subtracting these two measurements according to:

$$\cancel{V_{R+ND} = \alpha\left(T_R + T_{ND} + T_{rec}\right) \text{ and}} \qquad \cancel{(14)}$$

$$\cancel{V_R = \alpha\left(T_R + T_{rec}\right).} \qquad \cancel{(15)}$$

$$\cancel{V_{R+ND}}\,\alpha(\nu) = \frac{V_{R+nd}(\nu) - V_R(\nu)}{T_{nd}(\nu)}, \qquad (10)$$

where V_{R+nd} and V_R are the signals expressed in counts ~~number~~numbers measured with the noise diode turned on and off, respectively, and $\cancel{T_{ND}}T_{nd}$ is the noise diode emission temperature~~. The gain parameter can be obtained by subtracting these two measurements~~

$$\cancel{\alpha = \frac{V_{R+ND} - V_R}{T_{ND}},} \qquad \cancel{(16)}$$

~~where T_{ND} can be~~ at the various frequencies, estimated ~~by performing~~during a calibration procedure. The calibration consists in measuring the ~~emissions~~emission from two sources at two different known emission temperatures. The first source is a black body at ambient temperature made with an eccosorb CV-3 panel by Emerson and Cuming; the second source is, most of the times, the sky at an angle of 60° above the horizon. ~~In the calibration procedure~~Every 3 or 4 months, approximately, the sky emission can be replaced by a second ~~eccosorb~~ CV-3 panel immersed in ~~liquid nitrogen (~~LN_2~~)~~. The use of ~~liquid nitrogen~~LN_2 likely grants more accurate results, as the physical temperature of the emitting body has a smaller uncertainty with respect to the estimated sky temperature at 60°, but the LN_2 calibration cannot be performed automatically by the instrument and it was carried out so far ~~has been performed~~ in July and November, 2016, and in February, 2017.

The general calibration equations are described in what follows, whereas the tipping curve procedure that allows the use of the sky as calibration source is explained in ~~the next section.~~Section 3.4. Knowing the emission temperature of two sources α, T_{rec}, and T_{nd} can be obtained by using the following equations:

~~Knowing the emission temperature of two sources α, T_{rec} and T_{ND} can be obtained with:~~

$$\cancel{\alpha = \frac{V_{hot} - V_{cold}}{T_{hot} - T_{cold}},} \qquad \cancel{(17)}$$

$$\cancel{T_{rec} = \frac{T_{hot}V_{cold} - T_{cold}V_{hot}}{V_{hot} - V_{cold}}, \text{ and}} \qquad \cancel{(18)}$$

$$\cancel{T_{ND} = \frac{V_{cold+ND} - V_{cold}}{\alpha}}\,\alpha(\nu) = \frac{V_{hot}(\nu) - V_{cold}(\nu)}{T_{hot} - T_{cold}}, \qquad (11)$$

$$T_{rec}(\nu) = \frac{T_{hot}\left(V_{cold}(\nu) - V_0(\nu)\right) - T_{cold}\left(V_{hot}(\nu) - V_0(\nu)\right)}{V_{hot}(\nu) - V_{cold}(\nu)}, \text{ and} \qquad (12)$$

$$T_{nd}(\nu) = \frac{V_{cold+nd}(\nu) - V_{cold}(\nu)}{\alpha(\nu)}. \qquad (13)$$

$$\cancel{.} \qquad \cancel{(19)}$$

T_{hot} and T_{cold}, and V_{hot} and V_{cold} are the emission temperatures and the recorded counts ~~number~~numbers of the two sources, respectively. For the black body, the emission temperature is assumed to be equal to its physical temperature. ~~T_{ND} and all the quantities used in Eq. (17), (18), and (19) are spectral quantities. The noise diode produces a signal that can be considered constant in frequency within 1.5%.~~The noise diode produces a signal that is measured to be quite stable in frequency. In fact, single-channel T_{nd} values are always within 1.5% of the spectral mean of the diode temperature brightness $\overline{T}_{nd}$. The spectra originated from black body measurements (especially those from the CV-3 immersed in LN_2) can be affected by standing waves and in order to avoid to transfer them in the calibrated sky spectral measurements, T_{nd} is averaged over the central 11000 channels of the ~~FFT spectrometer~~FFTs, as suggested by Gomez et al. (2012). Therefore it can be written:

$$\cancel{T_{ND} = \left(T_{hot} - T_{cold}\right) \sum_{i=3000}^{14000} \frac{V_{cold+ND}(i) - V_{cold}(i)}{V_{hot}(i) - V_{cold}(i)}}\text{, ~~where~~} \qquad \cancel{(20)}$$

$$\cancel{V_{cold+ND}(i)}\overline{T}_{nd} = \left(T_{hot} - T_{cold}\right) \sum_i \frac{V_{cold+nd}(\nu_i) - V_{cold}(\nu_i)}{V_{hot}(\nu_i) - V_{cold}(\nu_i)}, \qquad (14)$$

where

$V_{cold+nd}(\nu_i)$ is the value of channel i with the noise diode turned on, while $V_{cold}\cancel{(i)}(\nu_i)$ is the value of the same channel with the the noise diode turned off.

3.4~~.3~~ Tipping curve ~~calibration~~procedure

In this section, the tipping curve calibration technique employed to calibrate the noise diodes using the sky signal is described. The tipping curve procedure is performed twice every hour as it is also used to measure the atmospheric opacity ~~of~~needed in Eq. ~~(13).~~(9). During a tipping curve, VESPA-22 collects the radiation coming from different elevation angles, approximately every 5° from 35° to 60° above the horizon. The measured spectra are averaged using the 11000 central channels of the spectrometer. Radiation from the stratosphere contributes less than 1% and can be neglected, so the signal intensity can ~~describe~~be described by means of the following equation:

$$\overline{T}(\theta_i) \cong T_0 e^{-\mu(\theta_i)\tau} + T_{trop}\left(1 - e^{-\mu(\theta_i)\tau}\right). \qquad (15)$$

$$\cancel{\overline{T}\left(\theta_i\right) \cong T_0 e^{-\mu(\theta_i)\tau} + T_{atm}\left(1 - e^{-\mu(\theta_i)\tau}\right)}. \qquad \cancel{(21)}$$

The atmospheric temperature $\cancel{T_{atm}}T_{trop}$ can be estimated from the surface temperature $T_{\cancel{sup}surf}$:

$$\cancel{T_{atm} = T_{sup} - d} \qquad \cancel{(22)}$$

$$T_{trop} = T_{surf} - d, \tag{16}$$

where the value of d can be affected by seasonal variations. In order to characterize this parameter several radiosoundings were launched during July, November, and December, 2016, and February, 2017. The value of the parameter d as a function of time is obtained from a linear interpolation between the mean values of $\cancel{T_{sup} - T_{atm}}T_{surf} - T_{trop}$ measured during these four periods, as described in ~~Table 1.~~Table 2. $\cancel{T_{atm}}T_{trop}$ is the average temperature obtained from radiosonde data by weighting the tropospheric temperature vertical profile with the -water vapor concentration profile.

Table 2~~: mean~~. Mean values and standard ~~deviation~~deviations of $\cancel{T_{sup}}T_{surf} - \cancel{T_{atm}}T_{trop}$ obtained from the radiosoundings

Month	Mean ($\cancel{T_{sup}}T_{surf} - \cancel{T_{atm}}T_{trop}$)
July	14.4±2.8 K
November	8.3±3.6 K
December	9.4 ±3.8 K
February	9.4±2.1 K

Using Eq. ~~(21)~~(15), it is possible to ~~explicit~~explicitly give the relation between the opacity and the mean brightness temperature of the received signal:

$$\cancel{\mu(\theta_i)\tau = \ln\left(\frac{T_0 - T_{atm}}{\bar{T}(\theta_i) - T_{atm}}\right).} \qquad \cancel{(23)}$$

$$\mu(\theta_i)\tau = ln\left(\frac{T_0 - T_{trop}}{\bar{T}(\theta_i) - T_{trop}}\right). \tag{17}$$

A linear regression ~~between~~of the opacities $ln\left(\frac{T_0 - T_{trop}}{\bar{T}(\theta_i) - T_{trop}}\right)$ observed at $\theta_i$$\cancel{, ln\left(\frac{T_0 - T_{atm}}{\bar{T}(\theta_i) - T_{atm}}\right),}$ and the air mass factors $\mu(\theta_i)$ allows us to retrieve the opacity at the zenith, τ (~~de Zafra,~~Nedoluha et al. 1995). Substituting for $\bar{T}(\theta_i)$ using Eq. ~~(12),~~ (8) and approximating all the spectral quantities with their mean values (indicated by a bar) over the central 11000 channels, Eq. ~~(23)~~ (17) can be written as:

$$\cancel{\mu(\theta_i)\tau = \ln\left(\frac{T_0 - T_{atm}}{\frac{\bar{V}(\theta_i)}{\alpha} - T_{rec} - T_{atm}}\right)} \qquad \cancel{(24)}$$

$$\mu(\theta_i)\tau = ln\left(\frac{T_0 - T_{trop}}{\frac{(\bar{V}(\theta_i)-\bar{V}_0)}{\bar{\alpha}} - \bar{T}_{rec} - T_{trop}}\right), \qquad (18)$$

where it appears that ~~T_{rec}~~the mean values $\bar{T}_{rec}$ and ~~α~~$\bar{\alpha}$ are needed to perform the calculation. ~~In order to obtain an estimate of these two parameters, during the tipping curve procedure VESPA-22 measures also the~~

The emission from ~~a CV-3 eccofoam sheet, considered as a black body at ambient temperature (hot load). The sky signal at an elevation angle of 60° (T_{cold}^{sky}) acts as second~~ two calibration ~~source (cold load). The emission from these two~~ sources at different temperatures is used to calculate ~~α~~$\bar{\alpha}$ and ~~T_{rec}~~$\bar{T}_{rec}$ according to Eq. ~~(17)~~(11) and Eq. ~~(18).~~(12). However, since the sky emission temperature T_{cold}^{sky} is not known, ~~VESPA-22 uses~~ an iterative procedure is used to obtain both τ and T_{cold}^{sky}. An initial opacity value, τ_0, is ~~used~~adopted as first guess to obtain $T_{cold,0}^{sky}$ using ~~Eq. (21) with θ = 60°.~~Equation 21 with $\theta = 60°$. $T_{cold,0}^{sky}$ is then used to obtain α_0 and T_{rec_0} ~~from~~ by means of Eq. (11) and Eq. ~~(17) and Eq. (18); $\mu(\theta_i)$~~(12); $\mu(\theta_i)\tau$ is calculated for different elevation angles using Eq. ~~(24)~~(18), and ultimately a linear fit ~~allow~~allows us to calculate a new estimate for τ, τ_1. The iterative procedure goes on until the intercept value is minimized. Figure 3 shows the results of a tipping curve measurement carried out on 10 Dec, 2016.

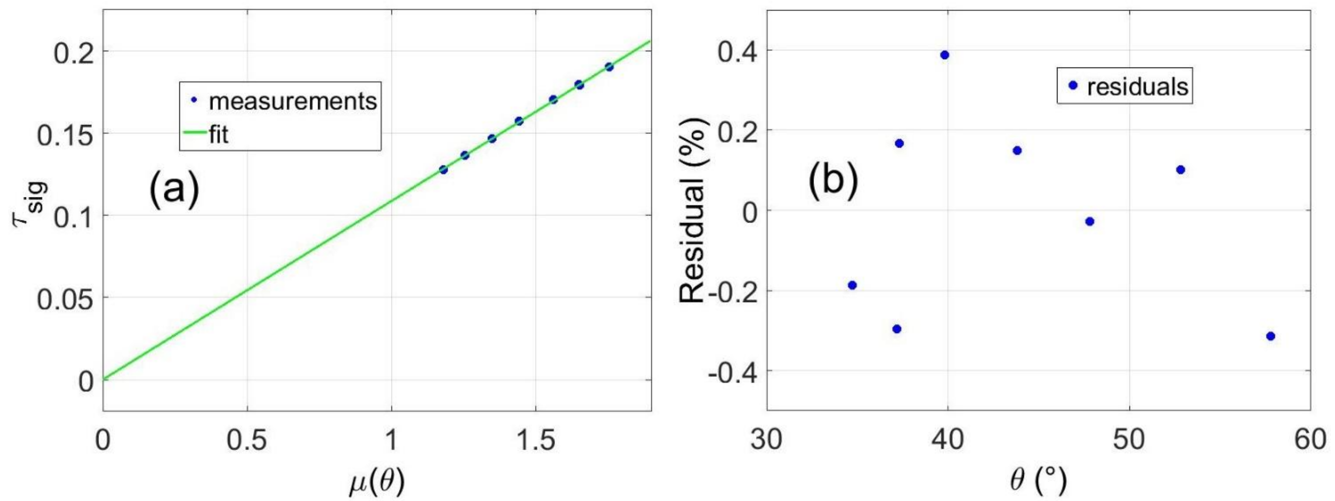

Figure 3: (a) The values of $ln\left(\frac{T_0-T_{trop}}{\bar{T}(\theta_i)-T_{trop}}\right)$ (indicated with τ_{sig} on the y-axis of panel a) as function of the air mass factor $\mu(\theta_i)$ (blue points) measured during a tipping curve on 10 Dec, 2016, and the fit result (green line). (b) The residuals (measurements minus fit) as a function of the elevation angle.

The value of T_{cold}^{sky} measured with this procedure is used in Eq. ~~(17) and Eq. (19) to estimate T_{nd}.~~(11) and Eq. (13) to estimate $\bar{T}_{nd}$. In order to avoid the use of data ~~measured~~acquired during inhomogeneous~~-~~ sky ~~condition~~conditions, all measurements producing linear fits (see Figure 3a) with a root mean square ~~higher~~larger than 0.~~8~~4 are discarded. ~~Figure 4~~Figure 4 shows the time series of both noise diodes mean emission temperatures (blue and cyan) from July 2016 to ~~May~~July 2017. The noise diode in blue is the one used as calibration diode. In the same plot, $\cancel{T_{nd}}\overline{T}_{nd}$ values obtained using a LN_2 cooled ~~eccofoam~~ CV-3 as the cold ~~source~~load are also depicted (orange and red stars). The mean relative difference between $\cancel{T_{nd}}\overline{T}_{nd}$ values calculated with ~~the two calibration schemes (tipping curve and~~ LN_2~~)~~ and with tipping curves carried out immediately before or after LN_2 calibrations is (0.4±0.4)% and (0.2±0.3)% for the calibration and the backup diodes, respectively.

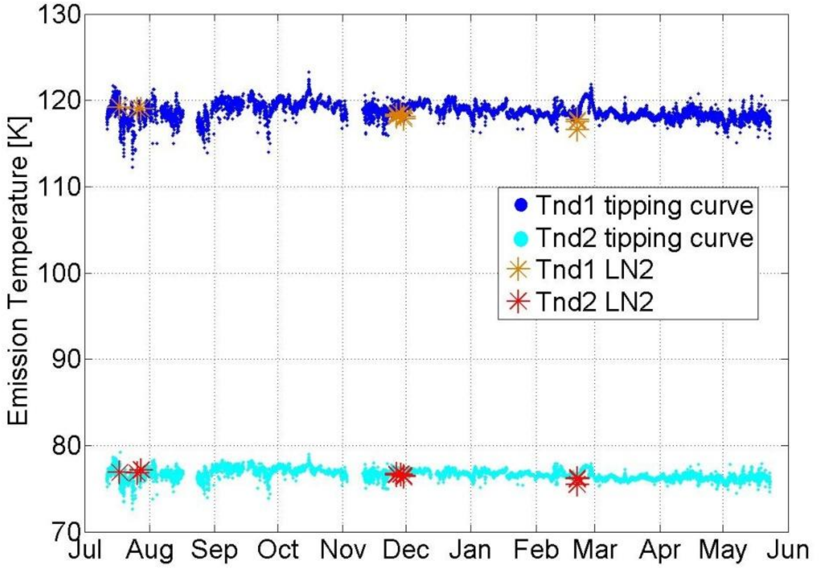

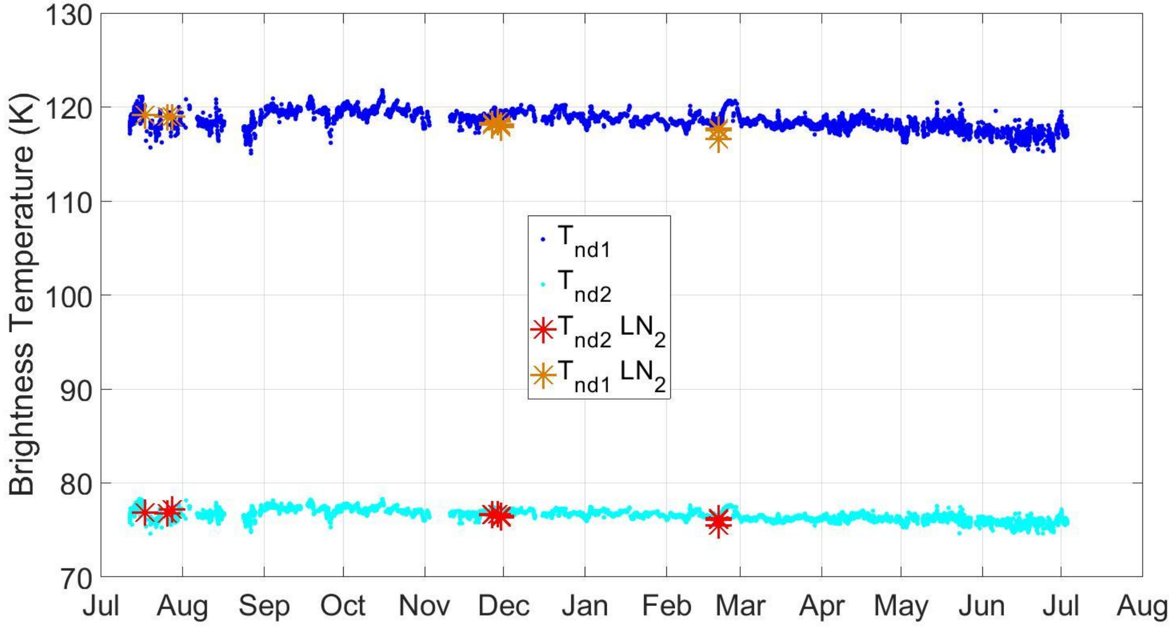

Figure ~~4:~~4: Time series of the noise diodes mean emission temperature calculated by means of the tipping curve procedure (blue and cyan ~~full~~solid circles) compared with values obtained ~~using a~~by means of LN_2 calibrations (~~red and~~ orange and red stars).

~~5~~4 Retrieval ~~Description~~process

VESPA-22 water vapor vertical profiles are obtained using the optimal estimation theory (Rodger, 2000). In what follows the retrieved water vapor profile is indicated as x, whereas x_a indicates the apriori profile and $\tilde{x}$ the real water vapor atmospheric profile. The quantity y and y_a represent the measured and apriori spectra, respectively. The matrix K is the weighting functions matrix, whereas S_e and S_a are the covariance matrices associated to the ~~The generic relation between the measured spectrum y and the real profile $\tilde{x}$ can be modeled by~~spectral measurements and the apriori vertical profile, respectively. The profile x can be used to calculate the synthetic spectrum y_{fit} according to:

$$\cancel{y = f(\tilde{x})\ .}\ y_{fit} = y_a + K(x - x_a)\ . \tag{19}$$

~~(25)~~

~~Eq. (25) can be expanded to the first order around an apriori profile obtaining the forward equation:~~

$$\cancel{y = y_a + K(\tilde{x} - x_a)\ ,} \qquad \cancel{(26)}$$

~~where $\tilde{x}$ is the true water vapor atmospheric profile, x_a is the water vapor apriori profile, y_a is the spectrum associated to the apriori vertical profile, and K is the weighting function matrix defined as~~

$$\cancel{K = \left.\frac{\partial y}{\partial x}\right|_{x_a}} . \quad (27)$$

~~According to Rodgers (2000), the profile x which best represents the atmospheric state $\tilde{x}$ given the measurements y and local climatology x_a and y_a can be retrieved by using~~

$$\cancel{x = x_a + G\left(y - y_a\right)} , \quad (28)$$

~~where G is the gain matrix and is defined by~~

$$\cancel{G = \left(K^T S_e^{-1} K + S_a^{-1}\right)^{-1} K^{-1} S_e^{-1}} . \quad (29)$$

~~S_e and S_a are the covariance matrices associated to the measurement and the apriori, respectively. S_a contains information on the uncertainties of the apriori, whereas S_e is related to the measurement spectral noise.~~

~~The profile x can be used to calculate the synthetic spectrum y_{fit}:~~

$$\cancel{y_{fit} = y_a + K\left(x - x_a\right)} . \quad (30)$$

The altitude grid used for VESPA-22 retrievals starts from 10 km and goes up to 110 km altitude, at steps of 1 km. This range is much larger than the sensitivity interval of the instrument which is in fact limited by the Doppler broadening at high altitudes and by the FFTS bandwidth and the tropospheric influence on the lower stratosphere at low altitudes. Only the central 400 MHz of the measured spectrum are used in the retrieval.

~~Just the central 400 MHz of the measured spectrum are used in the retrieval.~~

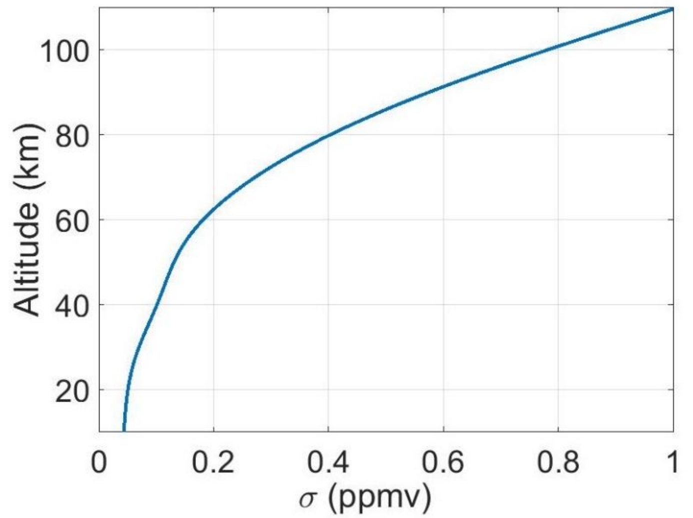

Figure 5: The value of σ_i used to compute the apriori covariance matrix as a function of altitude (Equation (20)).

The S_a matrix is computed according to:

$$\cancel{S_{a,ij} = \sigma_i \sigma_j e^{-\frac{|z_i - z_j|}{h}},} \qquad \cancel{(31)}$$

$$S_{a,ij} = \sigma_i \sigma_j e^{\frac{-|z_i - z_j|}{h}}, \qquad (20)$$

where σ_i ~~and z_i are respectively~~ is the root mean square of the variance of the apriori profile (expressed in volume mixing ratio, or vmr~~) and~~, see Figure 5) at the altitude ~~of the profile showed in Figure 5,~~ z_i, while h is a correlation altitude set to be 5 km.

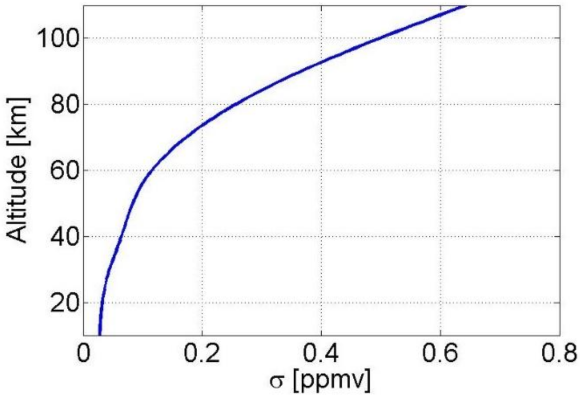

~~Figure 5: the value~~Values of ~~σ_i used~~σ_i were empirically chosen in order to ~~compute~~optimize the ~~apriori covariance matrix in Eq. (31) as function~~characteristics of the ~~altitude.~~retrieval (i.e., maximize sensitivity range and vertical resolution without introducing unphysical oscillations in the retrieved vertical profile).

In the inversion process for VESPA-22 spectra, S_e is a diagonal matrix with its diagonal elements ~~constant~~all equal and calculated using a two-step process. A first retrieval of the original, not smoothed (see Section 3.2), spectral measurement is performed using a fixed value (1x10^{-5}) for the S_e diagonal elements and the obtained profile, x_0, is used to calculate a synthetic spectrum $y_{0,fit}$ ~~by means of Eq. (30).~~by means of Eq. (19). In order to consider the spectral measurement noise in the retrieval process, a second and final inversion is then performed, this time with the S_e diagonal elements set to the ~~$(y - y_{0,fit})^2$ mean value.~~ $(y_{unsmoothed} - y_{0,fit})^2$ mean value. These values range from 3x10^{-4} K^2 (maximum value during summer) to 8 x 10^{-6} K^2 (minimum value obtained during winter).

A second~~-~~ order polynomial (light blue curve in Figure 7a) is also added to the retrieval in order to take into account the spectral emission from the upper troposphere and lower stratosphere ~~that would not otherwise be properly resolved by the retrieval algorithm, leaving a spectral baseline unaccounted for (see light blue curve in Figure 6 a).~~, and a potential contribution to the baseline from the delrin sheet. The polynomial is calculated independently for each retrieved profile. The addition of this extra degree of freedom to the retrieval process reduces the altitude interval in which VESPA-22 retrievals can be considered reliable, raising the lower limit of the sensitivity range (see definition below and Figure 8b) by approximately 6 km altitude. The use of a second-order term also introduces an additional source of uncertainty in the retrieved mixing ratio profile. Such a contribution is taken into account in the error analysis discussed in Section 4.3 (see Figure 11).

An important quantity used to characterize the retrieval quality is the averaging kernels matrix A ~~defined as:~~

~~$A = G K$.~~ ~~(32)~~

(Rodgers, 2000). The rows of A are called averaging kernels (AKs) and ~~represent~~can be used to characterize the sensitivity of the water vapor retrieval at a given altitude to variations in the water vapor concentration profile at all altitudes (Rodger, 2000). If the AKs are well-peaked functions, centered at their nominal altitude, a perturbation in the atmospheric water vapor concentration at a specific altitude is transferred by the algorithm to the correct altitude layer of the retrieved profile. Furthermore, the area enclosed under each AK is an indication of the total sensitivity of the retrieved ~~profile~~value at that altitude to atmospheric variations in water vapor concentration. ~~Sensitivity values~~A sensitivity value close to 1 at a certain ~~altitudes indicate~~altitude indicates that the major contribution to the ~~retrieval values~~retrieved value at ~~those altitudes~~that altitude comes from the spectral measurements rather than from the apriori water vapor profile. ~~Following the suggestion of Tschanz et al. (2013)~~ The retrieval is considered valid for scientific use in the ~~retrieval sensitivity~~ altitude range ~~adopted here is the altitude range in which~~where the sensitivity is above 0.8~~.~~ (e.g., Tschanz et al., 2013). The AKs ~~full width at half maximum (~~FWHM~~)~~ can ~~instead~~ be used as a rough estimate of the local vertical resolution of the obtained water vapor mixing ratio vertical profile.

~~5~~4.1 Forward model and apriori ~~profile~~profiles

~~In order to account for the variations of the mean atmospheric state during the eleven months of data presented in this study, a different water vapor apriori profile is used for each month of measurements. These profiles are obtained from the monthly averages of AURA/MLS water vapor vertical profiles (version 4.2) from the years 2014, 2015, and 2016. These monthly averages are "assigned" to the 15th day of each month and then, at each altitude, are linearly interpolated to build daily apriori profiles that vary gradually, day by day, from the 15th of one month to the next (hereafter this averaging and interpolating process is indicated as "daily smoothing monthly averages"). In the altitude region where MLS data have no scientific relevance, from 85 to 110 km altitude, the apriori profile slowly decreases with altitude as the tail of a gaussian distribution.~~

Figure 6 displays the apriori profiles used by the VESPA-22 retrieval algorithm during 10 out of the 12 months of the year and based on local climatology (3 years worth of data of Aura/MLS v4.2). They are identical below 48 km and diverge above, due to the large difference in Polar regions between summer and winter water vapor mesospheric profiles. The summer apriori (red line) is used during the period from June 1 to August 31, while the winter apriori (blue line) is used during the period from

October 1 to April 31. During the months of May and September, there is a transition period in which a linear daily interpolation from one apriori to the other was used for continuity.

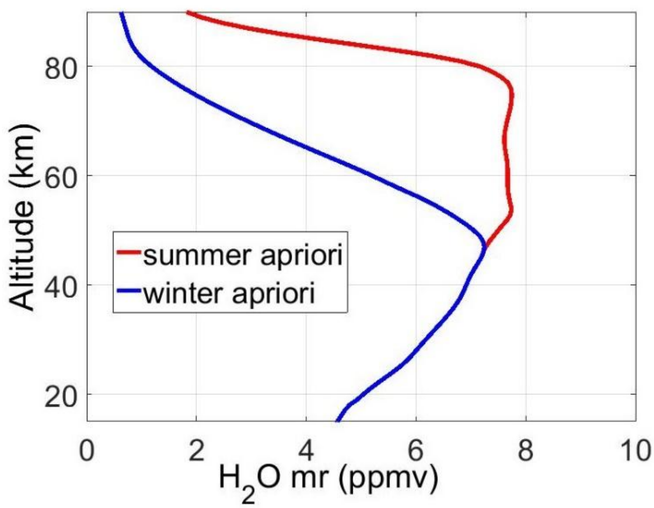

Figure 6: The apriori profiles employed by VESPA-22 for the October-April period (indicated as winter apriori, blue line) and for the Jun-Aug period (indicated as summer apriori, red line) obtained from climatology.

The matrix ~~*K*~~K and the y_a spectrum~~ of Eq. (26)~~ are calculated using the radiative transfer simulation software ARTS (Eriksson et al., 2011), adopting a Voigt-Kuntz lineshape and the line intensity provided by the JPL 2012 catalogue (Pickett et al., 1998, ~~reference site~~and https://spec.jpl.nasa.gov/). Following the work of ~~Selee~~Seele (1999) and Tschanz et al. (2013), the line described by the JPL 2012 catalogue is divided into three emission lines indicating the hyperfine splitting of the 22.235 GHz water vapor line. The employed pressure broadening and self-broadening parameters are those reported by Liebe (1989). ~~Table 2~~Table 3 summarizes the spectroscopic parameters used for the analysis of VESPA-22 spectral measurements which, in what follows, are indicated as “reference” model.

Table 3: Spectroscopic parameters (“reference” model) used ~~in~~for VESPA-22 ~~retrieval~~retrievals. Indicated parameters, from left to right, are: emission line frequency, intensity, lower state energy, pressure broadening ~~parameter~~coefficient, pressure broadening temperature dependence, self-broadening coefficient, and self-broadening temperature dependence. The line intensity is given for a reference temperature of 296 K.

ν_0 [GHz]	S [m^2 Hz]	E [J]	γ_{air} [Hz Pa^{-1}]	n_{air}	γ_{self} [Hz Pa^{-1}]	n_{self}
22.235043990	5.3648 10^{-19}	8.869693 10^{-21}	28110	0.69	134928	1

22.235077056	4.5703 10^{-19}	8.869693 10^{-21}	28110	0.69	134928	1
22.235120358	3.9740 10^{-19}	8.869693 10^{-21}	28110	0.69	134928	1

The profile x_{ARTS} is the profile used in the forward model calculations to compute the apriori spectrum and the weighting functions. x_{ARTS} matches the apriori profile from 12 km of altitude upward and, below 9 km, it is consistent with the measurements of precipitable water vapor (PWV) collected by the HATPRO radiometer (Rose and Czekala, 2009; Pace et al., 2015) installed at the THAAO. This lower part of x_{ARTS} is calculated according to:

~~$x_{ARTS}\left(from\, the\, ground\, to\, 9km\right) = \frac{PWV_{Hatpro}}{PWV_{Eu}} x_{Eu}$ (33)~~

$$x_{ARTS}(\text{from the ground to 9 km}) = \frac{PWV_{Hatpro}}{PWV_{Eu}} x_{Eu} \quad (21)$$

where x_{Eu} is a water vapor mixing ratio profile obtained by daily smoothing monthly averages calculated from the radiosoundings launched ~~at~~from the Eureka station~~ (80.0°N, 85.9°W)), Canada~~, PWV_{Eu} is the associated water vapor column content, and PWV_{Hatpro} is the column content measured by the HATPRO~~. x_{ARTS} therefore represents the monthly average x_{Eu} profile simply rescaled to be consistent with the column content measurements of the HATPRO at Thule.~~ located at the THAAO. Data from Eureka were chosen (instead of those from Alert, Canada, for example) because they show the closest resemblance to the tropospheric profiles measured at Thule by local radiosoundings, when the latter are available. In order to avoid discontinuities in x_{ARTS}, values at altitudes between 9 and 12 km are obtained with a linear interpolation between x_{ARTS}~~(9 km)~~(9 km) and x_{ARTS}~~(12 km)~~(12 km).

The pressure and temperature profiles needed to run the forward calculation are built merging NASA Goddard Space Flight Center (GSFC), ~~AURA~~Aura/MLS and climatological temperature and pressure profiles. The NASA GSFC profiles ~~by~~obtained through the Goddard Automailer Service (Lait et al., 2005) are used to build the tropospheric meteorological state, from the ground up to 9 km of altitude. ~~For the altitude range between~~Between 10 and 87 km~~ of~~ altitude, the MLS temperature and pressure profiles collected during VESPA-22 observations, in a radius of 300 km from the observation point of VESPA-22, are averaged together to produce a single set of daily meteorological vertical profiles. The VESPA-22 observation point coordinates are chosen to be 74.8° N and 73.5° W, and represent an estimate of the geographical coordinates of the air mass that is observed by VESPA-22 (which points South-West, at about 220°) at 60 km altitude when the instrument aims at an elevation of 15° above the horizon. Daily temperature and pressure profiles from ~~86~~97 to 110 km of altitude are obtained by daily smoothing zonal monthly averages from the COSPAR International Reference Atmosphere (Rees et al., 1990).

The absence of vertical discontinuities in the temperature and pressure daily profiles is assured by a smoothing process performed at the altitudes where the three different datasets (GSFC, MLS, and ~~climatological profiles~~COSPAR) are stitched together, between 9 and 12 km and between 87 and 97 km.

The software ARTS is employed to simulate the emission from the zenith, $\tilde{y}_r$, and from an angle close to the horizon, y_s. The emission $\tilde{y}_r$ is then rescaled using Eq. ~~(34)~~(22), therefore simulating the effect of the delrin compensating sheet~~.~~:

$$\cancel{y_r = \tilde{y}_r e^{-\tau_d} + T_d\left(1 - e^{-\tau_d}\right)} \qquad \cancel{(34)}$$

$$y_r = \tilde{y}_r + T_d(1 - e^{-\tau_d}), \qquad (22)$$

whereas the mean difference $y_s - y_r$ is:

$$y_s - y_r = y_a\left(\tilde{\mu}e^{-\tilde{\mu}\tilde{\tau}}\right) - e^{-\tilde{\tau}-\tau_d}\ . \qquad (23)$$

The opacity τ_d used in Eq. ~~(34)~~(22) is the opacity of the compensating sheet, ~~whereas~~ the temperature T_d is the temperature of the sheet, measured by a sensor installed next to it~~. The value of~~, and the signal beam observing angle ~~imposed in the simulation~~, $\tilde{\theta}$, is chosen in order to minimize the mean difference $y_s - y_r$, as it is in fact attained by VESPA-22 in its data taking process. The apriori spectrum is calculated according to the same equation used for the measured signal (Eq. ~~(10)~~(5) and ~~(11)).~~(6)),

$$\cancel{y_s - y_r = y_a\left(\tilde{\mu}e^{-\mu\tilde{\tau}} - e^{-\tilde{\tau}-\tau_d}\right)} \qquad \cancel{(35)}$$

$$\cancel{y_a = \frac{y_s - y_r}{\tilde{\mu}e^{-\mu\tilde{\tau}} - e^{-\tilde{\tau}-\tau_d}}} \qquad \cancel{(36)}$$

$$y_a = \frac{y_s - y_r}{\tilde{\mu}e^{-\tilde{\mu}\tilde{\tau}} - e^{-\tilde{\tau}-\tau_d}}, \qquad (24)$$

where $\tilde{\mu}$ and $\tilde{\tau}$ are the air mass factor associated to the simulated signal beam and the zenith opacity calculated from the x_{ARTS} profile.

Deriving Eq. ~~(36)~~(24) and Eq. (22), and using ~~Eq. (27) and Eq. (34),~~the K matrix definition (Rodgers, 2000), the retrieval weighting function matrix can be ~~obtained~~written as:

$$\cancel{K = \frac{\partial}{\partial x}\left(\frac{y_s - y_r}{\tilde{\mu}e^{-\mu\tilde{\tau}} - e^{-\tilde{\tau}-\tau_d}}\right)_{x_a} \cong \frac{\left.\frac{\partial y_s}{\partial x}\right|_{x_a} - \left.\frac{\partial y_r}{\partial x}\right|_{x_a}}{\tilde{\mu}e^{-\mu\tilde{\tau}} - e^{-\tilde{\tau}-\tau_d}} = \frac{K_s - K_r e^{-\tau_d}}{\tilde{\mu}e^{-\mu\tilde{\tau}} - e^{-\tilde{\tau}-\tau_d}}} \qquad \cancel{(37)}$$

$$K = \frac{\partial}{\partial x}\left(\frac{y_s - y_r}{\tilde{\mu}e^{-\tilde{\mu}\tilde{\tau}} - e^{-\tilde{\tau}-\tau_d}}\right)_{x_a} \cong \frac{\left[\frac{\partial y_s}{\partial x}\right]_{x_a} - \left[\frac{\partial y_r}{\partial x}\right]_{x_a}}{\tilde{\mu}e^{-\tilde{\mu}\tilde{\tau}} - e^{-\tilde{\tau}-\tau_d}} = \frac{K_s - K_r e^{-\tau_d}}{\tilde{\mu}e^{-\tilde{\mu}\tilde{\tau}} - e^{-\tilde{\tau}-\tau_d}} \qquad (25)$$

where K_s and K_r are the weighting function matrices that ARTS calculates for the simulated signal and reference beams. As a first approximation, the dependence of $\tilde{\tau}$ on the stratospheric water vapor profile in Eq. (25) is neglected.

~~5~~ 4.2 Retrieval example

~~Figure 6 a~~Figure 7a shows a VESPA-22 spectrum integrated for 24 hours (blue line) on 23 December, 2016, its corresponding synthetic spectrum y_{fit} (red line) and the apriori spectrum (green line), while the residual (defined as the difference between fit and measured spectrum, $y_{fit} - y$) is plotted in ~~Figure 6 b.~~Figure 7b. The cyan line is the second-degree polynomial retrieved by the inversion algorithm. ~~Figure 7~~Figure 8a shows the result of the inversion of the measured spectrum depicted in ~~Figure 6~~Figure 7 with the apriori profile and retrieval 1σ uncertainty. The details ~~about~~on the uncertainty calculation are discussed in ~~the~~ Section ~~6~~. 4.3.

~~Figure 8~~Figure 8, panel b, shows the ~~previous retrieval~~corresponding averaging kernels (AKs, black and colored solid lines~~),~~). AKs are multiplied by a factor of 10~~,~~ and the sensitivity ~~(~~in indicated with a red~~). In a typical VESPA-22 retrieval the sensitivity is above 0.8 in a range from 26 to 72 km~~ solid line.

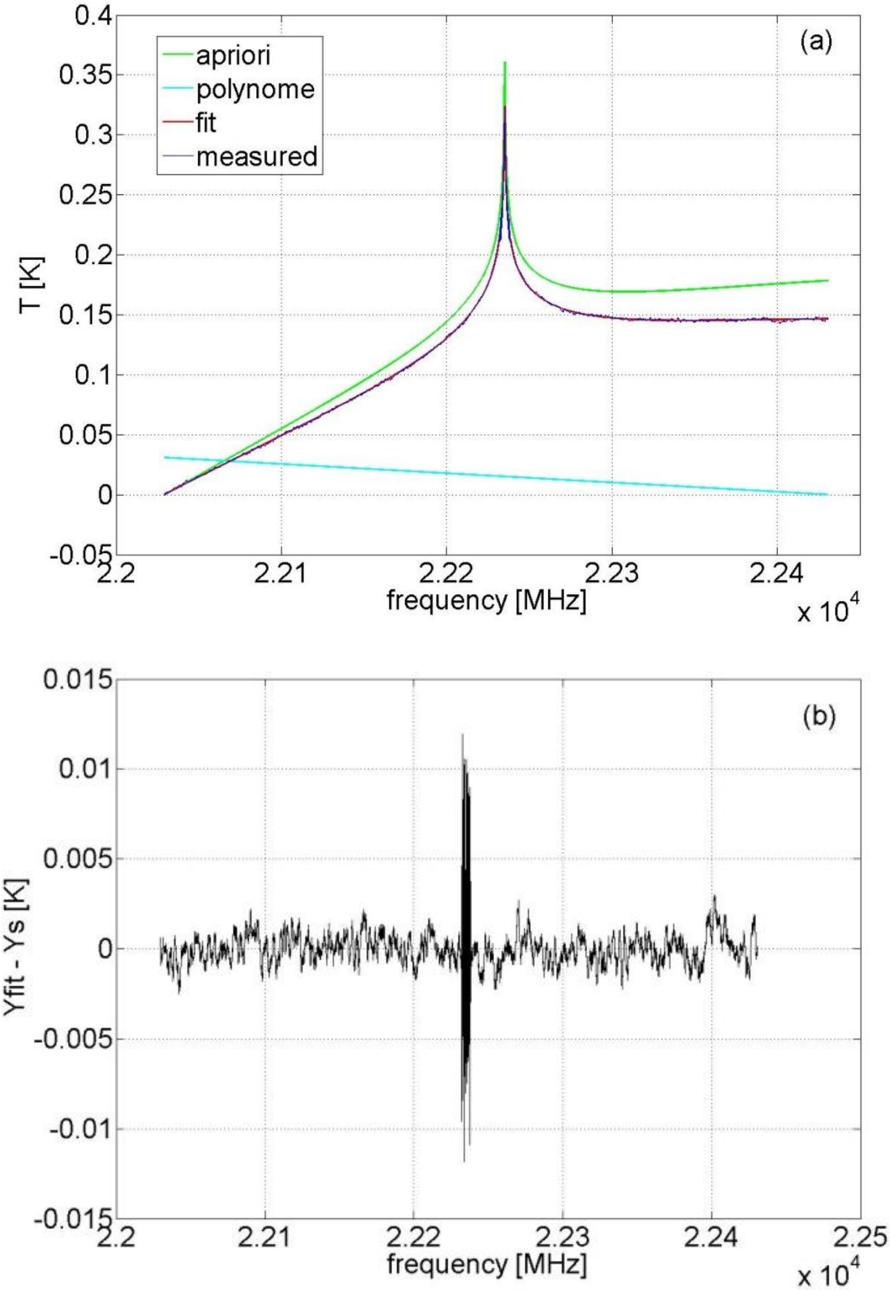
(a)
apriori
polynome
fit
measured
T [K]
0.4
0.35
0.3
0.25
0.2
0.15
0.1
0.05
0
-0.05
2.2
2.21
2.22
2.23
2.24
frequency [MHz]
x 10^4
(b)
Yfit - Ys [K]
0.015
0.01
0.005
0
-0.005
-0.01
-0.015
2.2
2.21
2.22
2.23
2.24
2.25
frequency [MHz]
x 10^4

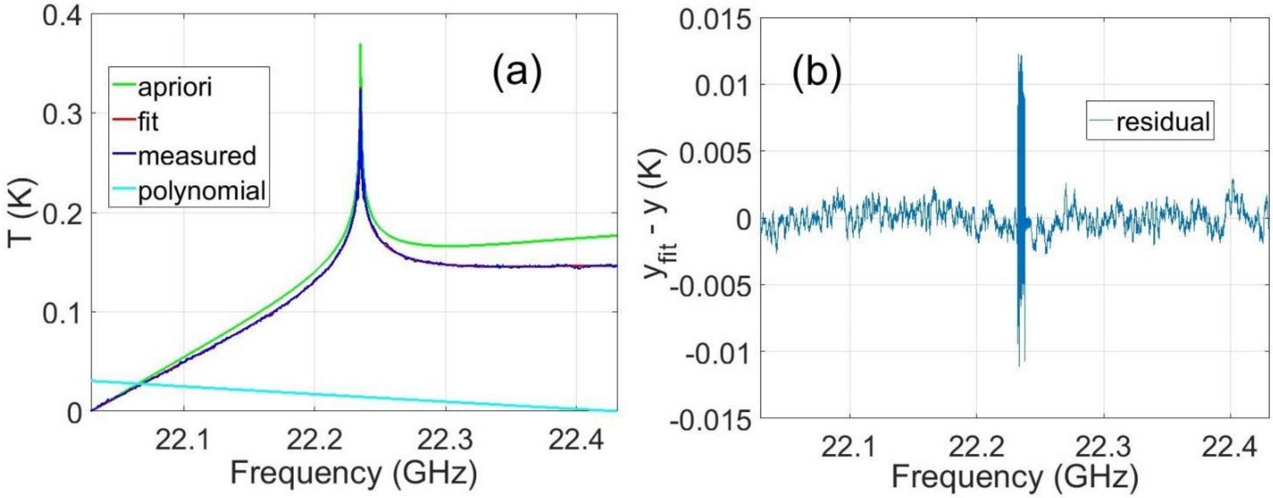

Figure ~~6: (a): an~~7: (a) An example of VESPA-22 measured spectrum (blue) collected on 23 December, 2016, with the apriori spectrum ~~(~~in green~~)~~ and the fit spectrum ~~(~~in red~~); (b): the~~. The second-order polynomial is indicated with a cyan solid line. (b) The residual ~~$y_{fit} - y$.~~ $y_{fit} - y$. The central part of the spectrum is unsmoothed in order to maintain the maximum spectral resolution near the peak and its residual is ~~higher~~larger.

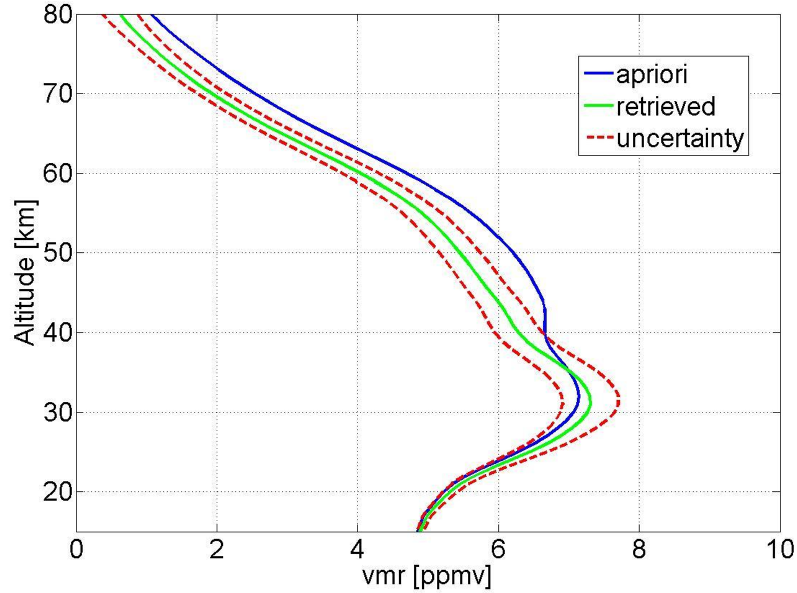

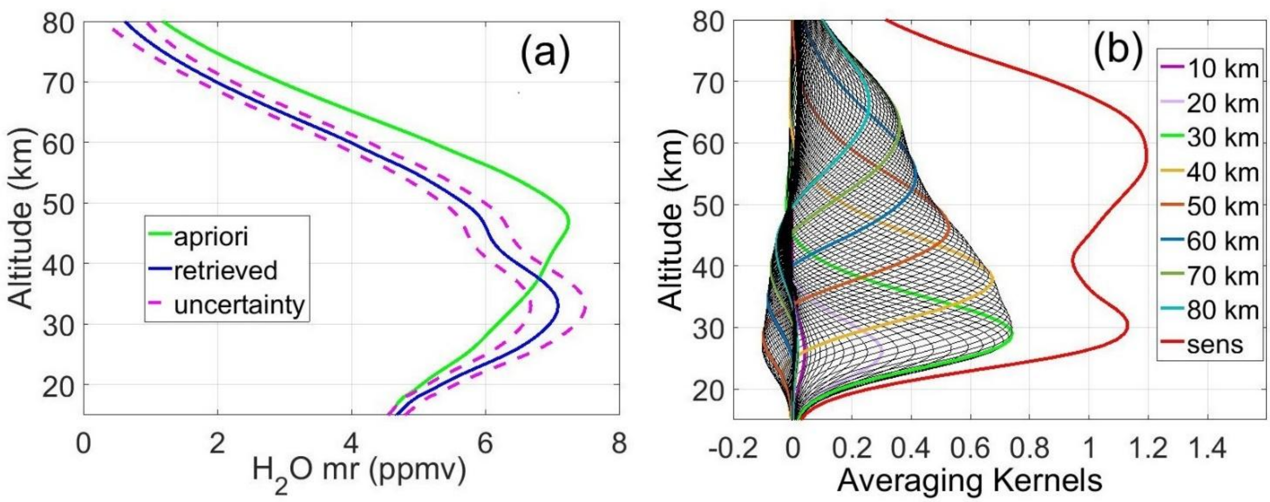

Figure ~~7: the~~8: (a) The retrieved VESPA-22 profile (~~green~~blue solid line) correspondent to the spectrum showed in ~~Figure 6 and the~~Figure 7. The apriori profile ~~(blue~~is indicated with a green solid line~~)~~.. The two red dashed lines describe the uncertainty of this VESPA-22 retrieval (for details on the estimated uncertainty ~~on~~of VESPA-22 mixing ratio vertical profiles see ~~the~~ Section ~~6).~~

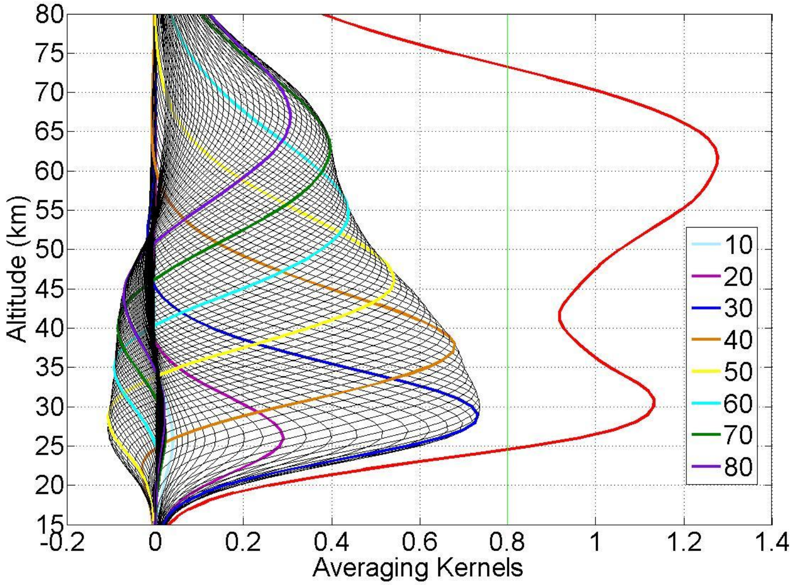

~~Figure 8:~~4.3). (b) Rows of the A matrix multiplied by a factor of 10 as a function of altitude (some A functions are highlighted in ~~color~~colors). The vertical profile of the sensitivity is shown in red.

~~6~~4.3 Retrieval uncertainty

The uncertainty characterizing VESPA-22 retrieved profiles can be divided in ~~three~~four major contributions: 1) the uncertainty due to the linear approximation used in ~~Eq. (26);~~the optimal estimation; 2) the ~~systematic~~ uncertainty due to the ~~uncertainties of the~~ various parameters used in the spectra calibration and pre-processing; ~~and~~ 3) the ~~retrieval~~ uncertainty due to spectral noise and potential artifacts; and 4) the uncertainty introduced by the use of the second order polynomial in the retrieval process. One additional error source is the limited vertical resolution inherent to concentration vertical profiles obtained by means of this ground-based observing technique. This leads to solution profiles that can be considered a smoothed version of the real atmospheric concentration profiles. In discussing the Optimal Estimation method, Rodgers (2000) suggests that this error, called “smoothing error”, should be estimated only if accurate knowledge of the variability of the atmospheric fine structure is available. This approach is used here and the smoothing error is not included in the error estimate.

The first contribution can be evaluated observing the difference Δy_{lin} between the fit spectrum without the addition of the second order polynomial, ~~y^*_{fit},~~y^*_{fit}, and the spectrum obtained using ARTS to calculate the emission expected from the retrieved profile x~~. In~~ (in the calculation, ARTS does not perform ~~a~~any linear approximation~~ to the general function f described in Eq. (25):~~):.:

$$\cancel{\Delta y_{lin} = y^{*}_{fit} - f\left(x\right)\ .} \qquad \cancel{(38)}$$

$$\Delta y_{lin} = y^{*}_{fit} - f(x)\ . \tag{26}$$

The uncertainty Δx_{lin} that Δy_{lin} causes on the retrieved profile can be calculated with

$$\cancel{\Delta x_{lin} = G\Delta y_{lin}} \qquad \cancel{(39)}$$

~~and it~~$\Delta x_{lin} = G\Delta y_{lin},$ (27)

where G is the gain matrix (Rodgers, 2000). The uncertainty Δx_{lin} has a negligible contribution to the total uncertainty (with a maximum of 0.1 % at 70 km altitude).

In order to evaluate the second contribution listed above, the effects on the retrieved profile due to the variation of each single parameter used in the measurements calibration and pre-processing was investigated. The difference between the profile retrieved using the "correct" value of a specific parameter and the retrieval obtained by changing such a value by the estimated relative uncertainty of the parameter is considered to be the contribution σ_i of this parameter to the total calibration and pre-processing uncertainty. The total uncertainty from these sources is defined ~~systematic~~ as calibration uncertainty. Table 4**Table 4** summarizes the uncertainties ~~of~~on the various parameters involved in the calibration and pre-processing of VESPA-22 spectra~~; when~~. When the uncertainty is a function of altitude the minimum and maximum values of the uncertainty are reported. The total calibration uncertainty σ_{cal} is given by:

~~The total systematic uncertainty σ_{cal} is therefore given by:~~

$$\cancel{\sigma_{cal} = \sqrt{\sum \sigma_i^2}} \qquad \cancel{(40)}$$

~~In Figure 9, the relative contributions of the various parameters used in the calibration and pre-processing are shown.~~

$$\sigma_{cal} = \sqrt{\textstyle\sum_i \sigma_i^2}\ . \tag{28}$$

Table 4: Uncertainties ~~of~~on the various parameters used in the calibration process. When the uncertainty is a function of altitude the minimum and maximum values of the uncertainty are reported.

Parameter	Uncertainty (relative or absolute)
Signal angle, θ	±0.1°
Noise ~~Diode~~diode brightness temperature, T_{nd}	±1.~~3~~7%
Atmospheric opacity at the zenith, τ	±5%
Air ~~Temperature~~temperature profile	[±2.1 ± 5.0] K
Geopotential height	[±30 ± 110] m
Delrin opacity, τ_d	±10%
Spectroscopic parameters	[±1% ±10%]

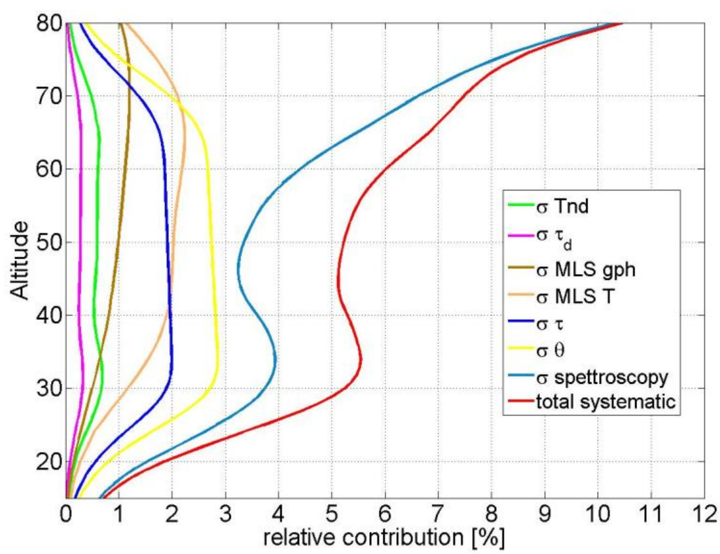

~~**Figure 9: Relative contributions to systematic uncertainty (red curve). The contributions are: the signal beam angle (yellow), the noise diode temperature (green), the opacity (blue), the MLS meteorological profile (orange and brown), the compensating sheet (Delrin®) opacity (magenta), the spectroscopic parameters (cyan).**~~

In Figure 9, the relative contributions of the various parameters needed in the calibration and pre-processing procedures are shown. The yellow line shows the σ_i contribution due to the uncertainty on the signal beam angle. In order to minimize this contribution, the choked antenna and the parabolic mirror are aligned using a He-Ne laser. During the period from April to

October, the VESPA-22 pointing offset can be verified by scanning rapidly at around the sun elevation angle and comparing the measured position of the center of the sun against the known ephemerides. For the measurements discussed here an offset $\Delta\theta = 0.2° \pm 0.1°$ was estimated.

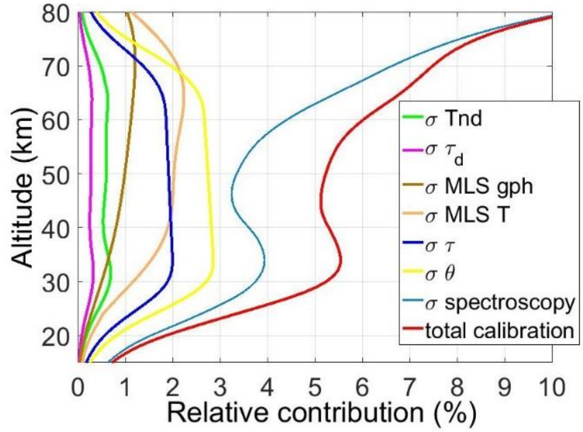

Figure 9: Relative contributions to the calibration uncertainty defined by Eq. (28) and indicated with a red solid curve. The contributions are the signal beam angle (yellow), the noise diode temperature (green), the sky opacity (blue), the MLS meteorological profiles (orange and brown), the compensating sheet opacity (magenta), the spectroscopic parameters (cyan).

The green solid line shows the potential relative error on the water vapor mixing ratio vertical profile due to the uncertainty on the estimated noise diode temperature $\cancel{T_{nd}}\bar{T}_{nd}$. In order to evaluate the uncertainty ~~of~~ $\cancel{T_{nd}}$on $\bar{T}_{nd}$, the 0.4% difference between the values obtained by means of the ~~skydip and~~ LN_2 calibrations and by means of the skydips immediately following or preceding the LN_2 calibrations (see Section 3.4~~.3 and Figure 4~~ and Figure 4) is considered. On top of this, also the fluctuations of the signal produced by the calibration ~~diode~~diodes must be taken into account. These can be evaluated by using the standard deviation of the difference over time between the $\cancel{T_{nd}}\bar{T}_{nd}$ values of the two noise diodes, measured to be 1.~~2%. These two~~1%. The tipping curve procedure allows to calculate the noise diodes brightness temperature averaged over the 11000 central channels of the spectrometer. Since the noise diodes brightness temperatures do have a small frequency dependence, using their mean values introduces a source of uncertainty which is estimated to be 0.9%. An additional source of uncertainty is due to sky inhomogeneities, and amounts approximately to 1%. All these sources of ~~error (0.4% and 1.2%)~~uncertainty for $\bar{T}_{nd}$ are added in quadrature to obtain ~~the~~ $\cancel{T_{nd}}$a total uncertainty of 1.~~3~~8%.

The blue line shows the contribution due to the uncertainty $\Delta\tau$ on the sky zenith opacity τ. In order to estimate this uncertainty, the uncertainties introduced by sky inhomogeneity and by the estimation of the effective tropospheric temperature $\cancel{T_{atm}}T_{trop}$ are considered. The first ~~contribute it is~~contributes to about 2% ~~but can increase depending from the sky condition. It~~ and is estimated using the uncertainty on the slope of the ~~slope parameter produced by the~~ linear fit ~~used in~~of the tipping curve ~~procedure~~ (see ~~the Measurement Technique section).~~Section 3.4 and Figure 3). The second ~~contribute~~contribution can be evaluated observing the daily fluctuations of $\cancel{T_{atm}}$$T_{trop}$ measured at ~~the meteorological station of~~ Eureka (~~Northern~~ Canada), Aasiaat ~~and Alert~~ (Southern Greenland), and Alert (Canada~~ respectively~~). The natural day to day temperature fluctuations and the lack of tropospheric meteorological data at Thule during long intervals of time led us to estimate an uncertainty on $\cancel{T_{atm}}$$T_{trop}$ of about 6 K, which then makes the total uncertainty $\Delta\tau$ ~~to be~~ ~5-%.

The brown and orange lines show the σ_i~~'s~~'s due to ~~the~~ temperature and geopotential height ~~uncertainties in the meteorological profile~~profiles used in the forward calculation. The uncertainties on these parameters are obtained from the MLS data quality and description document (Livesey et al., 2015).

~~The~~In Figure 9, the magenta line shows the contribution of the uncertainty on the compensating sheet opacity, $\Delta\tau_d$. ~~This value is measured observing the effect of the Delrin sheet on the incoming signal from the zenith direction. During regular measurement conditions, signal and reference beams are balanced with the signal angle at~~ $\cancel{\theta}$ ~~:~~Although the uncertainty on the measurements of τ_d is about 2% (see Table 1), the use of a linear interpolation suggests the use of a more conservative estimate, eventually set at 10%. The cyan line shows the contribution due to uncertainties in the employed spectroscopic parameters, and it has the largest impact on the calibration uncertainty. Following Straub et al. (2010), the emission line intensity and the pressure broadening coefficient were assigned an uncertainty of 8.7 10^{-22} m^2 Hz and of 1014 Hz Pa^{-1}, respectively.

$$\cancel{\bar{T}_S(\theta)=\bar{T}_R\,.} \qquad \cancel{(41)}$$

~~where~~ $\cancel{\overline{T_S}}$ ~~and~~ $\cancel{\overline{T_R}}$ ~~are the mean values of signal and reference beams respectively. The compensating sheet modifies the reference beam according~~In addition to~~:~~

$$\cancel{T_R = T_{R\_nod}e^{-\tau_d} + T_d\left(1-e^{-\tau_d}\right),} \qquad \cancel{(42)}$$

~~where~~ $\cancel{T_d}$ ~~is the sheet physical temperature and~~ $\cancel{T_{R\_nod}}$ ~~is the intensity of the reference beam without the sheet. In order to estimate~~ $\cancel{\tau_d}$~~, during normal data taking operations the signal angle is locked to its balanced position and the Delrin sheet is removed from the reference beam. Using Eq. (42) and (41),~~ $\cancel{\tau_d}$ ~~can be calculated as:~~

$$\cancel{\tau_d = -\ln\left(\frac{T_d-\bar{T}_S}{T_d-\bar{T}_{R\_nod}}\right),} \qquad \cancel{(43)}$$

~~Where~~ $\cancel{\bar{T}_{R\_nod}}$ ~~is the mean intensity of the reference beam without the sheet. The brightness temperature of~~ $\cancel{T_s}$ ~~and~~ $\cancel{T_{R\_nod}}$ ~~are calculated according to Eq. (15); the calibration parameters~~ $\cancel{\alpha}$ ~~and~~ $\cancel{T_{rec}}$~~, are obtained from a~~ ~~LN_2 calibration.~~

~~In order to carry out the mentioned procedure, qualified personnel must be at the observatory and therefore τ_a was measured only in July and November, 2016, and February 2017 (see Table 4). Were performed seven measurements of the grey body opacity, two during July, three during November and two during February. The half of the difference between the minimum and maximum values obtained during the same period is used as measurement uncertainty. The measurements mean values changes with time. This is caused by the degassing typical behavior of plastic sheets, i.e., the property to absorb/release water vapor molecules from/to the environment, which depends on atmospheric humidity. During wintertime the air is drier and the compensating sheets release some water vapor and lower their own opacity.~~

~~**Table 4: The mean value and standard deviation of the measured delrin opacity during different periods**~~

~~Thickness~~	~~July 2016~~	~~November 2016~~	~~February 2017~~
~~9 mm~~	~~0.159 ± 0.004~~	~~0.128 ± 0.003~~	~~0.123 ± 0.003~~
~~5 mm~~	~~0.088 ± 0.001~~	~~0.072 ± 0.001~~	~~0.070 ± 0.001~~

~~VESPA-22 spectral data are calibrated using a linear interpolation between the τ_a values measured over time. Although the uncertainty of the measurements is about 2%, the value of the Delrin sheet opacity varies through time and the use of a linear interpolation suggests caution. $\Delta\tau_a$ has therefore been conservatively estimated to be 10%.~~

~~The cyan line in Figure 9 shows the contribution due to~~ these uncertainties ~~in spectroscopic parameters. This spectroscopic contribution has the largest impact on the systematic uncertainty. Following Tschanz et al. (2013), the emission line intensity and the pressure broadening parameter were assigned an uncertainty of 8.7 10^{-22} m^2 Hz and of 1014 Hz Pa^{-1}, respectively.~~

~~Figure 10~~, Figure 10 shows the results of ~~the retrieval of the~~retrieving VESPA-22 data from October 2016 to May 2017 ~~analyzed with the spectroscopic model eventually adopted~~ using different sets of values for the ~~analysis of VESPA-22 spectra, hereafter reference model, and the same data analyzed with other spectroscopic models. As stated in section 5.1, the reference model line intensity is taken from the JPL 2012 catalogue, modified by adding the hyperfine splitting of the H_2O line (Tschantz et al., 2013) while the pressure broadening parameters are taken from the work of Liebe (1989). Parameters coming from~~ spectroscopic parameters (see also~~HITRAN (Rothman et al., 2012) and JPL catalogues (Pickett et al., 1998) from different years were compared with one another, as described in the work of~~ Haefele et al~~. (~~., 2009). ~~The JPL catalogue does not include the pressure broadening parameters, so JPL models were integrated with information coming from the work of Liebe (1989) or Cazzoli et al.~~ In the figure,~~(2007).~~

~~Figure 10, panel a, shows~~ the mean profiles retrieved using the different models listed in the legend are depicted. Such models include values taken from HITRAN (Rothman et al., 2012) and JPL catalogues (Pickett et al., 1998), for different years, and from Liebe (1989) and Cazzoli et al. (2007). ~~.~~The blue line represents the mean profile obtained using ~~the~~VESPA-22 reference model~~. Figure 10,~~ (RM). In panels b~~ and c, shows~~, the mean ~~absolute and~~ relative difference ~~between the retrieved~~ profiles between retrievals obtained using the reference model and the other spectroscopic models ~~and the reference model. It can be noticed that the~~are drawn (see legend). The water vapor mixing ratio retrieved ~~profile strongly depends~~profiles show a strong dependence on the spectroscopic model of choice, with a relative difference between profiles obtained using different models reaching a maximum of ~~10~~8% at the top of the sensitivity range. ~~The correlation coefficient (Figure 10, panel d) of the datasets obtained with the different models respect to the reference model dataset is above 0.9 in the sensitivity range. This strong correlation indicates that the time series variation of the water vapor profile measured by VESPA-22 is quite independent from the model used.~~

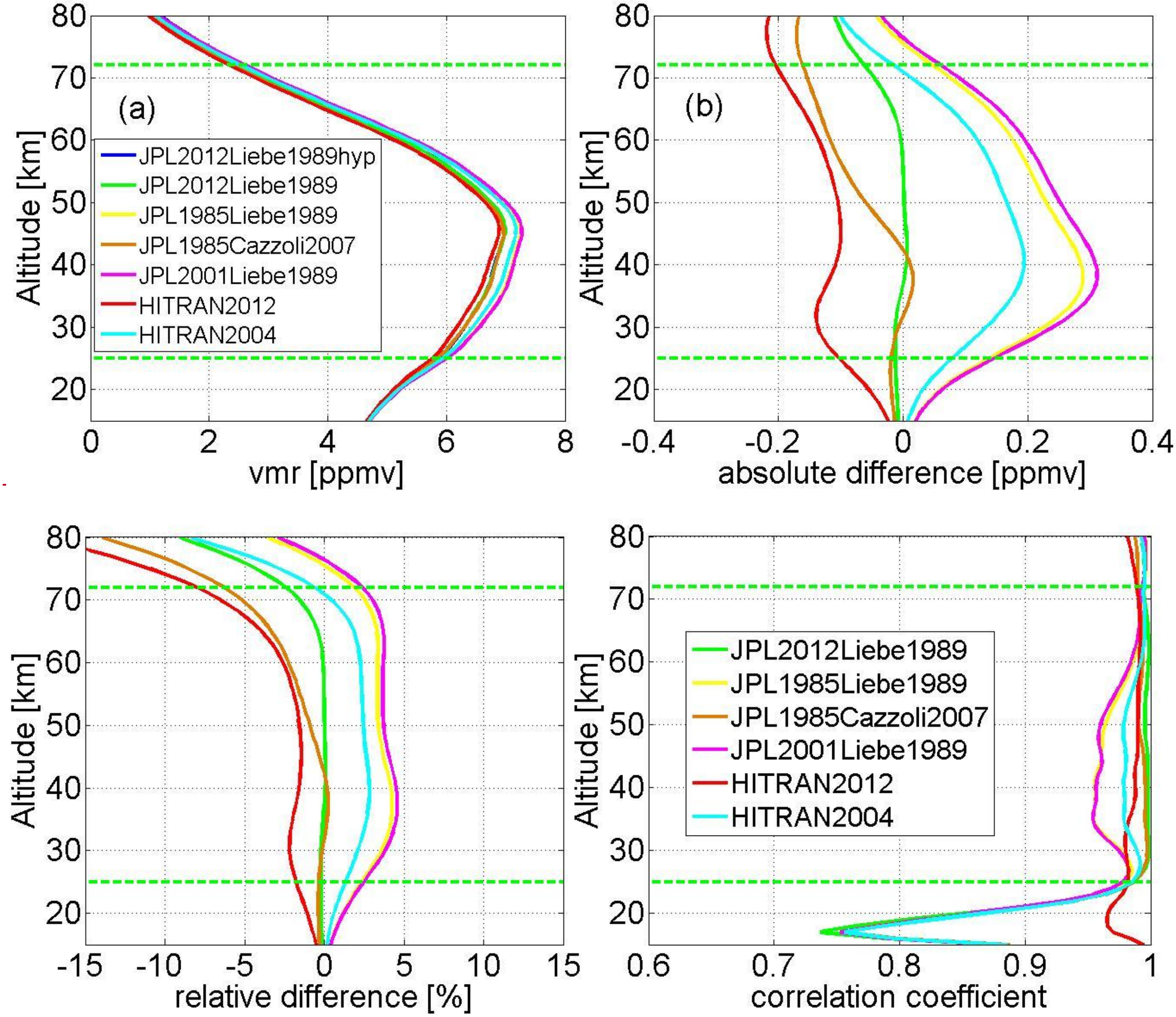
(a)
Altitude [km]
vmr [ppmv]
JPL2012Liebe1989hyp
JPL2012Liebe1989
JPL1985Liebe1989
JPL1985Cazzoli2007
JPL2001Liebe1989
HITRAN2012
HITRAN2004
(b)
absolute difference [ppmv]
relative difference [%]
correlation coefficient

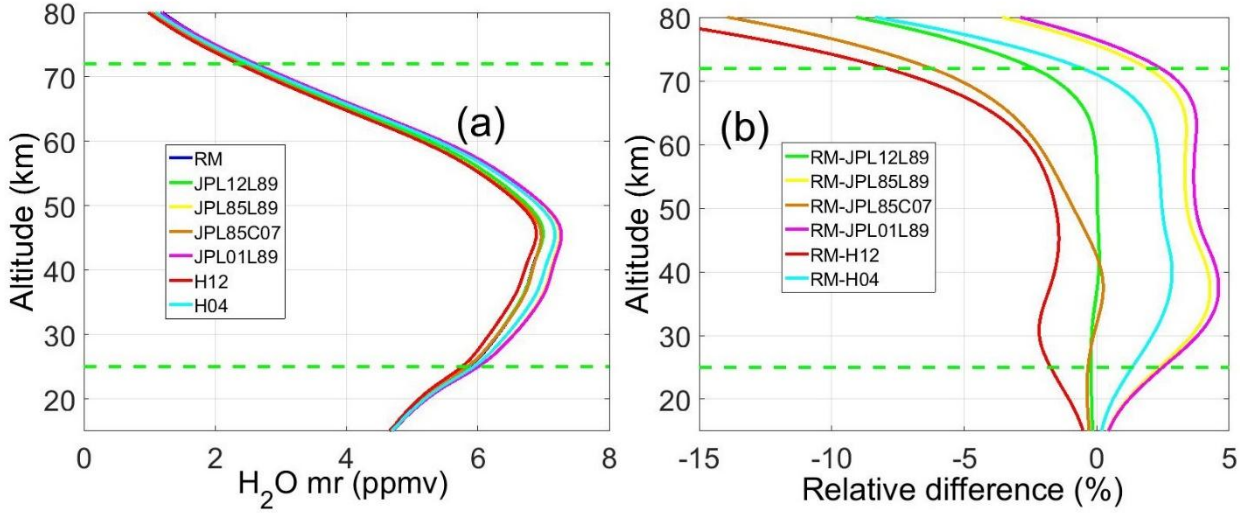

Figure ~~10:~~10: (a) ~~mean~~Mean retrieved water vapor profiles obtained using different spectroscopic models (the blue line is the model eventually adopted for the analysis of VESPA-22 spectra, called reference model~~) and vertical~~, or RM). The spectroscopic parameters for the additional models tested are obtained from different versions of the JPL catalogue (years 1985, 2001 and 2012; Pickett et al., 1998) with the pressure broadening parameters taken from Liebe (1989) and Cazzoli et al. (2007). Two models include values from HITRAN 2004 and 2012 (Rothman et al., 2012). Models are indicated in the legend with their abbreviations: JPL2012Liebe1989 (JPL12L89), JPL1985Liebe1989 (JPL85L89), JPL1985Cazzoli2007 (JPL85C07), JPL2001Liebe1989 (JPL01L89), HITRAN2012 (H12), and HITRAN2004 (H04). (b) Vertical profiles of ~~(b) and (c) the~~ mean ~~absolute and~~ relative ~~difference and (d) the correlation coefficient~~differences between VESPA-22 profiles obtained using ~~different spectroscopic models and the~~ the reference model~~. The data~~ and the different spectroscopic models. Data represented here range from 4 October, 2016, to 22 May, 2017. The average retrieval sensitivity range is marked by ~~the~~ dashed horizontal green lines. ~~The spectroscopic parameters are taken from different versions of the JPL catalogue (versions of years 1985, 2001 and 2012) with the pressure broadening parameter taken from the works of Liebe (1989) or Cazzoli et al. (2007) or from the HITRAN catalogue (version of years 2004 and 2012).~~

~~Figure 11~~Figure 11 shows the uncertainty calculated for the retrieval ~~shown in Figure 7 of the~~of 23 December, 2016~~.~~, shown in Figure 8. The overall ~~systematic~~calibration uncertainty is shown with a red curve. The ~~retrieval~~ uncertainty due to spectral noise and artefacts can be evaluated using the ~~S~~S uncertainty matrix ~~obtained as~~ (Rodger, 2000) obtained as:

$$\cancel{S=(K^T S_e^{(-1)} K + S_a^{(-1)})^{(-1)}.} \quad \cancel{(44)}$$

$$S = (K^T S_e^{-1} K + S_a^{-1})^{-1}. \quad (29)$$

The square root of the diagonal elements of S represents the spectral uncertainty of the retrieved profile at different altitudes and is indicated in ~~Figure 11~~Figure 11 with a blue line. ~~The retrieval uncertainty~~ This term depends on the ~~level~~S_e value of ~~noise of~~the retrieval and its value increases during summer and poor weather conditions. The green curve displays the

~~spectrum. Finally,~~estimated uncertainty due to the use of the second order polynomial in the retrieval process. The total uncertainty is ~~obtained~~calculated as

$$\sigma_{tot} = \sqrt{\sigma_{cal}^2 + \sigma_{spec}^2 + \sigma_{poly}^2} \tag{30}$$

$$\cancel{\sigma_{tot} = \sqrt{\sigma_{cal}^{\ 2} + \sigma_{ret}^{\ 2}}} \qquad \cancel{(45)}$$

and is represented with a purple line in ~~Figure 11.~~Figure 11.

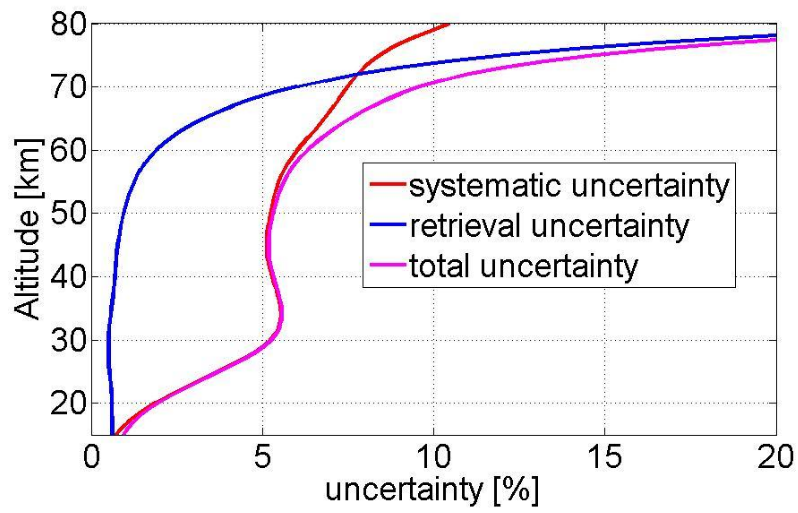

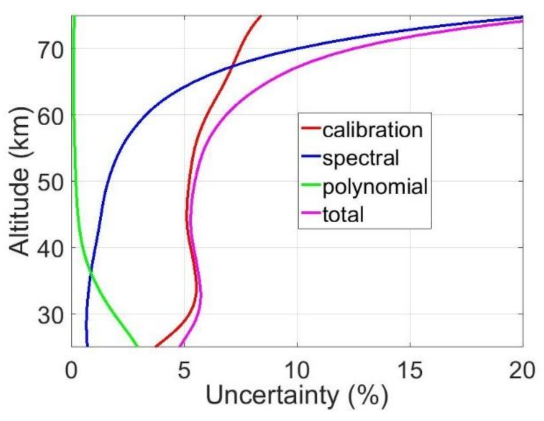

Figure ~~11:~~11: Vertical profiles of the ~~systematic~~calibration uncertainty (red), the retrieval uncertainty (blue), and the total uncertainty (magenta) of VESPA-22 water vapor mixing ratio vertical profiles obtained inverting a ~~24-hour integration~~ spectrum collected on 23 December 2016 and integrated for 24 hours.

~~7~~5 VESPA-22 and Aura/MLS water vapor profiles intercomparison

VESPA-22 water vapor vertical retrievals obtained from 24-hour integration spectra (from 00:00 to 23:59 UT) have been compared with version 4.2 of ~~AURA~~Aura/MLS water vapor vertical profiles. The MLS profiles used for this intercomparison are daily mean profiles obtained averaging all MLS profiles collected within a radius of 300 km centered around VESPA-22 observation point (74.8° N, 73.5° W, see Section ~~5.1). A measurement of the horizontal resolution of VESPA-22 is the horizontal area highlighted by the half power full beam angle; for an observation angle of 15° at a height of 60 km it is an ellipse with axes of about 55 x 14 km.~~4.1).

The intercomparison is carried out using data from 15 ~~Jul~~July, 2016, to ~~21 May~~02 July, 2017. ~~The~~In general, spectra collected during July, August, and September are less continuous and noisier than spectra observed during the rest of the selected period. This is due to extensive testing of the equipment, poor weather conditions, and snow covering the zenith observing window (in November 2016 a ~~more~~second powerful fan was installed outside the ~~windows~~roof window in order to ~~minimize~~reduce snow deposition). ~~Additionally~~In particular, there are no stratospheric measurements carried out by VESPA-22 between 4 and 22 November, 2016, ~~and between 12 and 16 February, 2017,~~ due to ~~poor weather conditions and~~ snow covering the lower portion of the reference beam window~~, and from 11 to 16 December, 2016, due to technical issues.~~. During the second part of March, April, and May, 2017, the spatial distance between concurrent MLS and VESPA-22 profiles increases, on average~~;~~. As a result, during these periods the MLS water vapor profiles compared to VESPA-22 profiles are composed by averaging ~~less data~~ together fewer profiles with respect to other periods and there are several days ~~in this period~~of VESPA-22 data with no concurrent MLS data. A few isolated days in which large sky inhomogeneities do not allow the correct balance of signal and reference beams have also been removed from the intercomparison. It is worth recalling that the signal to noise ratio of VESPA-22 spectra, and therefore the quality of the retrievals, depends on the sky opacity and, consequently, on the season, being noticeably better during winter and poorer in summer. This is particularly true for microwave ~~instruments installed~~spectrometers operating in ~~the~~ Polar regions, where ~~the~~ seasonal fluctuations ~~in~~of the tropospheric water vapor column content are significant.

~~Table 5 summarizes the characteristics of the Aura/MLS water vapor version 4.2 retrievals (Livesey et al., 2015).~~

Table 5: The main specifications of Aura/MLS water vapor mixing ratio profiles version 4.2 (Livesey et al., 2015~~)~~).

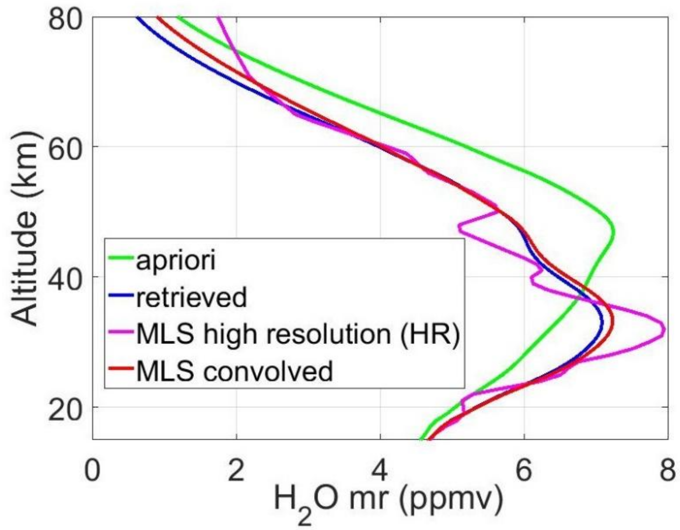

Pressure ~~[~~(hPa~~]~~)	Altitude ~~[~~(km~~]~~)	Resolution V x H ~~[~~(km~~]~~)	Single profile precision ~~[%]~~(%)	Accuracy ~~[%]~~(%)
0.002	86	10.3 x 350	152	34
0.01	76	8.8 x 725	55	11
0.046	66	7.4 x 540	35	8
0.21	55	3.6 x 670	19	7
1.0	44	2.5 x 400	6	4
4.6	35	3.4 x 350	4	7
22	26	3.2 x 265	5	7

68	18	3.1 x 190	5	6

Figure 12: The MLS profile measured on 23 December, 2016, with its high original vertical resolution (HR, magenta line) compared with the apriori profile (green line), the MLS convolved profile obtained from Eq. (31) (red line), and the VESPA-22 retrieved profile (blue line).

Table 5 summarizes the characteristics of the Aura/MLS water vapor version 4.2 retrievals (Livesey et al., 2015). In order to compare the two datasets, MLS vertical profiles are convolved with VESPA-22 averaging kernels in order to match the resolution of VESPA-22 profiles according to~~:~~ Rodgers (2000):

$$\cancel{x_{MLS} = x_a + A\left(\tilde{x}_{MLS} - x_a\right)} \tag{46}$$

$$x_{MLS} = x_a + A(\tilde{x}_{MLS} - x_a), \tag{31}$$

where $\tilde{x}_{MLS}$ is the raw (high resolution or HR) MLS water vapor vertical profile, x_a is the apriori profile, ~~A is Averaging Kernel Matrix~~A is the averaging kernel matrix, and x_{MLS} is the convolved MLS profile.

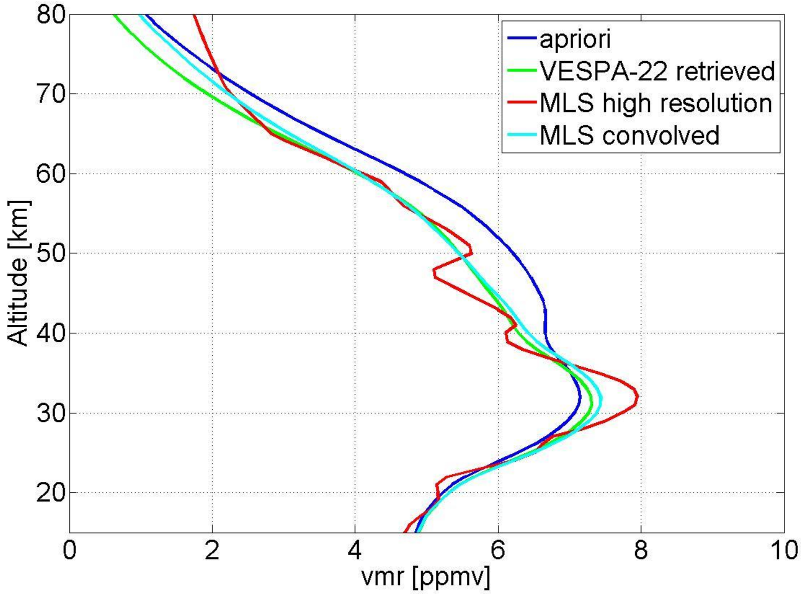

~~Figure 12: the MLS profile measured on 23 December 2016 with high vertical resolution (red line)~~ Additionally, VESPA-22 profiles were also compared with ~~the~~ MLS profiles smoothed in the vertical by using a 10 km moving average. This second set of degraded MLS profiles was generated in order to study the correlation between VESPA-22 and MLS datasets without introducing the dependency from one another brought by the convolution process (affecting MLS convolved profiles).

Figure 12 shows the MLS measured profile on 23 December, 2016, (magenta line), the MLS convolved profile obtained from Eq. ~~(46) and with the~~ (31) (red line), the apriori profile (green line), and the VESPA-22 retrieved profile (~~green line) and the apriori profile (~~blue line~~).~~

~~Figure 12 shows the MLS measured profile on 23 December 2016 (red line~~) ~~convolved using Eq. (46) (cyan line), together with the apriori profile (blue line) and the VESPA-22 retrieved profile (green line).~~for the same day. The MLS convolved profile tends to the apriori profile below ~~25~~26 km and above 72 km, where the retrieval sensitivity drops. ~~Figure 13,~~Figure 13, panel a, shows the mean VESPA-22 retrieved profile (in blue) and the mean MLS convolved profile (in red), with their standard deviations indicated with dashed lines~~, whereas panel b shows the~~ . The mean sensitivity of VESPA-22 retrieved profiles ~~with its standard deviation (solid and dashed lines respectively), which~~ is larger than 0.8 from ~~25~~about 26 to 72 km altitude~~.~~ and is indicated by the two green horizontal dashed lines. This interval can vary from day to day depending ~~from~~on the noise level of the 24-hour integrated ~~spectrum. Panels c and d display~~spectra (see white solid lines in Figure 15). Panel b displays the relative ~~and absolute differences~~difference of VESPA-22 water vapor mixing ratio mean vertical profile with respect to the MLS mean convolved profile (red line) and with respect to the MLS ~~high resolution~~smoothed mean vertical profile (~~i.e., not convolved;~~ blue line~~).~~) with their standard deviations (blue and red dashed lines, respectively). The largest relative and absolute (not shown) differences between the two datasets ~~occurs~~occur at 72 km, the upper limit of the VESPA-22 sensitivity range, and ~~are~~is about -6% ~~and -0.2 ppmv, respectively,~~ with Aura/MLS convolved mean profile being larger than VESPA-22 mean retrieval. The standard deviation of the differences increases in the mesosphere as a result of the larger atmospheric variability and the larger relative uncertainty of both instruments at these altitudes (see Figure 11 and Table 5) with respect to lower levels.

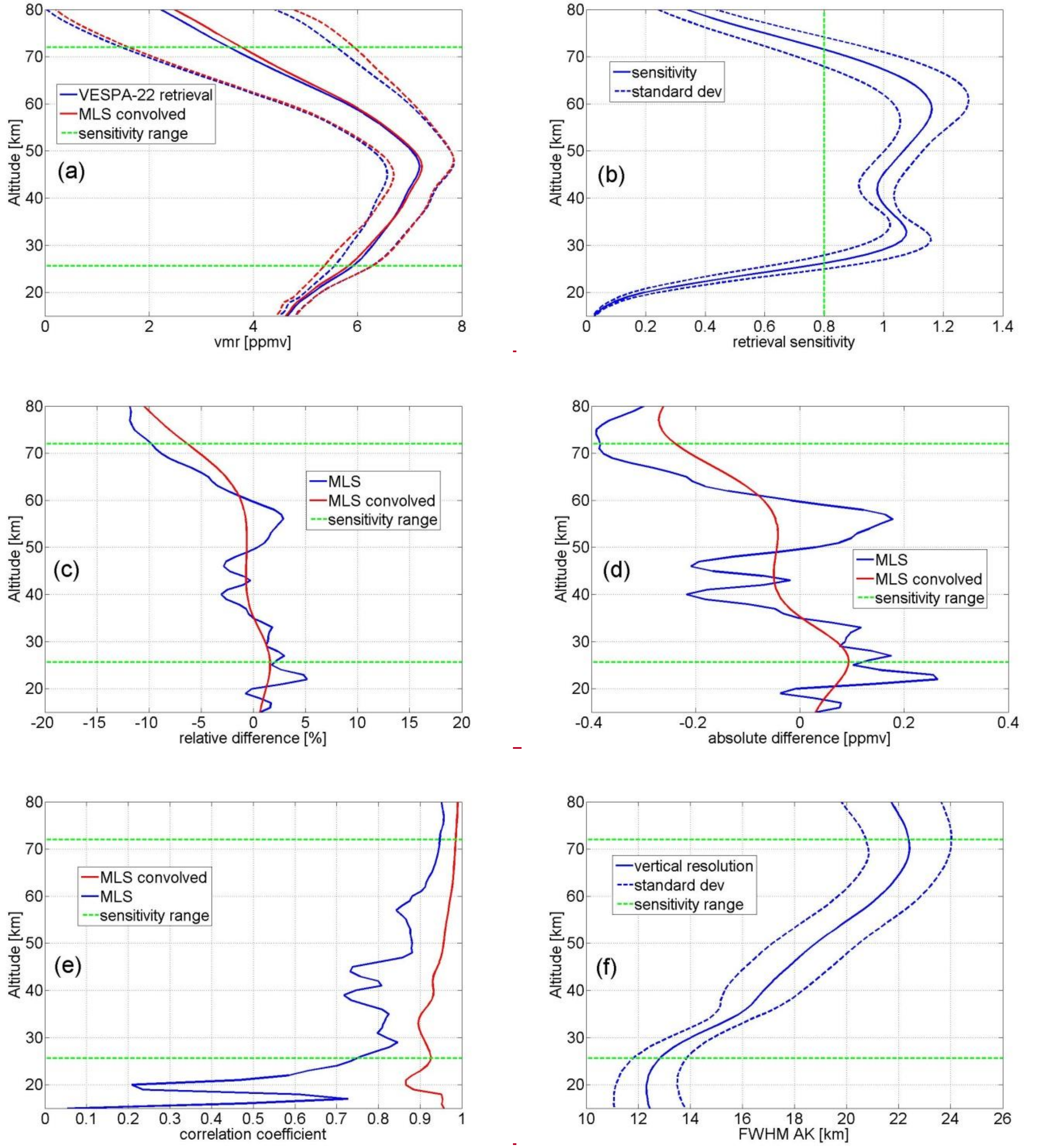

Figure ~~**13: (a) VESPA-22 averaged water vapor mixing ratio vertical profile with its standard deviation (blue line and blue dotted lines) and the mean MLS convolved profile with its standard deviation (red line and red dotted lines); (b) the mean retrieval sensitivity profile; (c) relative and (d) absolute differences vertical profiles between VESPA-22 and MLS convolved mean profiles**~~

~~(red line), and between VESPA-22 and MLS high resolution (not convolved) mean profiles (blue line); (e) vertical profiles of the~~ 13, panel c, shows the vertical profiles of the correlation coefficient between VESPA-22 and MLS convolved ~~profiles (red line), and between VESPA-22 and MLS high resolution profiles (blue line); (f) vertical profile of the mean full width at half maximum of VESPA-22 averaging kernels. The data used for the intercomparison range from 15 July 2016 to 21 May 2017.~~

~~The mean difference between the two datasets at the extremes of the sensitivity range could be reduced using an apriori for VESPA-22 retrievals that is closer to the real atmospheric state, as it would be for example a monthly average of MLS mean profiles collected during the same month of the measurement. However, as already discussed in Section 5, a climatological apriori, i.e., the monthly average of three years (2014-2016) of MLS~~data (red), and between VESPA-22 and MLS smoothed data ~~has been chosen instead, as this approach allows the identification and study of potential interannual water vapor variations. In Figure 13, panel e, the vertical profiles of the correlation coefficient between VESPA-22 and MLS convolved data (red), and between VESPA-22 and MLS not convolved data (blue) are shown. The former correlation is about 0.9~~(blue). The latter shows values of 0.8 or higher over the entire sensitivity range~~ while the latter is between 0.7 and 0.94.~~. The good correlation ~~between~~of VESPA-22 ~~and~~with MLS ~~high resolution water vapor~~smoothed profiles ~~is useful~~down to ~~illustrate how the two completely independent datasets correlate over the extended~~26 km altitude ~~range from 10 to 80 km.~~

~~Figure 13, panel f, shows the vertical profile of mean values of the full width at half maximum (FWHM)~~suggests that VESPA-22 retrievals are reliable at these stratospheric altitudes. Such a high correlation was obtained by using for the VESPA-22 retrieval algorithm an apriori profile held constant in time up to 48 km, therefore providing no contribution to the correlation. Below 25 km the correlation with MLS smoothed quickly deteriorates, whereas the correlation of VESPA-22 with MLS convolved profiles remains high, emphasizing the dependency of both datasets on VESPA-22 apriori profile and averaging kernels. Figure 13, panel d, shows the vertical profile of the mean values of the FWHM of VESPA-22 averaging kernels (blue solid line) calculated over the comparison period~~ with its standard deviation (blue dashed lines).~~. The FWHM of the averaging kernels is a measure of the retrieval vertical resolution (Rodgers, 2000). The single profile vertical resolution can vary depending ~~from~~on the level of noise affecting the measured spectrum.

~~The correlation between the water vapor mixing ratio profiles of VESPA-22 and Aura/MLS can be evaluated also by looking at Figure 14, where MLS values at three different altitude levels (high resolution in blue and convolved in red) are displayed as a function of the VESPA-22 values at the same altitudes, with the green line representing the linear regression of the MLS convolved vs. VESPA-22 measurements and the orange lines the ideal case of perfect agreement. Table 6 displays the parameters of the three linear regressions.~~

~~Table 6: Values obtained from the linear regressions between MLS convolved and VESPA-22 measurements at the indicated altitudes.~~

~~$y = ax + b$~~	~~a~~	~~b [ppmv]~~

~~35 km~~	~~0.92~~	~~0.52~~
~~50 km~~	~~0.91~~	~~0.69~~
~~65 km~~	~~1.01~~	~~0.09~~

~~Figure 15~~

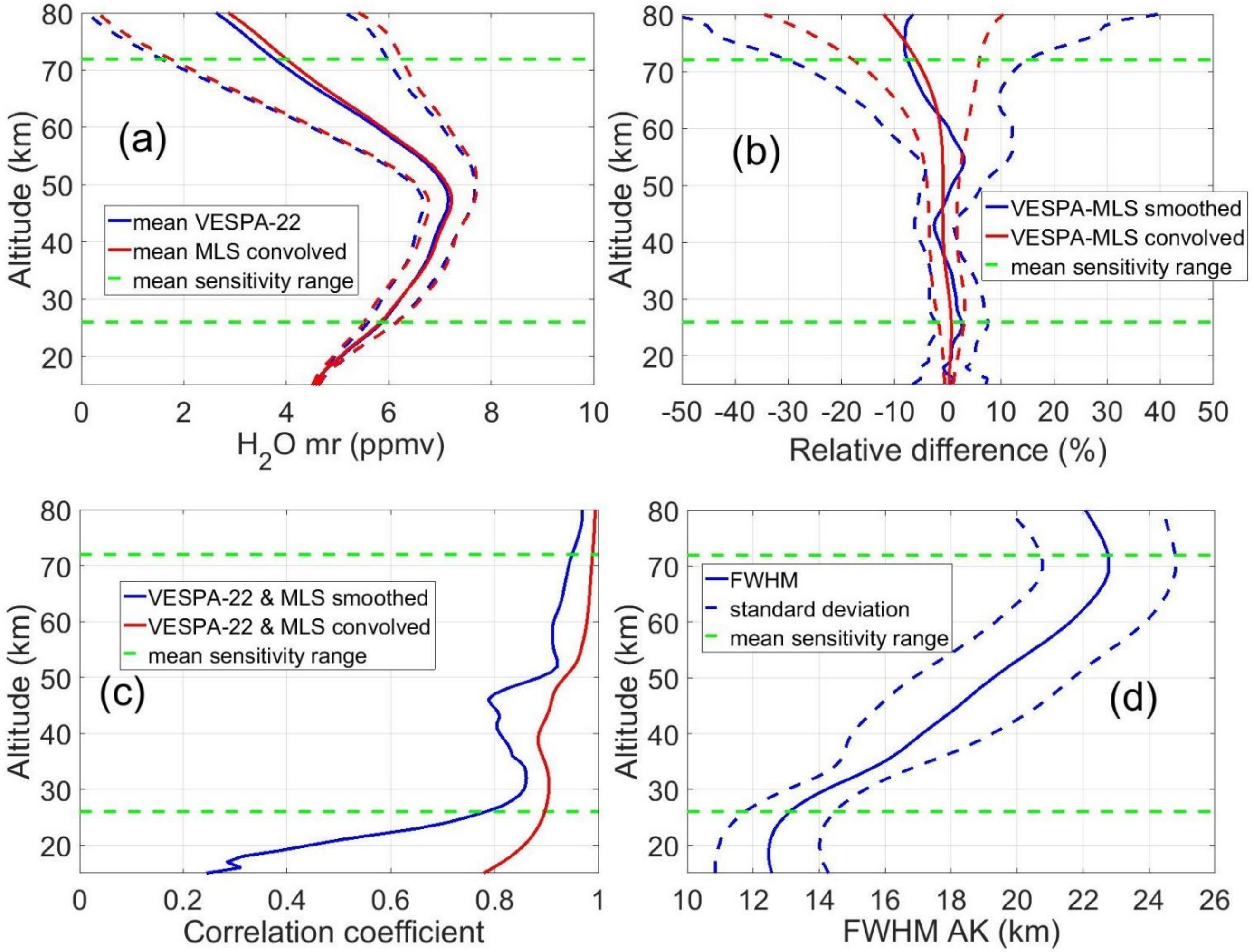

Figure 13: (a) VESPA-22 averaged water vapor mixing ratio vertical profile with its standard deviation (blue line and blue dashed lines) and the mean MLS convolved profile with its standard deviation (red line and red dashed lines); (b) Vertical profiles of the mean relative difference between VESPA-22 and MLS convolved (red line), and between VESPA-22 and MLS smoothed (blue line) with their standard deviations (red and blue dashed lines, respectively); (c) Vertical profiles of the correlation coefficient between VESPA-22 and MLS convolved profiles (red line), and between VESPA-22 and MLS smoothed profiles (blue line); (d) Vertical profile of the mean FWHM of VESPA-22 averaging kernels with its standard deviation. The data used for the intercomparison range from 12 July, 2016, to 02 July, 2017. The green dashed horizontal lines display the mean altitudes of the sensitivity range extremes.

Figure 14 shows the time series ~~of water vapor mixing ratio values measured~~ at different altitudes ~~by means of~~ of water vapor mixing ratio values from VESPA-22 (blue dots~~) and obtained by convolving MLS original vertical profiles~~), MLS convolved (red dots~~).~~), and MLS smoothed (yellow dots) datasets. The time series at ~~50~~65 km and ~~65~~75 km altitude show some ~~oscillations~~scattering in the MLS ~~convolved measurements after the 13th of~~ smoothed data from mid-March to mid-May, possibly due to the increased distance in this period between VESPA-22 and MLS observed air masses ~~and the less available data~~, to a relatively small number of MLS profiles averaged together to compute the MLS daily ~~averaged profiles. In the same period the increasing sky opacity and poor weather produced nosier~~profiles, and to the reduced MLS single profile precision at these altitudes (see Table 5). The 25 and 35 km water vapor time series display rapid and intense variations in winter caused by the polar vortex moving over Thule in mid-December and then away from Thule at the end of January. The 25 km time series is also useful to evaluate the quality of the VESPA-22 measurements at the bottom limit of the sensitivity range. Figure 14 shows that, at this altitude, VESPA-22 ~~measurement, decreasing the retrieval~~is capable of depicting the rapid variations in water vapor but does not have the necessary sensitivity~~.~~ to match the most intense variations observed by MLS (mid-January and early February).

In order to provide a more complete, albeit less quantitative, overview of the VESPA-22 and convolved MLS time series, ~~Figure 16~~Figure 15 shows contour maps of VESPA-22 (in color) and MLS convolved (black ~~line~~lines) water vapor profiles. The data collected by both instruments ~~revealed~~reveal an absolute maximum in August 2016 at 50 km of height of about 8.3 ppmv. During fall and winter the maximum of the water vapor mixing ratio profile lowers its altitude to reach about ~~30~~35 km in January 2017, due also to the downward motion of air ~~subsidence~~ inside the ~~polar~~Polar vortex. ~~A~~The two steep ~~gradient~~gradients in water vapor mixing ratio ~~is observed between 25 and 40 km altitude in the second half of January,~~ due to the ~~polar~~Polar vortex ~~that shifts~~moving away from Thule ~~for about two weeks.~~ are clearly visible between 25 and 40 km altitude., .

Both instruments also observe the return of the water vapor mixing ratio to pre-winter values in mid-April, possibly indicating the occurrence of the vortex final warming, with the re-establishment of a maximum in the mixing ratio profile at about 50 km altitude.

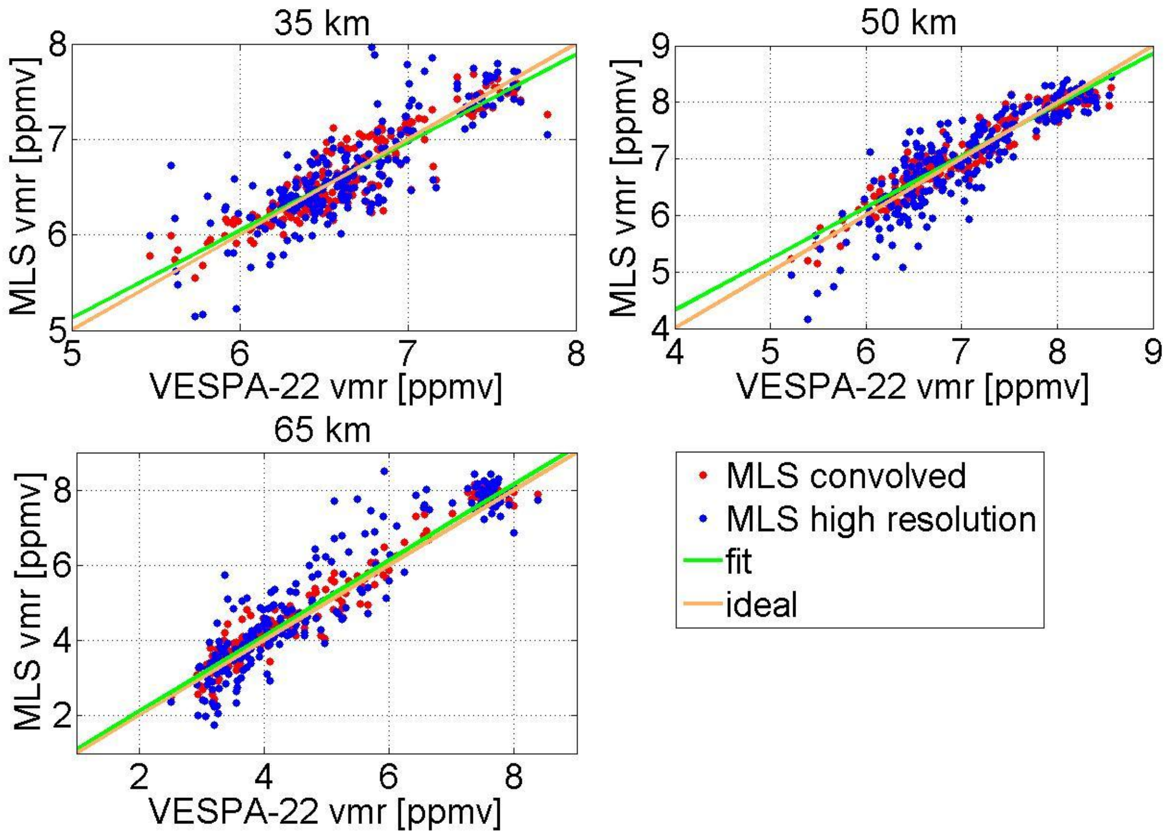

~~**Figure 14: High resolution (blue dots) and convolved (red dots) MLS water vapor mixing ratio values at three different altitudes plotted as a function of the corresponding VESPA-22 measurements obtained during the intercomparison period. The green line shows the linear regression between MLS convolved and VESPA-22 measurements while the orange line represents the ideal case of perfect agreement. The data used for the intercomparison range from 15 July 2016 to 21 May 2017.**~~

~~Given the large variability that stratospheric water vapor mixing ratio profiles can experience in Polar regions, in particular during winter and spring, Figure 17 is meant to illustrate the variations of VESPA-22 averaged mixing ratio profiles over the eleven months of reported measurements, and how the difference between VESPA-22 and MLS profiles varies from month to month. Figure 17, panel a, shows the monthly average profiles collected by VESPA-22, whereas panel b shows their relative difference with the monthly average profiles of convolved MLS. The maximum of mixing ratio in summer can be noticed in panel a, decreasing over time and lowering its altitude from September to January. The relative difference between the two datasets shows a similar shape during fall and winter, with a maximum absolute difference at the top of the sensitivity range from -5% to -10%, depending from the month. During summer the VESPA-22 data are characterized by a bias of about +7% at the~~

~~lower extreme of the sensitivity range, that slowly disappear in October. During April and May the Vespa-22 and MLS have a better agreement but it is due to the reduced sensitivity of VESPA-22 retrieval.~~

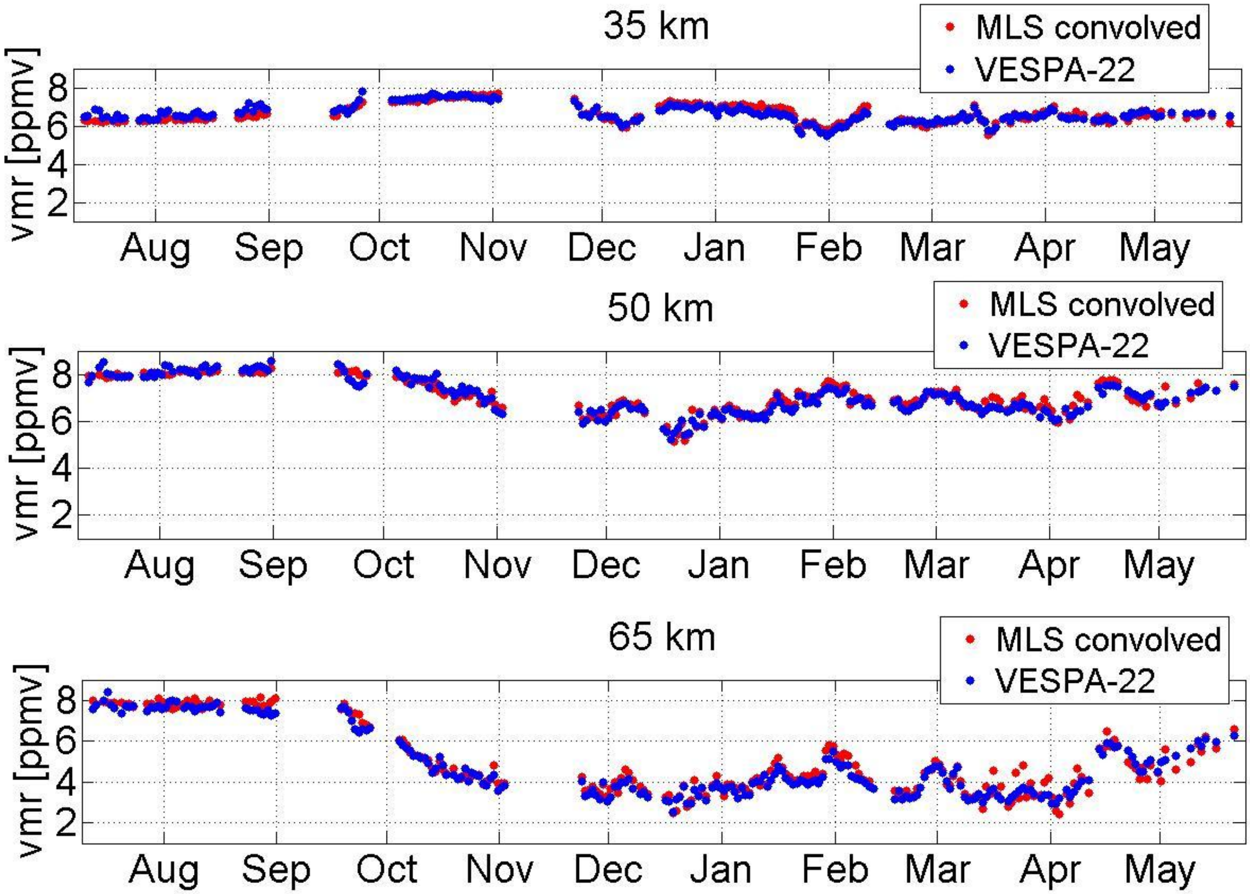
35 km
MLS convolved
VESPA-22
vmr [ppmv]
8
6
4
2
Aug
Sep
Oct
Nov
Dec
Jan
Feb
Mar
Apr
May
50 km
MLS convolved
VESPA-22
vmr [ppmv]
8
6
4
2
Aug
Sep
Oct
Nov
Dec
Jan
Feb
Mar
Apr
May
65 km
MLS convolved
VESPA-22
vmr [ppmv]
8
6
4
2
Aug
Sep
Oct
Nov
Dec
Jan
Feb
Mar
Apr
May

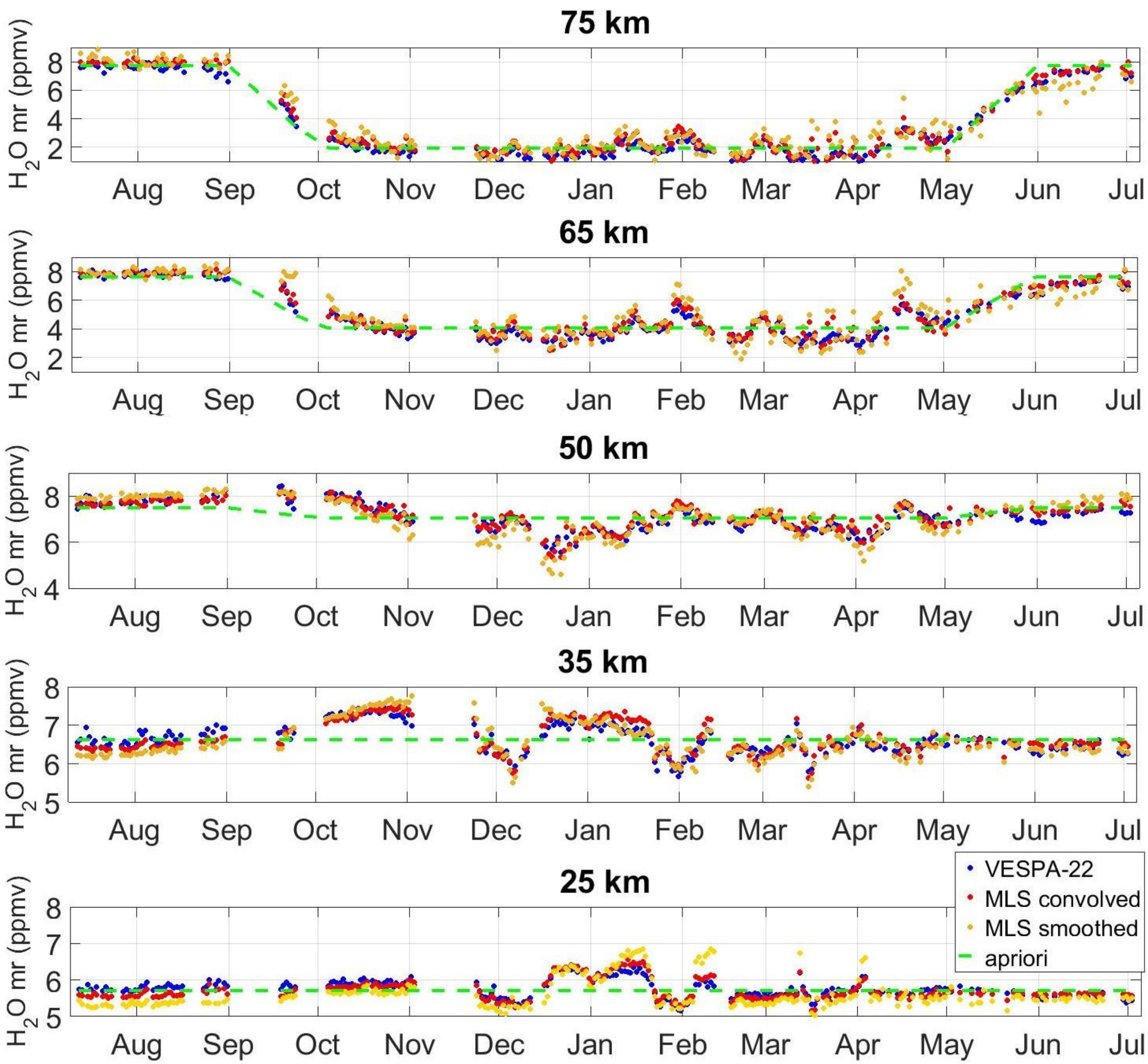

~~Figure 15:~~**Figure 14: Time series at different altitudes of water vapor mixing ratio values obtained with VESPA-22 (blue~~) and by convolving MLS vertical profiles (red).~~), by convolving MLS HR vertical profiles with VESPA-22 averaging kernels (red), and**

by smoothing MLS HR vertical profiles with a 10-km running average (yellow). Please note that the time series at the five different altitude levels have different scales on the Y-axis in order to better show the differences between datasets

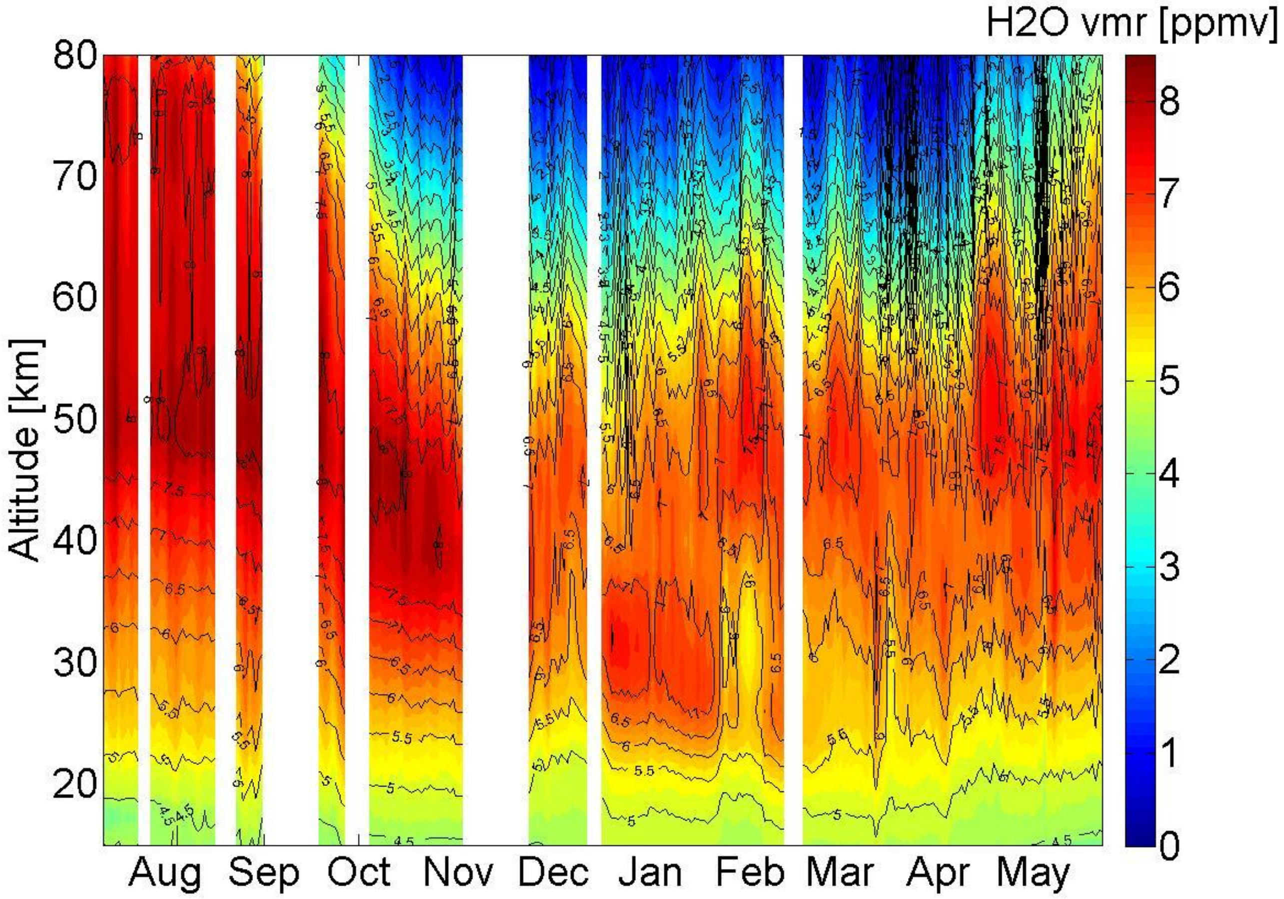

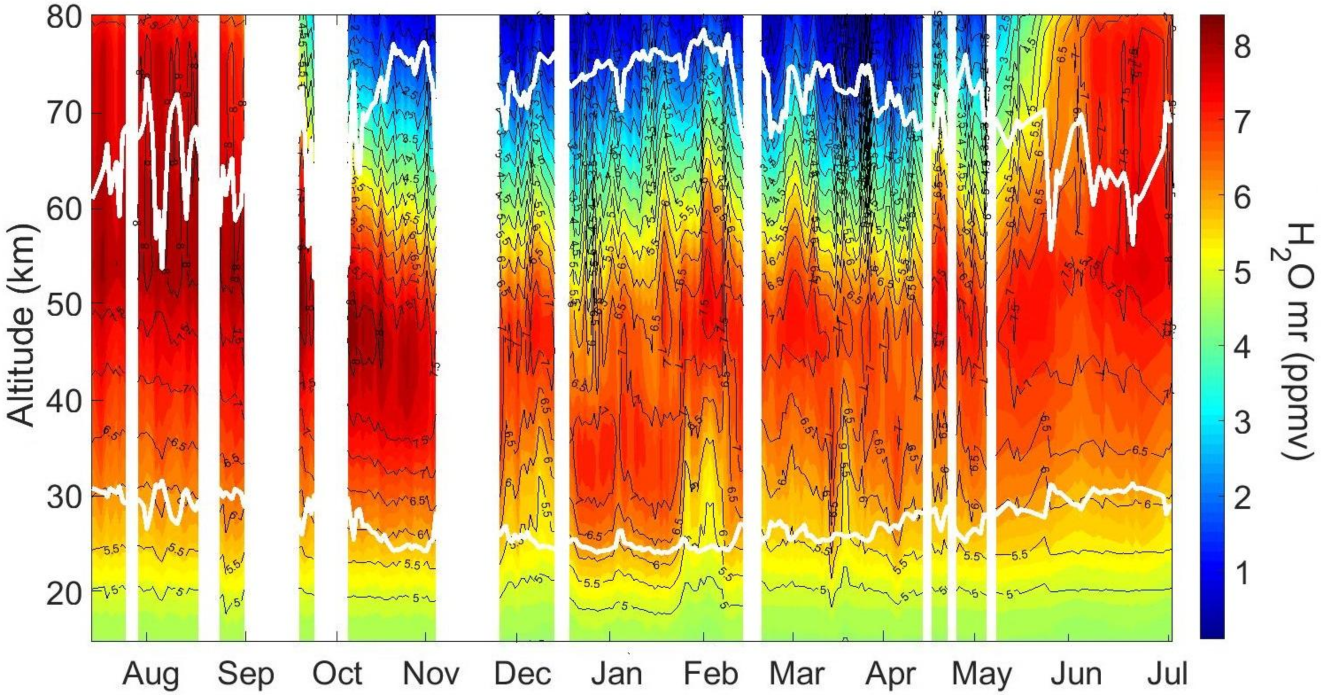

Figure ~~16: a~~15: A map showing the VESPA-22 retrieved profiles (colored map) compared to MLS convolved profiles (black lines). The blank areas ~~characterize~~indicate the ~~interruption period longer~~lack of VESPA-22 data for more than three days. White solid lines indicate the time series of the sensitivity interval.

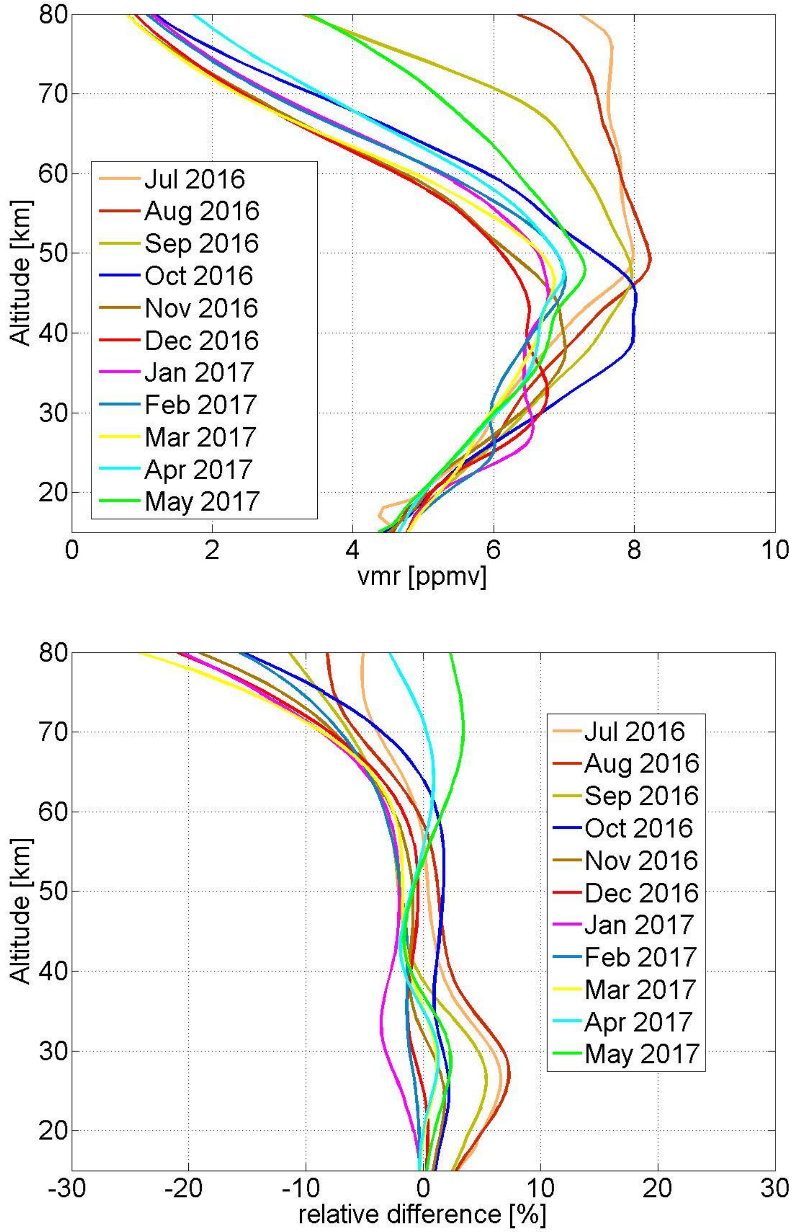

~~**Figure 17: (a) Monthly averages of the VESPA-22 water vapor mixing ratio profiles, and (b) monthly averages of the difference between VESPA-22 and convolved MLS dataset.**~~

Summary

VESPA-22 was installed at the Thule High Arctic Atmospheric Observatory (THAAO~~)~~; http://www.thuleatmos-it.it/) located at Thule Air Base ~~(~~, Greenland~~)~~, in July 2016 for long-term observations of the Polar middle atmospheric water vapor~~.~~ and column content. The instrument is characterized by a ~~full beam at half power~~FWHM encompassing 3.5~~°,~~° (Bertagnolio et al., 2012), granting the observation of the signal beam at angles as low as about 12° above the horizon. The instrument is installed indoor in a wooden annex to the main laboratory and observes the sky emission through ~~observation~~ windows made of 5-cm thick Plastazote LD15 sheets. ~~There~~During clear sky conditions, there are no evident artifacts larger than 2 mK affecting the measured spectra. VESPA-22 operated automatically with minimum need of maintenance for about one year, proving the robustness of hardware and acquiring system.

~~Instrument~~The instrument calibration is regularly performed using two noise diodes. The emission temperature of these elements is measured during tipping curve calibrations and checked periodically ~~against~~with liquid nitrogen calibrations. The calibrating noise diode temperature is estimated with an uncertainty of 1.~~3%, evaluated confronting calibration results obtained by means of tipping curves and liquid nitrogen, and the standard deviation of the differences between the two noise diodes time series.~~8%.

VESPA-22 retrieval algorithm is based on the optimal estimation technique~~;~~ (Rodgers, 2000); the retrieved profiles from 24-hour integration spectra have ~~a~~an average sensitivity larger than 0.8 from about ~~25~~26 to 72 km of altitude and a vertical resolution from about 12 to 23 km.

The forward model is provided by the ARTS software (Eriksson et al., 2013~~) and it simulates~~), which is tuned to reproduce the VESPA-22 measurement technique. In order to perform a realistic simulation of the troposphere, the PWV measured by the HATPRO radiometer (Rose and Czekala, 2009; Pace et al., 2015) operating side by side with VESPA-22 is taken into account in the forward model.

The uncertainty on VESPA-22 retrieved water vapor mixing ratio vertical profiles is evaluated as the sum of the contributions ~~of~~from calibration, pre-processing~~ and~~, spectroscopic parameters~~ and measurement noise.~~, measurements noise, and use of a second-order polynomial baseline in the retrieval process. In the sensitivity range of VESPA-22 retrievals, the total uncertainty is estimated to be about 5-6 % from 26 to 60 km increasing to about ~~12~~18% at 72 km.

VESPA-22 and MLS ~~retrieved~~water vapor profiles are compared during a period from July 2016 to ~~May~~July 2017. The VESPA-22 data used in the comparison are the results of retrievals from 24-hour integration spectra, ~~from 00:00 to 23:59,~~ while MLS data are the daily mean vertical profiles collected by MLS in a radius of 300 km around VESPA-22 observation point~~. VESPA-22 and MLS~~, convolved ~~datasets show a good correlation~~ with ~~a correlation coefficient of about 0.9 or higher.~~VESPA-22 averaging kernels. No significant ~~bias~~ biases were observed between the two datasets ~~was observed~~ in the altitude range from 25 to 60 km, whereas ~~in the altitude range~~ from 60 to 72 km the value of the mean difference (VESPA-22 – MLS) increases reaching -6% (-0.2 ppmv) at 72 km. A good correlation is also found between VESPA-22 and MLS smoothed (see Section 5) vertical profiles in the entire vertical range (from 26 to 72 km altitude, on average) where VESPA-22 profiles are considered valid.

The results described in this manuscript proved that VESPA-22 is capable of carrying out reliable middle atmospheric water vapor ~~stratospheric~~ measurements during different seasons and weather conditions, ~~even during spring and summer,~~ although the ~~data collected in these periods are affected by larger noise~~vertical range where the dataset is recommended for scientific use is reduced in summer with respect to ~~other seasons, due to the larger amount of tropospheric water vapor. VESPA-22 is capable of observing the seasonal variations of the water vapor concentration vertical profile in the stratosphere, as for example the water vapor subsidence occurring inside and at the edge of the polar vortex. The VESPA-22 and MLS convolved retrieved monthly averaged profiles show an agreement within 10%, with the maximum difference measured during~~ winter~~ at the top of the sensitivity range (Figure 17, panel a and b). Furthermore,~~. VESPA-22 retrievals are capable of correctly represent the rapid variations in water vapor concentrations that can occur in the stratosphere, as ~~demonstrated~~revealed by the large water vapor gradients measured ~~in~~both by VESPA-22 and Aura/MLS in mid-December 2016, late January/early February 2017, and then again during April and May (see ~~Figure 16) by both VESPA-22 and Aura/MLS~~Figure 15). At the same time, VESPA-22 spectral measurements and corresponding mixing ratio retrievals appear to have the necessary stability and consistency to observe slow seasonal variations, such as the water vapor subsidence occurring inside and at the edge of the Polar vortex.

~~*Acknowledgements.*~~*Acknowledgements*. The development of VESPA-22 and measurements at Thule were supported by the Italian Antarctic Programme (PNRA) funded by MIUR through Projects 2013/C3.03 and 2015/B3.01. This study has been also partially supported by Progetto Premiale ARCA. Bob de Zafra, Mike Gomez, and Axel Murk helped with the development of VESPA-22 by suggesting useful solutions to technical problems related to the instrument design. We are indebted to them. Additionally, G. Muscari is very thankful to Nik ~~Kaempfer~~Kämpfer and Axel Murk for donating to the VESPA-22 project the firmware that the FFTS is currently employing. We are grateful to Stephan Buehler and Patrick Eriksson for helping with the ARTS software, and to the MLS team of the Jet Propulsion Laboratory for providing access to the Aura/MLS data.

References

Bertagnolio, P. P., Muscari, G~~.~~., and Baskaradas, J.: Development of a 22 GHz ground-based spectrometer for middle atmospheric water vapor monitoring~~. European Journal of~~, Eur. J. Remote ~~Sensing~~Sens. 45~~.1~~, 51-61, doi: 10.5721/EuJRS20124506, 2012.

Cazzoli, G., ~~C.~~ Puzzarini, ~~G.~~C., Buffa, G., and ~~O.~~ Tarrin~~;~~, O.: Experimental and theoretical investigation on pressure-broadening and pressure-shifting of the 22.2 GHz line of water, J. Quant. Spectrosc. Radiat. Transfer, 105, 438–449, doi: 10.1016/j.jqsrt.2006.11.003, 2007.

~~De~~de Zafra, R. L.: The Ground-Based Measurement of Stratospheric Trace Gases Using Quantitative Millimeter Wave Emission Spectroscopy, in Diagnostic Tools in Atmospheric Physics: Varenna on Lake Como, Villa Monastero, 22 June-2 July 1993, edited by G. Fiocco and G. Visconti, Società Italiana di Fisica, pp. 23–54, 1995.

Eriksson, P., Buehler, S. A., Davis, C. P., Emde, C., ~~&~~and Lemke, O.: ARTS, the atmospheric radiative transfer simulator, version 2~~. Journal of Quantitative Spectroscopy and Radiative~~, J. Quant. Spectrosc. Radiat. Transfer, 112(10), 1551-1558, doi:10.1016/j.jqsrt.2011.03.001, 2011.

Gomez, R. M., Nedoluha, G. E., Neal, H. L., ~~&~~and McDermid, I. S.: The fourth-generation Water Vapor millimeter-Wave Spectrometer~~.~~, Radio Science, 47(1), doi:10.1029/2011RS004778, 2012.

Haefele, A., ~~E.~~ De Wachter, ~~K.~~E. , Hocke, K., Kämpfer, N~~. Ka¨mpfer, G. E.~~., Nedoluha, ~~R. M.~~G. E., Gomez, ~~P.~~R. M., Eriksson, P~~.~~., Forkman, ~~A.~~P., Lambert, A., and ~~M. J.~~ Schwartz~~:~~, M. J.: Validation of ground-based microwave radiometers at 22 GHz for stratospheric and mesospheric water vapor, J. Geophys. Res., 114, D23305, doi:10.1029/2009JD011997, 2009.

Lait, L., Newman, P~~.~~., and Schoeberl, R.: Using the Goddard Automailer, NASA Goddard Space Flight Cent., Greenbelt, Md. Available at http://code916. gsfc. nasa.gov/Dataservices/, 2005.

Liebe, H. J.: MPM – An atmospheric millimeter-wave propagation model, Int. J. Infrared. Millim., 10, 631–650, doi:10.1007/BF01009565, 1989.

Livesey, N. J., Read, W. G., Wagner, P. A., Froidevaux, L., Lambert, A., Manney, G. L., Millan Valle, L. F., Pumphrey, H. C., Santee, M. L., Schwartz, M. L., Wang, S., Fuller, R. A., Jarnot, R. F., Knosp, R. F. and Martinez, E.: Earth Observing System (EOS) Aura Microwave Limb Sounder (MLS) Version 4.2x Level 2 data quality and description document~~.~~, Jet Propulsion Laboratory California Institute of Technology, Pasadena, California, 2015.

Nedoluha, G. E., Bevilacqua, R. M., Gomez, R. M., Thacker, D. L.,~~ William, B.~~ Waltman, W. B., and ~~Thomas, A.~~ Pauls~~:~~, T. A.: Ground-based measurements of water vapor in the middle atmosphere~~. Journal of Geophysical Research~~, J. Geophys. Res. 100.D2, 2927-2939, doi: 10.1029/94JD02952, 1995.

Nedoluha, G. E., Bevilacqua, R. M., Gomez, R. M., Hicks, B. C., ~~&~~and Russell, J. M.: Measurements of middle atmospheric water vapor from low latitudes and midlatitudes in the Northern Hemisphere, 1995–1998~~. Journal of Geophysical Research: Atmospheres,~~, J. Geophys. Res., 104(D16), 19257-19266, doi: 10.1029/1999JD900419, 1999.

Pace, G., Junkermann, W., Vitali, L., ~~Di~~di Sarra, A., Meloni, D., Cacciani, M., Cremona G., Iannarelli A. M., Zanini G.: On the complexity of the boundary layer structure and aerosol vertical distribution in the coastal Mediterranean regions: a case study~~.~~, Tellus B, 67, doi: 10.3402/tellusb.v67.27721, 2015.

Parrish, A., ~~Dezafra~~de Zafra, R. L., Solomon, P. M~~.~~., and Barrett, J. W.: A ground-based technique for millimeter wave spectroscopic observations of stratospheric trace constituents, Radio Science, *23*(2), 106-118, doi: 10.1029/RS023i002p00106, 1988.

Pickett, H. M., Poynter, R. L., Cohen, E. A., Delitsky, M. L., Pearson, J. C~~.~~., and Müller, H. S. P.: Submillimeter, millimeter, and microwave spectral line catalog, ~~Journal of Quantitative Spectroscopy and Radiative~~J. Quant. Spectrosc. Radiat. Transfer, 60(5), 883-890., doi: 10.1016/S0022-4073(98)00091-0, 1998.

Oltmans, S. J., Vömel, H., Hofmann, D. J., Rosenlof, K. H., and Kley, D.: The increase in stratospheric water vapor from baloonborne frostpoint hygrometer measurements at Washington, D. C., and Boulder, Colorado, Geophys. Res. Lett., vol. 27, no. 21, 3453–3456, doi: 10.1029/2000GL012133, 2000.

Rees, D., Barnett, J. J~~.~~., and Labitzke, K.: COSPAR International Reference Atmosphere: 1986. Pt. 2: Middle atmosphere models~~. Advances in space research,~~, Adv. Space Res., 10, 1990.

Rodgers, C. D.: Inverse method for atmospheric sounding, Series on atmospheric, oceanic and Planetary Physics – Vol. 2, edited by: Taylor, F. W., World Scientific Publishing Co. Pte LTd, Singapore, 2000.

Rose, T~~.,~~. and Czekala, J~~.,~~.: RPG-HATPRO Radiometer Operating Manual~~.~~, Radiometer Physics GmbH, Version, 2009

Rosenlof, K. H., Oltmans, S. J., Kley, D., Russell III, J. M., Chiou, E. -W., Chu, W. P., ~~• D. G.~~ Johnson, D. G., Kelly, K. K., Michelsen, H. A., Nedoluha, G. E., Remsberg, E. E., Toon, G. C., McCormick, M. P.: Stratospheric water vapor increases over the past half-century~~. Geophysical research letters,~~, Geophys. Res. Let., 28(7), 1195-1198, doi: 10.1029/2000GL012502, 2001.

Rothman, L. S., Gordon, I. E., Babikov, Y., Barbe, A., Chris Benner, D~~. C~~., Bernath, P. F., Birk, M., Bizzocchi, L., Boudon, V., Brown, L. R., Campargue, A~~.~~., Chance, K., Cohen, E. A., Coudert, L. H., Devi, V.M., Drouin, B. J., Fayt, A., Flaud, J.-M., Gamache, R. R., Harrison, J. J., Hartmann, J.-M., Hill, C., Hodges, J. T., Jacquemart, D., Jolly, A., Lamouroux, J., Le Roy, R. J., Li, G., Long, D. A., Lyulin, O. M., Mackie, C. J., Massie, S. T. , Mikhailenko, S., Müller, H. S. P., Naumenko, O. V., Nikitin, A. V., Orphal, J., Perevalov, V., Perrin, A., Polovtseva, E. R., Richard, C., Smith, M. A. H., Starikova, E., Sung, K., Tashkun, S., Tennyson, J., Toon, G. C., Tyuterev, Vl. G., and Wagner, G.: The HITRAN2012 molecular spectroscopic database~~. Journal of Quantitative Spectroscopy and Radiative~~, J. Quant. Spectrosc. Radiat. Transfer,~~-~~ 130, 4-50, doi: 10.1016/j.jqsrt.2013.07.002, 2013.

Seele, C.: Bodengebundene Mikrowellenspektroskopie vonWasserdampf in der mittleren polaren ~~Atmosph¨are~~Atmosphäre, Ph.D. thesis, University of Bonn, 1999.

Serreze, M. C~~.,~~. and Francis, J. A.: The Arctic amplification debate~~.~~, Climatic change, 76(3-4), 241-264, doi: 10.1007/s10584-005-9017-y, 2006.

Solomon, S.: Stratospheric ozone depletion: A review of concepts and history~~. Reviews of Geophysics,~~, Rev. Geophys., 37(3), 275-316, doi:10.1029/1999RG900008, 1999.

Solomon, S., Rosenlof, K. H., Portmann, R. W., Daniel, J. S., Davis, S. M., Sanford, T. J., and Plattner, G. K.: Contributions of stratospheric water vapor to decadal changes in the rate of global warming~~.~~, Science, 327(5970), 1219-1223, doi: 10.1126/science.1182488, 2010.

Straub, C., Murk, A., and N. Kämpfer: MIAWARA-C, a new ground based water vapor radiometer for measurement campaigns, Atmos. Meas. Tech., 3, 1271–1285, doi:10.5194/amt-3-1271-2010 , 2010.

Teniente, J., Goñi, D., Gonzalo, R., del Río, C.: Choked Gaussian antenna: Extremely low sidelobe compact antenna design~~.~~, IEEE Antennas and Wireless Propagation Letters,- 1(1), 200-202, doi: 10.1109/LAWP.2002.807959, 2002.

Tschanz, B., Straub, C., Scheiben, D., Walker, K. A., Stiller, G. P., and Kämpfer, N.: Validation of middle-atmospheric campaign-based water vapour measured by the ground-based microwave radiometer MIAWARA-C~~. Atmospheric Measurement Techniques,~~, Atmos. Meas. Tech., 6(7), 1725-1745, doi: 10.5194/amt-6-1725-2013, 2013.

Waters, J. W., Froidevaux, L., Harwood, R. S., Jarnot, R. F., Pickett, H. M., Read, W. G., Siegel, P., Cofield, R. E., Filipiak, M., Flower, D., Holden, J., Lau, G. K., Livesey, N. J., Manney, G. L., Pumphrey, H., Santee, M. L.,Wu, D. L., Cuddy, D. T., Lay, R. R., Loo, M., Perun, V. S., Schwartz, M. J., Stek, P. C., Thurstans, R. P., Boyles, M., Chandra, S., Chavez, M., Chen, G.-S., Chudasama, B., Dodge, R., Fuller, R. A., Girard, M., Jiang, J. H., Jiang, Y. B., Knosp, B. W., LaBelle, R. C., Lam, J., Lee, K. A., Miller, D., Oswald, J. E., Patel, N., Pukala, D., Quintero, O., Scaff, D., Snyder,W. V., Tope, M.,Wagner, P. A.,

~~andWalch~~and Walch, M.: The Earth Observing System Microwave Limb Sounder (EOS MLS) on the Aura satellite, IEEE T. Geosci. Remote, 44, 1075– 1092, doi:10.1109/TGRS.2006.873771, 2006.